



Theses and Dissertations

2004-07-08

Consensus Seeking, Formation Keeping, and Trajectory Tracking in Multiple Vehicle Cooperative Control

Wei Ren

Brigham Young University - Provo

Follow this and additional works at: <https://scholarsarchive.byu.edu/etd>



Part of the [Electrical and Computer Engineering Commons](#)

BYU ScholarsArchive Citation

Ren, Wei, "Consensus Seeking, Formation Keeping, and Trajectory Tracking in Multiple Vehicle Cooperative Control" (2004). *Theses and Dissertations*. 153.

<https://scholarsarchive.byu.edu/etd/153>

This Dissertation is brought to you for free and open access by BYU ScholarsArchive. It has been accepted for inclusion in Theses and Dissertations by an authorized administrator of BYU ScholarsArchive. For more information, please contact scholarsarchive@byu.edu, ellen_amatangelo@byu.edu.

CONSENSUS SEEKING, FORMATION KEEPING, AND
TRAJECTORY TRACKING IN MULTIPLE VEHICLE
COOPERATIVE CONTROL

by

Wei Ren

A dissertation submitted to the faculty of

Brigham Young University

in partial fulfillment of the requirements for the degree of

Doctor of Philosophy

Department of Electrical and Computer Engineering

Brigham Young University

August 2004

Copyright © 2004 Wei Ren

All Rights Reserved

BRIGHAM YOUNG UNIVERSITY

GRADUATE COMMITTEE APPROVAL

of a dissertation submitted by

Wei Ren

This dissertation has been read by each member of the following graduate committee and by majority vote has been found to be satisfactory.

Date

Randal W. Beard, Chair

Date

Timothy W. McLain

Date

Sean C. Warnick

Date

Wynn C. Stirling

Date

A. Lee Swindlehurst

BRIGHAM YOUNG UNIVERSITY

As chair of the candidate's graduate committee, I have read the dissertation of Wei Ren in its final form and have found that (1) its format, citations, and bibliographical style are consistent and acceptable and fulfill university and department style requirements; (2) its illustrative materials including figures, tables, and charts are in place; and (3) the final manuscript is satisfactory to the graduate committee and is ready for submission to the university library.

Date

Randal W. Beard
Chair, Graduate Committee

Accepted for the Department

Michael A. Jensen
Graduate Coordinator

Accepted for the College

Douglas M. Chabries
Dean, College of Engineering and Technology

ABSTRACT

CONSENSUS SEEKING, FORMATION KEEPING, AND TRAJECTORY TRACKING IN MULTIPLE VEHICLE COOPERATIVE CONTROL

Wei Ren

Electrical and Computer Engineering

Doctor of Philosophy

Cooperative control problems for multiple vehicle systems can be categorized as either formation control problems with applications to mobile robots, unmanned air vehicles, autonomous underwater vehicles, satellites, aircraft, spacecraft, and automated highway systems, or non-formation control problems such as task assignment, cooperative transport, cooperative role assignment, air traffic control, cooperative timing, and cooperative search. The cooperative control of multiple vehicle systems poses significant theoretical and practical challenges. For cooperative control strategies to be successful, numerous issues must be addressed. We consider three important and correlated issues: consensus seeking, formation keeping, and trajectory tracking.

For consensus seeking, we investigate algorithms and protocols so that a team of vehicles can reach consensus on the values of the coordination data in the presence of imperfect sensors, communication dropout, sparse communication topologies, and noisy and unreliable communication links. The main contribution of this dissertation in this area is that we show necessary and/or sufficient conditions for consensus seeking with limited,

unidirectional, and unreliable information exchange under fixed and switching interaction topologies (through either communication or sensing).

For formation keeping, we apply a so-called “virtual structure” approach to spacecraft formation flying and multi-vehicle formation maneuvers. As a result, single vehicle path planning and trajectory generation techniques can be employed for the virtual structure while trajectory tracking strategies can be employed for each vehicle. The main contribution of this dissertation in this area is that we propose a decentralized architecture for multiple spacecraft formation flying in deep space with formation feedback introduced. This architecture ensures the necessary precision in the presence of actuator saturation, internal and external disturbances, and stringent inter-vehicle communication limitations. A constructive approach based on the satisficing control paradigm is also applied to multi-robot coordination in hardware.

For trajectory tracking, we investigate nonlinear tracking controllers for fixed wing unmanned air vehicles and nonholonomic mobile robots with velocity and heading rate constraints. The main contribution of this dissertation in this area is that our proposed tracking controllers are shown to be robust to input uncertainties and measurement noise, and are computationally simple and can be implemented with low-cost, low-power micro-controllers. In addition, our approach allows piecewise continuous reference velocity and heading rate and can be extended to derive a variety of other trajectory tracking strategies.

ACKNOWLEDGMENTS

I would first like to acknowledge my advisor, Dr. Randy Beard for his assistance and guidance over the past four years. He has not only been a great mentor but a good friend to me. I particularly appreciate his patience and encouragement to help me with my study, and his suggestions and insights to help me solve challenging research problems and develop new ideas.

I would like to acknowledge Dr. Tim McLain for his assistance, both technically and socially. Being a great source of knowledge and experience, he is always willing to give me suggestions and support. I would also like to thank the other members of my committee: Dr. Sean Warnick, Dr. Wynn Stirling, and Dr. A. Lee Swindlehurst for their support.

I gratefully acknowledge Dr. Dah-Jay Lee for his help and support all the time. I am thankful for Dr. Wayne Barrett and Dr. Chris Grant from the Mathematics Department for their technical guidance. I am also indebted to Dr. David Long for his advice.

I owe special thanks to Will Curtis at the Air Force Research Lab and Jisang Sun, Derek Kingston, Jeff Anderson, Matt Blake, Walt Johnson, Carolyn Cornaby, and Reed Christiansen at the BYU MAGICC Lab for their help over the past few years.

I am also thankful for the friendship with Wei Li, Chris Peel, Lihong Bu, Dahai Lin, Xiaojun Wang, Zhihong Ding, Mike Turner, and Shon Hiatt at BYU.

Most importantly, I would like to acknowledge my wife, Fei for her love and constant help. Despite her non-engineering background in economics law, she has been very patient and supportive to me. She has also been willing to “discuss” control theory with me whenever I met technical difficulties. I am also very grateful for the ubiquitous encouragement and love brought to my life by my parents and sister.

Contents

Acknowledgments	vii
List of Tables	xiii
List of Figures	xvii
1 Introduction	1
1.1 Motivation	1
1.2 Contributions	3
1.2.1 Multi-agent Consensus Seeking	3
1.2.2 Multi-agent Formation Keeping	4
1.2.3 Trajectory Tracking with Input Constraints	5
1.3 Organization	5
2 Literature Review	7
2.1 Consensus Seeking	7
2.2 Formation Keeping	8
2.3 Trajectory Tracking	10
2.4 CLF and Satisficing Control	11
2.5 Constrained Control	12
3 Consensus Seeking Under Fixed and Switching Interaction Topologies	13
3.1 Introduction	13
3.2 Problem Statement	14
3.3 Consensus Under Fixed Interaction Topologies	19
3.3.1 Consensus Using Continuous-Time Update Scheme	19

3.3.2	Consensus Using Discrete-Time Update Scheme	28
3.4	Consensus Under Dynamically Changing Interaction Topologies	32
3.4.1	Consensus Using Discrete-Time Update Scheme	32
3.4.2	Consensus Using Continuous-Time Update Scheme	34
3.4.3	Discussion	36
3.4.4	Simulation Results	38
4	Multi-agent Formation Control	41
4.1	Introduction	41
4.2	Multiple Spacecraft Formation Flying	41
4.2.1	Problem Statement	42
4.2.2	Decentralized Architecture via the Virtual Structure Approach	46
4.2.3	Decentralized Formation Control Strategies	52
4.2.4	Simulation Results	63
4.3	Satisficing Approach to Multi-agent Coordinated Control	68
4.3.1	Satisficing Theory	69
4.3.2	Satisficing Control for Formation Maneuvers	71
4.3.3	Application Example	76
5	Trajectory Tracking Control with Input Constraints	83
5.1	Introduction	83
5.2	Trajectory Tracking for UAVs with Velocity and Heading Rate Constraints	83
5.2.1	Problem Statement	85
5.2.2	CLF for Tracking Control with Saturation Constraints	89
5.2.3	Nonlinear Tracking Control based on CLF	96
5.2.4	Simulation Results	103
5.3	Experimental Study of Saturated Tracking Control for Mobile Robots	106
5.3.1	Experimental Setup	108
5.3.2	Tracker Design	110
5.3.3	Experimental Results	116

6 Conclusion and Future Work	125
6.1 Summary of Main Results	125
6.2 Future Work	126
6.3 Conclusion	127
Bibliography	141

List of Tables

5.1	Parameter values used in simulation.	104
5.2	Specifications of the robot and velocity controller parameters.	116

List of Figures

3.1	A graph that contains a spanning tree.	15
3.2	A spanning tree of the graph (Example 1).	15
3.3	A spanning tree of the graph (Example 2).	16
3.4	A spanning tree of the graph (Example 3).	16
3.5	Communication topology.	27
3.6	Consensus of τ_i and s_i using update law (3.4).	28
3.7	Consensus of τ_i and s_i without link from A_2 to A_1 using update law (3.4).	29
3.8	Consensus and evolution of τ_i and s_i using update law (3.8).	29
3.9	Possible interaction topologies for $\mathcal{A} = \{A_i i = 1, \dots, 5\}$	38
3.10	The union of \mathcal{G}_s	39
3.11	Consensus with $\mathcal{G}[k]$ and $\mathcal{G}(t_k)$ randomly switching from \mathcal{G}_s	39
3.12	Consensus with $\mathcal{G}[k]$ and $\mathcal{G}(t_k)$ randomly switching from \mathcal{G}'_s	40
4.1	Coordinate Frame Geometry.	43
4.2	The centralized architecture based on the virtual structure approach.	47
4.3	The decentralized architecture via the virtual structure approach.	49
4.4	Plot of \tilde{r}_{Fxi} with initial conditions $\tilde{r}_{Fxi} = 1$ and $\dot{\tilde{r}}_{Fxi} = 0$ for different choices of Γ_{Gi}	63
4.5	The geometric configuration of nine spacecraft.	64
4.6	The average coordination error of the coordination vector instantiations.	64
4.7	The absolute position and attitude tracking errors.	65
4.8	The relative position and attitude errors.	65
4.9	The control effort for spacecraft #1.	68
4.10	The desired trajectories for robot #1 and #2.	77
4.11	The formation function $F(x, s)$ with $F(x(t_0), s(t_0)) = 0.1$	77

4.12	The tracking errors for robot #1 and #2 with $F(x(t_0), s(t_0)) = 0.1$	78
4.13	The formation function $F(x, s)$ with $F(x(t_0), s(t_0)) = 0.43$	80
4.14	The tracking errors for robot #1 and #2 with $F(x(t_0), s(t_0)) = 0.43$	80
4.15	Canister robots used in the experiment.	81
4.16	The commanded desired distance and actual distance between the two robots with $F_U = 0.1$	81
4.17	Formation measure function $F(x, s)$ with $F_U = 0.1$	82
5.1	System architecture.	85
5.2	The feasible control set $\mathcal{F}(t, x)$ at some time $t = \hat{t}$	97
5.3	The reference and actual trajectories of the 6-DOF model.	105
5.4	The trajectory tracking errors of the 6-DOF model.	105
5.5	The reference and commanded control inputs of the 6-DOF model.	106
5.6	The simulation scenario of the 6-DOF model with model uncertainties and disturbances.	107
5.7	The trajectory tracking errors of the 6-DOF model with model uncertainties and disturbances.	107
5.8	Hardware/software structure for the mobile robot testbed.	108
5.9	Canister robots.	109
5.10	Software architecture.	110
5.11	PID control loop for v^c and ω^c	110
5.12	Desired and actual robot trajectories using velocity controllers when there are two targets and $\epsilon_{\omega_1} = \epsilon_{\omega_2} = 0.75$ (rad/s).	117
5.13	Tracking errors using velocity controllers when there are two targets and $\epsilon_{\omega_1} = \epsilon_{\omega_2} = 0.75$ (rad/s).	118
5.14	Reference and commanded velocities using velocity controllers when there are two targets and $\epsilon_{\omega_1} = \epsilon_{\omega_2} = 0.75$ (rad/s).	118
5.15	Desired and actual robot trajectories using nonsmooth backstepping when there are two targets and $\epsilon_{\omega_1} = \epsilon_{\omega_2} = 0.75$ (rad/s).	119
5.16	Tracking errors using nonsmooth backstepping when there are two targets and $\epsilon_{\omega_1} = \epsilon_{\omega_2} = 0.75$ (rad/s).	120

5.17	Reference and actual velocities using nonsmooth backstepping when there are two targets and $\epsilon_{\omega_1} = \epsilon_{\omega_2} = 0.75$ (rad/s).	120
5.18	Control forces and torques using nonsmooth backstepping controller when there are two targets and $\epsilon_{\omega_1} = \epsilon_{\omega_2} = 0.75$ (rad/s).	121
5.19	Desired and actual robot trajectories using the saturation controller when there are three targets and $\epsilon_{\omega_1} = \epsilon_{\omega_2} = 0.2$ (rad/s).	122
5.20	Tracking errors using the saturation controller when there are three targets and $\epsilon_{\omega_1} = \epsilon_{\omega_2} = 0.2$ (rad/s).	122
5.21	Reference and commanded velocities using the saturation controller when there are three targets and $\epsilon_{\omega_1} = \epsilon_{\omega_2} = 0.2$ (rad/s).	123

Chapter 1

Introduction

1.1 Motivation

In the last ten years, advances in networking and distributed computing have facilitated a paradigm shift from large, monolithic mainframe computers to networks of less expensive, less powerful workstations. One motivation for multi-agent systems is to achieve the same gains for mechanically controlled systems as has been gained in distributed computation. Rather than having a single monolithic (and therefore expensive and complicated) machine do everything, the hope is that many inexpensive, simple machines, can achieve the same, or enhanced functionality, through coordination. In essence, the objective is to replace expensive complicated hardware with software and multiple copies of simple hardware.

There are numerous applications for multi-agent systems including space-based interferometry, future autonomous combat systems, autonomous household appliances, enhanced surveillance systems, hazardous material handling systems, and active reconfigurable sensing systems. The objective of our research in multi-agent coordination is to facilitate a similar paradigm shift from large, monolithic vehicles (e.g., spacecraft, robots, unmanned air vehicles, autonomous underwater vehicles etc.) to groups of smaller, less expensive vehicles that coordinate their action to achieve their objective. Examples include replacing large space-based telescopes with multiple spacecraft interferometers, search and rescue missions with air, land and sea vehicles, and mine detection operations.

The cooperative control problems for multi-agent systems can be categorized as either formation control problems with applications to mobile robots [1, 2, 3, 4, 5, 6],

unmanned air vehicles (UAVs) [7], autonomous underwater vehicles (AUVs) [8], satellites [9, 10], aircraft [11], spacecraft [12, 13, 14, 15], and automated highway systems [16], or non-formation control problems such as task assignment [17, 18], cooperative transport [19, 20, 21], cooperative role assignment [22], air traffic control [23], cooperative timing [24, 25], and cooperative search [26]. The cooperative control of multi-agent systems poses significant theoretical and practical challenges. For cooperative control strategies to be successful, numerous issues must be addressed. We will consider three important and correlated issues: consensus seeking, formation keeping, and trajectory tracking.

The study of information flow and interaction among multiple agents in a group plays an important role in understanding the coordinated movements of these agents. For cooperative control strategies to be effective, a team of vehicles must be able to respond to unanticipated situations or changes in the environment that are sensed as a cooperative task is carried out. As the environment changes, the vehicles on the team must be in agreement as to what changes took place. A direct consequence of the assumption that shared information is a necessary condition for coordination is that cooperation requires that the group of agents reach a consensus on the coordination data. In other words, the instantiation of the coordination data on each agent must asymptotically approach a sufficiently common value.

The study of formation keeping is motivated by the obvious advantages achieved by using formations of multiple vehicles to accomplish an objective. These include increased feasibility, accuracy, robustness, flexibility, cost and energy efficiency, and probability of success. For example, the probability of success will be improved if multiple vehicles are used to carry out a mission in a coordinated manner, e.g. multiple UAVs are assigned to a certain target [27] or multiple AUVs are used to search for an underwater object [8]. In addition, cost and energy efficiency may be maximized if multiple agents can coordinate their movements in a certain way, e.g. multiple aircraft flying in a V-shape formation to maximize fuel efficiency. Furthermore, in spacecraft interferometry applications in deep space, using formations of multiple microspacecraft instead of a monolithic spacecraft can reduce the mission cost and improve system robustness and accuracy [28].

The study of nonlinear tracking control techniques for vehicle systems with input constraints is essential for the success of cooperative timing (see e.g. [29, 27]) and formation keeping missions (see e.g. [15]). While control systems are needed to enhance performance, increase operational speeds, and reduce costs in many areas of modern technology, current control system design tools are mostly limited to systems modeled by linear dynamics. As engineers push the limits of technology, it is becoming necessary to consider inherent nonlinearities in the system. Unfortunately there are few design tools for vehicle systems with inherent nonlinear dynamics. This motivates the research of a new approach to constructive nonlinear control design called “satisficing control” [30]. Meanwhile, the study of the satisficing control paradigm in turn facilitates the design of nonlinear tracking controllers for vehicle systems subject to polytopic input constraints.

1.2 Contributions

1.2.1 Multi-agent Consensus Seeking

We investigate algorithms so that a team of vehicles can reach consensus on the values of the coordination data in the presence of (i) imperfect sensors, (ii) communication dropout, (iii) sparse communication topologies, and (iv) noisy and unreliable communication links. A necessary and sufficient condition is shown for consensus seeking under fixed communication topologies to answer the question of “With whom does the communication take place?” and explore the minimum requirement to achieve consensus in multiple vehicle systems [31]. Discrete-time and continuous-time consensus protocols as well as necessary/sufficient conditions are also given for consensus of information under dynamically switching interaction topologies due to limited and unreliable information exchange [32, 33]. The consensus seeking problem is also considered when the information state of each vehicle is driven by exogenous input and random noise [34].

One feature of this dissertation in this area is that unidirectional information exchange is allowed instead of requiring bidirectional information exchange (e.g. [35]). This will be important in applications where bidirectional communication or sensing are not available. Another feature is that dynamic consensus problems are studied for time-varying

information states and an analysis about the final consensus equilibrium is performed. Furthermore, we extend some results of the Perron-Frobenius theorem in matrix theory and some properties of the Laplacian matrix in graph theory.

1.2.2 Multi-agent Formation Keeping

We apply a so-called “virtual structure” approach to treat the entire desired formation as a single entity with place-holders corresponding to each vehicle embedded in the virtual structure to represent the desired position and orientation for each vehicle. As the entire desired formation evolves in time, the place-holders trace out trajectories corresponding to each vehicle’s desired states. As a result, single vehicle path planning and trajectory generation techniques can be employed for the virtual structure while trajectory tracking strategies can be employed for each vehicle.

Regarding actuator saturation and internal and external disturbances to each vehicle, an idea of introducing formation feedback from each vehicle to the virtual structure is also proposed in the context of spacecraft formation flying to improve group stability and robustness [36, 37]. In the case when a large number of vehicles are involved in the group and stringent inter-vehicle communication limitations are exerted, a decentralized framework is proposed, where a local copy of the coordination vector is instantiated on each vehicle and brought into consensus through low-bandwidth communication between neighboring vehicles using a bidirectional ring topology [38, 39]. The proposed framework can achieve the following characteristics: First, formation feedback is included in the framework to improve group robustness. Second, the group maneuvers are easy to prescribe and direct in the framework. Finally, the framework guarantees high precision for maintaining the formation during maneuvers.

Under the virtual leader / virtual structure framework, a constructive approach based on the satisficing control paradigm is applied to multi-agent formation maneuvers. This approach generates a group of control laws that guarantee bounded formation-keeping error, finite completion time, and reasonable formation velocity as well as inverse optimality and desirable stability margins [40]. This technique is applied to multiple robot coordination in an experimental study.

1.2.3 Trajectory Tracking with Input Constraints

We extend the satisficing control paradigm [30] to the case of time-varying nonlinear systems with input constraints and explore applications of the approach to trajectory tracking for nonholonomic mobile robots [41] and unmanned air vehicles [42, 43, 44, 45] subject to velocity and heading rate constraints. In addition, a similar idea can be applied to multi-agent coordinated control [40] and human interaction schemes [46] to guarantee stability.

The design methodology as applied to nonlinear systems with polytopic input constraints can be summarized as follows: If a constrained control Lyapunov function can be found for a system with polytopic input constraints, the feasible control set that defines all the stabilizing controls with respect to the control Lyapunov function satisfying the input constraints can be specified accordingly. A direct parametrization of this feasible control set or selection from this feasible control set is applicable, e.g. finding the geometric mean of the feasible control set or a parametrization based on the vertices of the feasible control set (a polygon in this case).

The salient features of our approach are as follows. First, under the proposed tracking CLF framework with input constraints, we allow the reference velocity and angular velocity to be piecewise continuous while other approaches to tracking control constrain them to be uniformly continuous in order to apply Barbalat's lemma. Second, using different selection schemes, our approach can be used to derive a variety of other trajectory tracking strategies. Finally, it is computationally simple and can be implemented with a low-cost, low-power microcontroller.

1.3 Organization

The remainder of this dissertation is organized as follows. In Chapter 2, we review the relevant literature. In Chapter 3, we propose consensus algorithms and show necessary and/or sufficient conditions for consensus of information under fixed and switching interaction topologies. In Chapter 4, we address the problem of formation keeping in the context of multiple spacecraft formation flying and multi-robot coordination respectively. In Chapter 5, we present a control Lyapunov function approach to unmanned air vehicle

trajectory tracking with input constraints and demonstrate an experimental study of saturated trajectory tracking control for a nonholonomic mobile robot. In Chapter 6, we offer our concluding remarks.

Chapter 2

Literature Review

2.1 Consensus Seeking

Distributed control of multi-agent systems has received significant attention in recent years (c.f. [47, 48, 49, 50]). In some applications of distributed multi-agent systems, shared information plays a central role and facilitates the coordination of the group. As a result, a critical problem for coordinated control is to design appropriate protocols and algorithms so that the group of agents can converge to a consistent view of the shared information in the presence of limited and unreliable information exchange and dynamically changing interaction topologies.

Convergence to a common value is called the consensus or agreement problem in the literature. Consensus problems have a history in the computer science literature (see e.g. [51] and have recently found applications in cooperative control of multi-agent systems [52, 53, 35, 54, 55, 56, 57, 58, 59, 31, 32].

One avenue of the research in consensus seeking relies on algebraic graph theory, in which graph topologies are connected with the algebraic properties of the corresponding graph matrices. In [52] information exchange techniques are studied to improve stability margins and formation performance for vehicle formations. In [35], sufficient conditions are given for consensus of the heading angles of a group of agents under undirected switching interaction topologies. In [55], average consensus problems are solved for a network of integrators using directed graphs. Using directed graphs, Ref. [31] and [32] show necessary and/or sufficient conditions for consensus of information under time-invariant and switching interaction topologies respectively.

Meanwhile, some other researchers make use of nonlinear tools to study consensus problems. In [56], a set-valued Lyapunov approach is used to consider consensus problems with unidirectional time-dependent communication links. In [60, 61], nonlinear contraction theory is used to study synchronization and schooling applications, which are related to the consensus problem.

Optimality issues related to consensus problems are also studied in the literature. In [58], the fastest distributed linear averaging (FDLA) problem are addressed in the context of consensus seeking among multiple autonomous agents. In [62], the authors consider distributed consensus protocols that minimize a team objective function.

There is other research in the literature that is related to the consensus problem. In [63], the authors study the flocking phenomenon observed in Reynolds by constructing local control laws that allow a group of mobile agents to align their velocities, move with a common speed and achieve desired inter-agent distances while avoiding collisions with each other. In [64], the authors address some new directions for decentralized coordination with local interactions. In [65], the authors study connections between phase models of coupled oscillators and kinematic models of groups of self-propelled particles.

2.2 Formation Keeping

The concept of formation control has been studied extensively in the literature with application to the coordination of multiple robots [1, 2, 3, 66, 4, 5, 67, 52, 53, 68, 6], unmanned air vehicles (UAVs) [7], autonomous underwater vehicles (AUVs) [8], satellites [9, 10], aircraft [11], and spacecraft [12, 28, 13, 14, 69].

Various strategies and approaches have been proposed for formation control. These approaches can be roughly categorized as leader-following, behavioral, and virtual structure approaches, to name a few. In the leader-following approach, some agents are designated as leaders while others are designated as followers. The leaders track predefined trajectories, and the followers track transformed versions of the states of their nearest neighbors according to given schemes. In the behavioral approach, the control action for each agent is defined by a weighted average of the control corresponding to each desired behavior for the agent. In the virtual structure approach, the entire formation is treated as a

single rigid body. The virtual structure can evolve as a whole in a given direction with some given orientation and maintain a rigid geometric relationship among multiple agents. Similar ideas to the virtual structure approach include the perceptive reference frame proposed in [9] and the virtual leader proposed in [70].

There are numerous studies on the leader-following approach. In [1], nearest neighbor tracking strategies are used to control a fleet of autonomous mobile robots moving in formation. In [12], various schemes and explicit control laws for formation keeping and relative attitude alignment are derived for the coordination and control of multiple microspacecraft. While the leader-following approach is easy to understand and implement, there are limitations. For example, the leader is a single point of failure for the formation. In addition, there is no explicit feedback from the followers to the leader: if the follower is perturbed by some disturbances, the formation cannot be maintained.

As an alternative to leader-following, the virtual structure approach was proposed in [3] to acquire high precision formation control for mobile robots. In [15], the virtual structure approach is applied to the spacecraft interferometry problem, where formation maneuvers are easily prescribed but no formation feedback is included from spacecraft to the virtual structure. In [6], a Lyapunov formation function is used to define a formation error and formation feedback is incorporated to the virtual leaders through parameterized trajectories. In [71], the virtual structure approach is used to perform elementary formation maneuvers for mobile robots, where group feedback is incorporated from the followers to the virtual structure to improve group stability and robustness. Also in [36], following the idea of [71], formation feedback is applied to spacecraft formation flying scenario via the virtual structure approach. One advantage of the virtual structure approach is that it is easy to prescribe the behavior for the group. Another advantage is that the virtual structure approach can maintain tight formation during maneuvers. The main disadvantage of the current virtual structure implementation is that it is centralized, which results in a single point of failure for the whole system. Decentralization of the virtual structure approach is addressed in this dissertation.

The behavioral approach is a decentralized implementation and can achieve more flexibility, reliability, and robustness than centralized implementations. In [2], the behavioral approach is applied to formation keeping for mobile robots, where control strategies are derived by averaging several competing behaviors. In [72], several behavioral strategies are presented for formation maneuvers of groups of mobile robots, where a bidirectional ring topology is used to reduce the communication overhead for the whole system and formation patterns are also defined to achieve a sequence of maneuvers. In [73], the behavioral approach is used to maintain attitude alignment among a group of spacecraft. An advantage of the behavioral approach is that explicit formation feedback is included through the communication between neighbors. Unfortunately, the behavioral approach is hard to analyze mathematically. Based on the way the formation patterns are defined in [72], the behavioral approach has limited application in directing rotational maneuvers for the group. In addition, the behavioral approach has limited ability for precise formation keeping, that is, the group cannot maintain accurate formation during maneuvers.

2.3 Trajectory Tracking

The stabilization and tracking of dynamical systems with nonholonomic constraints has received recent attention in the literature. Ref. [74] provides a nice overview of the developments in control of nonholonomic systems. An inherent challenge, identified by Brockett's well-known necessary condition for feedback stabilization [75], is that nonholonomic systems cannot be stabilized via smooth time-invariant state feedback. A simple but classical example of a nonholonomic system is a mobile robot which serves as an interesting topic for stabilization [76] and tracking [76, 77, 78, 79].

With unmanned air vehicles (UAVs) equipped with low-level altitude-hold, velocity-hold, and heading-hold autopilots, the resulting UAV/autopilot models are assumed to be first order for heading and Mach hold, and second order for altitude hold [80]. Therefore, the planar kinematic equations of motion for the UAV/autopilot models are similar to those of nonholonomic mobile robots. As a result, we will focus on reviewing some literature on mobile robot tracking control.

Current approaches to tracking control of mobile robots includes linear model [81, 82], sliding-mode [78], backstepping [83, 77, 79, 84], and passivity based approaches [85], to name a few. Ref. [78] proposes a robust tracking strategy for nonholonomic wheeled mobile robots using sliding modes. The approach asymptotically stabilizes the mobile robot to a desired trajectory and is robust to bounded external disturbances. In [77], a tracking control methodology using time-varying state feedback based on the backstepping technique is proposed for both a kinematic and simplified dynamic model of a two-degree-of-freedom mobile robot, where local and global tracking problems are solved under certain conditions. Using the backstepping technique and the LaSalle's invariance principle, [84] proposed a controller with saturation constraints which can simultaneously solve both the tracking and regulation problems of a unicycle-modelled mobile robot. With their approach, mobile robots can globally follow any path specified by a straight line, a circle, or a path approaching the origin using a single controller. Ref. [85] developed a model-based control design strategy via passivity and normalization approaches to deal with the problem of global stabilization and global tracking control for the kinematic model of a wheeled mobile robot in the presence of input saturations.

2.4 CLF and Satisficing Control

Control Lyapunov function (CLF) proposed in [86, 87] can be applied to generate stabilizing control laws. In [88], robust control Lyapunov functions are used to derive pointwise min-norm control laws, which are shown to be optimal with respect to some meaningful cost functionals. In [6], control Lyapunov functions are used to define a robot formation so that a constrained motion control problem of multiple systems is converted into a stabilization problem for one single system.

CLF-based satisficing control [30] evolved from the recently introduced notion of satisficing decision theory [89, 90, 91] which can be seen as a formal application of cost-benefit analysis to decision making problems. When combined with the global properties of CLFs, satisficing is a powerful design tool which conveniently parameterizes the entire class of continuous control laws which stabilize the closed-loop system with respect to a known CLF. Additionally, robust satisficing [30] parameterizes a large class of satisficing

controls which have the added benefit of desirable stability margins and which are inverse-optimal.

2.5 Constrained Control

Controller design for nonlinear systems subject to input constraints offers both practical significance and theoretical challenges. Two effective approaches for the design of nonlinear controllers are control Lyapunov functions (CLFs) [87, 86] and receding horizon control (RHC)/model predictive control (MPC), [92, 93]. Both approaches can be extended to find control laws for nonlinear systems subject to certain input constraints. In [94] and [95], constrained CLFs are applied to construct stabilizing universal formulas respectively for systems with control inputs bounded in a unit ball and systems with a scalar control input that is positive and/or bounded. Input constraints can also be incorporated into the MPC framework, which is known as the constrained MPC (see [93] and references therein). The issues limiting the utility of the RHC approach are its computation requirements and stability concerns.

Chapter 3

Consensus Seeking Under Fixed and Switching Interaction Topologies

3.1 Introduction

This chapter presents some new results on consensus seeking in distributed multiple vehicle cooperative control. The usefulness of cooperative control technologies will be greatly enhanced if we understand the fundamental issues inherent in all coordination problems. Toward this end, we offer the following, intuitively appealing, fundamental axiom:

Axiom 3.1.1 *Shared information is a necessary condition for coordination.*

In cooperative control problems, shared information may take the form of common objectives, common control algorithms, relative position information, or a world map. Underlying this axiom are two important questions: “What information should be shared?” and “With whom should information be shared?”

In every cooperative control problem, there must be an identifiable cooperation objective. To achieve the team objective, specific kernels of information must be shared among members of the team. Identification of the key pieces of information to be shared is a critical step in the formulation of a cooperative control solution. One approach is to collect the information that must be jointly shared to facilitate cooperation into a vector quantity called the *coordination variable* [96]. The coordination variable represents the minimal amount of information needed to effect a specific coordination objective.

Information necessary for cooperation may be shared in a variety of ways. For example, relative position sensors may enable vehicles to construct state information for

other vehicles [10], or knowledge may be communicated between vehicles using a wireless network [53], or joint knowledge might be pre-programmed into the vehicles before a mission begins [97].

For cooperative control strategies to be effective, a team of vehicles must be able to respond to unanticipated situations or changes in the environment that are sensed as a cooperative task is carried out. As the environment changes, the vehicles on the team must be in agreement as to what changes took place. A direct consequence of Axiom 3.1.1 is that cooperation requires that the group of agents reach a consensus on the coordination data. In other words, the instantiation of the coordination variable on each agent must asymptotically approach a sufficiently common value.

A critical problem for cooperative control is to determine algorithms so that a team of vehicles can reach consensus on the values of the coordination data in the presence of (i) imperfect sensors, (ii) communication dropout, (iii) sparse communication topologies, and (iv) noisy and unreliable communication links. The question of “With whom does communication take place?” is of great significance in seeking consensus among a team of vehicles. The focus of this chapter is on providing answers to this question.

In Section 3.2, we establish the notation and formally state the consensus seeking problem. Section 3.3 and 3.4 state some results on multi-agent consensus seeking for fixed and switching interaction topologies respectively.

3.2 Problem Statement

Let $\mathcal{A} = \{A_i | i \in \mathcal{I}\}$ be a set of n agents, where $\mathcal{I} = \{1, 2, \dots, n\}$. A directed graph \mathcal{G} will be used to model the interaction topology among these agents. In \mathcal{G} , the i th node represents the i th agent A_i and a directed edge from A_i to A_j denoted as (A_i, A_j) represents a unidirectional information exchange link from A_i to A_j , that is, agent j can receive or obtain information from agent i , $(i, j) \in \mathcal{I}$. If there is a directed edge from A_i to A_j , A_i is defined as the parent node and A_j is defined as the child node. The interaction topology may be dynamically changing, therefore let $\bar{\mathcal{G}} = \{\mathcal{G}_1, \mathcal{G}_2, \dots, \mathcal{G}_M\}$ denote the set of all possible directed interaction graphs defined for \mathcal{A} . In applications, the possible interaction topologies will likely be a subset of $\bar{\mathcal{G}}$. Obviously, $\bar{\mathcal{G}}$ has a finite number of

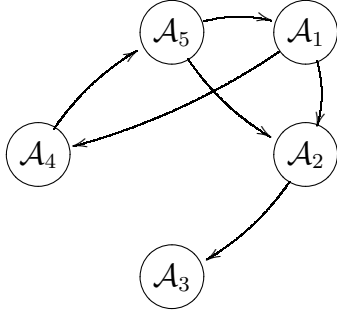


Figure 3.1: A graph that contains a spanning tree.

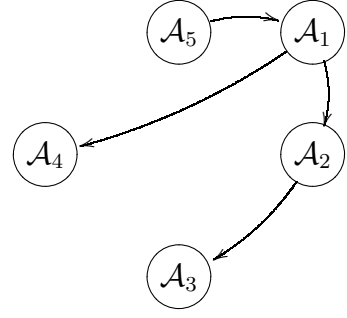


Figure 3.2: A spanning tree of the graph (Example 1).

elements. The union of a group of directed graphs $\{\mathcal{G}_{\ell_1}, \mathcal{G}_{\ell_2}, \dots, \mathcal{G}_{\ell_m}\} \subset \bar{\mathcal{G}}$ is a directed graph with nodes given by $A_i, i \in \mathcal{I}$ and edge set given by the union of the edge sets of \mathcal{G}_{ℓ_j} , where $\ell_j \in \{1, 2, \dots, M\}$.

A directed path in graph \mathcal{G} is a sequence of edges $(A_{k_1}, A_{k_2}), (A_{k_2}, A_{k_3}), (A_{k_3}, A_{k_4}), \dots$ in that graph, where $k_j \in \mathcal{I}$. Graph \mathcal{G} is called strongly connected if there is a directed path from A_i to A_j and A_j to A_i between any pair of distinct nodes A_i and $A_j, \forall (i, j) \in \mathcal{I}$. A directed tree is a directed graph, where every node, except the root, has exactly one parent. A spanning tree of a directed graph is a directed tree formed by graph edges that connect all the nodes of the graph (c.f. [98]). We say that a graph has (or contains) a spanning tree if a subset of the edges forms a spanning tree. Note that a spanning tree of a directed graph may not be unique. Fig. 3.1 shows an interaction graph between five agents, which contains a spanning tree as shown by Fig. 3.2. Two other spanning trees contained by the interaction graph are shown by Figs. 3.3 and 3.4 as an example to show that a spanning tree of a directed graph may not be unique.

Let $M_n(\mathbb{R})$ represent the set of all $n \times n$ real matrices. Given a matrix $A = [a_{ij}] \in M_n(\mathbb{R})$, the directed graph of A , denoted by $\Gamma(A)$, is the directed graph on n nodes $V_i, i \in \mathcal{I}$, such that there is a directed edge in $\Gamma(A)$ from V_j to V_i if and only if $a_{ij} \neq 0$ (c.f. [99]).

Let $\xi_i \in \mathbb{R}^p, i \in \mathcal{I}$, represent the i th information variable associated with the i th agent. Here each information variable represents an instantiation of the coordination

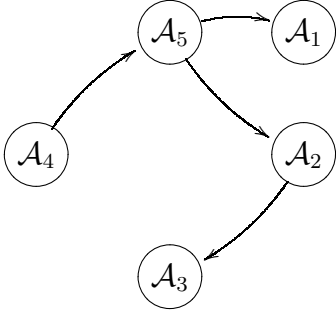


Figure 3.3: A spanning tree of the graph (Example 2).

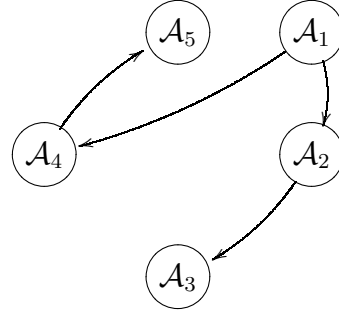


Figure 3.4: A spanning tree of the graph (Example 3).

data for the team. The set of agents \mathcal{A} is said to achieve consensus asymptotically if for any $\xi_i(0)$, $i \in \mathcal{I}$, $\|\xi_i(t) - \xi_j(t)\| \rightarrow 0$ as $t \rightarrow \infty$ for each $(i, j) \in \mathcal{I}$. In the sequel, we assume that the information variable ξ_i is a scalar for simplicity. However, all the results are valid for $\xi_i \in \mathbb{R}^p$.

Given T as the sampling period, we propose the following discrete-time consensus scheme:

$$\xi_i[k+1] = \frac{1}{\sum_{j=1}^n \alpha_{ij}[k]G_{ij}[k]} \sum_{j=1}^n \alpha_{ij}[k]G_{ij}[k]\xi_j[k], \quad (3.1)$$

where $k \in \{0, 1, 2, \dots\}$ is the discrete-time index, $(i, j) \in \mathcal{I}$, $\alpha_{ij}[k] > 0$ is a weighting factor, $G_{ii}[k] \triangleq 1$, and $G_{ij}[k]$ equals one if information flows from A_j to A_i at time $t = kT$ and zero otherwise, $\forall j \neq i$. Eq. (3.1) can be written in matrix form as

$$\xi[k+1] = D[k]\xi[k], \quad (3.2)$$

where $\xi = [\xi_1, \dots, \xi_n]^T$, $D = [d_{ij}]$, $(i, j) \in \mathcal{I}$, with $d_{ij} = \frac{\alpha_{ij}[k]G_{ij}[k]}{\sum_{j=1}^n \alpha_{ij}[k]G_{ij}[k]}$.

In addition, we propose the following continuous-time consensus scheme:

$$\dot{\xi}_i(t) = - \sum_{j=1}^n \sigma_{ij}(t)G_{ij}(t)(\xi_i(t) - \xi_j(t)), \quad (3.3)$$

where $(i, j) \in \mathcal{I}$, $\sigma_{ij}(t) > 0$ is the weighting factor, $G_{ii}(t) \triangleq 1$, and $G_{ij}(t)$ equals one if information flows from A_j to A_i at time t and zero otherwise, $\forall j \neq i$. Eq. (3.3) can be written in matrix form as

$$\dot{\xi}(t) = C(t)\xi(t), \quad (3.4)$$

where $C = [c_{ij}]$, $(i, j) \in \mathcal{I}$, with $c_{ii} = -\sum_{j \neq i} (\sigma_{ij}(t)G_{ij}(t))$ and $c_{ij} = \sigma_{ij}(t)G_{ij}(t)$, $j \neq i$.

Note that the interaction topology \mathcal{G} may be dynamically changing due to unreliable transmission or limited communication/sensing range. This implies that $G_{ij}[k]$ in Eq. (3.1) and $G_{ij}(t)$ in Eq. (3.3) may be time-varying. We use $\mathcal{G}[k]$ and $\mathcal{G}(t)$ to denote the dynamically changing interaction topologies corresponding to Eq. (3.1) and Eq. (3.3) respectively. We also allow the weighting factors $\alpha_{ij}[k]$ in Eq. (3.1) and $\sigma_{ij}(t)$ in Eq. (3.3) to be dynamically changing to represent possibly time-varying relative confidence of each agent's information variable or relative reliabilities of different information exchange links between agents. As a result, both matrix $D[k]$ in Eq. (3.1) and matrix $C(t)$ in Eq. (3.3) are dynamically changing over time.

Compared to the models in [35], we do not constrain the weighting factors $\alpha_{ij}[k]$ in Eq. (3.1) other than to require that they are positive. This provides needed flexibility for some applications. The Vicsek model and simplified Vicsek model used in [35] can be thought of as special cases of our discrete-time consensus scheme. If we let $\alpha_{ij}[k] \triangleq 1$ in Eq. (3.1), we obtain the Vicsek model. Also the simplified Vicsek model can be obtained if we let $\alpha_{ij}[k] \triangleq \frac{1}{g}$, $\forall j \neq i$, and $\alpha_{ii}[k] \triangleq 1 - \sum_{j \neq i} \frac{1}{g} G_{ij}[k]$, where $g > n$ is a constant. Compared to [57], where the interaction graph is assumed to be time-invariant and weighting factors σ_{ij} are specified a priori to be constant and equal to each other, we study continuous-time consensus schemes with dynamically changing interaction topologies and weighting factors. The continuous-time update rule in [35] can also be regarded as a special case of our continuous-time update scheme by letting $\sigma_{ij} \triangleq \frac{1}{n}$.

The main result of this chapter is that the update schemes (3.1) and (3.3) achieve asymptotic consensus for \mathcal{A} if the union of the collection of directed interaction graphs across some time intervals has a spanning tree frequently enough as the system evolves. Toward that end we have the following preliminary results.

Lemma 3.2.1 *The discrete update scheme (3.1) achieves asymptotic consensus for \mathcal{A} if and only if*

$$D[k-1]D[k-2]\cdots D[2]D[1]D[0] \rightarrow \mathbf{1}c^T \quad (3.5)$$

as $k \rightarrow \infty$, where $\mathbf{1}$ denotes the $n \times 1$ column vector with all the entries equal to 1, and c is an n vector of constant coefficients.

Proof: Note that the set of agents \mathcal{A} reaches consensus asymptotically if and only if the set

$$\mathcal{S} = \{\xi \in \mathbb{R}^n : \xi_1 = \xi_2 = \dots = \xi_n\},$$

is attractive and positively invariant.

Since

$$\xi[k] = D[k-1]D[k-2]\cdots D[1]D[0]\xi[0],$$

Eq. (3.5) implies that

$$\lim_{k \rightarrow \infty} \xi[k] = \mathbf{1}c^T \xi[0] = \begin{pmatrix} c^T \xi[0] \\ \vdots \\ c^T \xi[0] \end{pmatrix},$$

which implies that \mathcal{S} is attractive and positively invariant.

Conversely if \mathcal{S} is attractive and positively invariant, then

$$\lim_{k \rightarrow \infty} \xi[k] = \lim_{k \rightarrow \infty} D[k-1]D[k-2]\cdots D[1]D[0]\xi[0] = \mathbf{1}\alpha,$$

where α is a constant coefficient. Which in turn implies that

$$\lim_{k \rightarrow \infty} D[k-1]D[k-2]\cdots D[1]D[0] = \mathbf{1}c^T. \quad \blacksquare$$

Lemma 3.2.2 *The continuous update scheme (3.3) achieves asymptotic consensus for \mathcal{A} if and only if*

$$\Phi(t, 0) = I + \int_0^t C(\sigma_1) d\sigma_1 + \int_0^t C(\sigma_1) \int_0^{\sigma_1} C(\sigma_2) d\sigma_2 d\sigma_1 + \cdots \rightarrow \mathbf{1}c^T \quad (3.6)$$

as $t \rightarrow \infty$.

Proof: Noting that $\xi(t) = \Phi(t, 0)\xi(0)$, the proof is similar to that of Lemma 3.2.1. \blacksquare

3.3 Consensus Under Fixed Interaction Topologies

In this section, we assume that the graph \mathcal{G} is time-invariant and weighting factors in Eqs. (3.1) and (3.3) are constant. That is, matrix D and C in Eqs. (3.2) and (3.4) are constant. We will derive necessary and sufficient conditions for consensus of information using both the discrete-time and continuous-time update schemes.

3.3.1 Consensus Using Continuous-Time Update Scheme

In this section, we first consider the case when the information variable is inherently constant. We then consider the case when the information variable is dynamically evolving in time. This is the case, for example, in formation control problems where the information variable is the dynamic state of a virtual leader.

Static Consensus

Before moving on, we need the following definitions from matrix theory (c.f. [99]). Let I_n denote the $n \times n$ identity matrix. A matrix $A = [a_{ij}] \in M_n(\mathbb{R})$ is nonnegative, denoted as $A \geq 0$, if all its entries are nonnegative. Furthermore, if all its row sums are +1, A is said to be a (row) stochastic matrix.

We need the following lemma to derive our main results.

Lemma 3.3.1 *Given a matrix $A = [a_{ij}] \in M_n(\mathbb{R})$, where $a_{ii} \leq 0$, $a_{ij} \geq 0$, $\forall i \neq j$, and $\sum_{j=1}^n a_{ij} = 0$ for each i , then A has at least one zero eigenvalue and all of the non-zero eigenvalues are in the open left half plane. Furthermore, A has exactly one zero eigenvalue if and only if the directed graph associated with A has a spanning tree.*

Proof:

For the first statement, note that A is diagonally dominant, has zero row sum, and non-positive diagonal elements. Therefore, from the Gersgorin disc theorem (c.f. [99]), A has at least one zero eigenvalue and all the other non-zero eigenvalues are in the open left half plane.

The second statement will be shown using an induction argument.

(Sufficiency.) *Step 1.* The first step is to show that A has exactly one zero eigenvalue if the directed graph associated with A is itself a spanning tree.

Noting that the graph associated with A is a spanning tree, renumber the agents consecutively by depth in the spanning tree, with the root numbered as agent A_1 . In other words, children of A_1 are numbered A_2 to A_{q_1} , children of A_2 to A_{q_1} are labelled A_{q_1+1} to A_{q_2} and so on. Note that the associated matrix A is lower diagonal with only one diagonal entry equal to zero [57].

Step 2. Let $Q = [q_{ij}] \in M_n(\mathbb{R})$, where $q_{ii} \leq 0$, $q_{ij} \geq 0$, $\forall i \neq j$, and $\sum_{j=1}^n q_{ij} = 0$ for each j . Let $S = [s_{ij}] \in M_n(\mathbb{R})$ satisfy the similar properties to those of matrix Q . Also let \mathcal{G}_1 and \mathcal{G}_2 be the interaction graphs associated with Q and S respectively. We assume that $s_{\ell\ell} = q_{\ell\ell} - \sigma_{\ell m}$, $s_{\ell m} = q_{\ell m} + \sigma_{\ell m}$, and $s_{ij} = q_{ij}$ otherwise, where $\sigma_{\ell m} > 0$ denotes the weighting factor for the information link from agent m to agent ℓ , $m \neq \ell$. That is, \mathcal{G}_2 corresponds to an interaction graph where one more directed link from node m to node ℓ is added to graph \mathcal{G}_1 , where $m \neq \ell$. Denote $p_Q(t) = \det(tI - Q)$ and $p_S(t) = \det(tI - S)$ as the characteristic polynomial of Q and S respectively. Let $Q_t = tI - Q$ and $S_t = tI - S$. Given any matrix M , denote $M([i, j])$ as the sub-matrix of M formed by deleting the i^{th} row and j^{th} column.

Next, we will show that if matrix Q has exactly one zero eigenvalue, then so does matrix S . Without loss of generality, we assume that the new directed information link added to graph \mathcal{G}_1 is from node m to node 1, where $m \neq 1$, for simplicity since we can always renumber node ℓ as node 1.

Obviously matrix S has at least one zero eigenvalue and all the other non-zero eigenvalues are in the open left half plane following the first statement of this Lemma. Below we will show that S has only one zero eigenvalue.

Assume that $Q_t = [q_{tij}]$, and $S_t = [s_{tij}]$, $(i, j) \in \mathcal{I}$. Accordingly, it can be seen that $s_{t11} = t - s_{11} = t - q_{11} + \sigma_{1m} = q_{t11} + \sigma_{1m}$, $s_{t1m} = -s_{1m} = -q_{1m} - \sigma_{1m} = q_{t1m} - \sigma_{1m}$, and $s_{tij} = q_{tij}$ otherwise. Also note that $\det S_t([1, j]) = \det Q_t([1, j])$, $j \in \mathcal{I}$. Then we

know that

$$\begin{aligned}
\det S_t &= \sum_{j=1}^n (-1)^{1+j} s_{t1j} \det S_t([1, j]) \\
&= \sum_{j=1}^n (-1)^{1+j} q_{t1j} \det S_t([1, j]) \\
&\quad + \sigma_{1m} \det S_t([1, 1]) - (-1)^{1+m} \sigma_{1m} \det S_t([1, m]) \\
&= \det Q_t + \sigma_{1m} (\det S_t([1, 1]) + (-1)^m \det S_t([1, m])).
\end{aligned}$$

Consider a matrix $E = [e_{ij}]$, $(i, j) = 1, \dots, n-1$, given by adding $[s_{21}, s_{31}, \dots, s_{n1}]^T$ to the $(m-1)^{\text{th}}$ column of matrix $S([1, 1])$. Matrix E can be denoted as

$$E = \begin{bmatrix} s_{22} & s_{23} & \cdots & s_{2m} + s_{21} & \cdots & s_{2n} \\ s_{32} & s_{33} & \cdots & s_{3m} + s_{31} & \cdots & s_{3n} \\ \vdots & \vdots & \vdots & \ddots & \vdots & \vdots \\ s_{n2} & s_{n3} & \cdots & s_{nm} + s_{n1} & \cdots & s_{nn} \end{bmatrix}.$$

Thus $e_{i(m-1)} = s_{(i+1)m} + s_{(i+1)1}$, $i = 1, \dots, n-1$. Using the properties of determinants, it can be verified that

$$\det(tI - E) = \det S_t([1, 1]) + (-1)^m \det S_t([1, m]).$$

Obviously matrix E has zero row sum and nonpositive diagonal elements. Also matrix E is diagonally dominant. From the Gersgorin disc theorem, we know that E has at least one zero eigenvalue and all the other non-zero eigenvalues are on the open left half plane. As a result, the Routh stability criterion implies that the characteristic polynomial of E denoted as $\det(tI - E)$ has a nonnegative coefficient in the first power of t . We also know that matrix Q has a positive coefficient for the first power of t in its characteristic polynomial $\det Q_t$ since Q has exactly one zero eigenvalue and all the others are in the open left half plane.

Noting that $\det S_t = \det Q_t + \sigma_{1m} \det(tI - E)$, it is obvious that S has a positive coefficient for the first power of t . Therefore, S can only have one zero eigenvalue.

Step 3. If graph \mathcal{G} associated with A is itself a spanning tree, we know that A has exactly one zero eigenvalue from Step 1. If not, graph \mathcal{G} can be constructed by

consecutively adding information links to the spanning tree. Step 2 implies that adding one additional information link to the spanning tree results in an associated matrix that also has exactly one zero eigenvalue. We can recursively add additional information links, where Step 2 implies that the matrix associated with the new graph has exactly one zero eigenvalue, until we obtain the graph \mathcal{G} . By induction, we know that A has exactly one zero eigenvalue if graph \mathcal{G} has a spanning tree.

(Necessity.) If graph \mathcal{G} does not have a spanning tree, then there exist at least two separate subgroups or at least two agents in the group who do not receive any information. For the first case, there is no information exchange between these subgroups and matrix A can be written as block diagonal form by renumbering these agents based on their subgroup. It is straightforward to see that each block has at least one zero eigenvalue. Therefore, A has at least two zero eigenvalues. For the second case, A has at least two zero rows, which implies that A has at least two zero eigenvalues. ■

Corollary 3.3.1 *The Laplacian matrix of a graph has a simple zero eigenvalue if and only if the graph has a spanning tree.*

Proof: If we multiply the Laplacian matrix by -1, we get a matrix satisfying the properties defined in Lemma 3.3.1. ■

Next, we will show that the group of vehicles \mathcal{A} reach consensus asymptotically using the update scheme (3.3) if matrix C in Eq. (3.4) has exactly one zero eigenvalue and all the others are in the open left half plane. The following result also computes the value of the information variable that is reached through the consensus process.

Lemma 3.3.2 *If C is given by Eq. (3.4), then e^{Ct} , $\forall t > 0$, is a stochastic matrix with positive diagonal entries. Furthermore, if C has exactly one zero eigenvalue, then $e^{Ct} \rightarrow \mathbf{1}\nu^T$ and $\xi_i(t) \rightarrow \sum_{i=1}^n (\nu_i \xi_i(0))$ as $t \rightarrow \infty$, where $\mathbf{1} = [1, \dots, 1]_{n \times 1}^T$, $\nu = [\nu_1, \dots, \nu_n]^T \geq 0$, and $\sum_{i=1}^n \nu_i = 1$.*

Proof: Given eigenvalues $\lambda_i \in \sigma(C)$ with eigenvectors z_i , $i = 1, \dots, n$, where $\sigma(A)$ represents the spectrum of A , we know that $e^{\lambda_i t} \in \sigma(e^{Ct})$ with the same eigenvectors as C (c.f. [99]). Noting that C has a zero eigenvalue with an associated eigenvector given by $\mathbf{1}$,

then e^{Ct} has an eigenvalue 1 with the same eigenvector $\mathbf{1}$. Thus we know that $e^{Ct}\mathbf{1} = \mathbf{1}$, which implies that e^{Ct} always has row sum equal to 1. Also note that C can be written as the sum of a nonnegative matrix M and $-\beta I_n$, where β is the maximum absolute value of the diagonal entries of C . We can see that $e^{Ct} = e^{-\beta t}e^{Mt}$, which is obviously nonnegative and has positive diagonal entries. As a result, $e^{Ct}, \forall t > 0$, is a stochastic matrix with positive diagonal entries.

Furthermore, if C has exactly one zero eigenvalue, then e^{Ct} has exactly one eigenvalue equal to 1 and all the other eigenvalues have modulus less than 1. Let $J = [j_{ml}]$, $(m, l) = 1, \dots, n$, be the Jordan matrix corresponding to matrix C , then $j_{mm} = \lambda_m$. Without loss of generality, assume that $\lambda_n = 0$ and λ_m is on the open left half plane, $m = 1, \dots, n - 1$.

Let $C = PJP^{-1}$, where $P = [p_1, \dots, p_n]$ is an $n \times n$ matrix. Note that p_n can correspond to an eigenvector associated with eigenvalue $\lambda_n = 0$. Without loss of generality, choose $p_n = \mathbf{1}$ as the eigenvector.

We know that $e^{Ct} = Pe^{Jt}P^{-1}$. It can be verified that

$$e^{Jt} \rightarrow \begin{bmatrix} 0 & 0 & \cdots & 0 \\ \vdots & \vdots & \ddots & \vdots \\ 0 & 0 & \cdots & 0 \\ 0 & 0 & \cdots & 1 \end{bmatrix}$$

as $t \rightarrow \infty$ from the property of C (c.f. [99]). After some manipulation, we know that $e^{Ct} \rightarrow \mathbf{1}\nu^T$ as $t \rightarrow \infty$, where $\nu_i, i = 1, \dots, n$, corresponds to the last row of matrix P^{-1} . The result $\sum_{i=1}^n \nu_i = 1$ comes from the fact that e^{Ct} has row sum equal to 1 for any t .

We also need to show that $\nu \geq 0$. Now consider matrix $e^{Ck}, k = 0, 1, 2, \dots$. Obviously e^{Ck} should also approach to $\mathbf{1}\nu^T$ as $k \rightarrow \infty$. From Lemma 8.2.7 in [99], ν should be an eigenvector of matrix $(e^C)^T$ associated with the simple eigenvalue 1. From Theorem 8.3.1 in [99], $(e^C)^T$ has a nonnegative eigenvector $x \geq 0$ associated with the simple eigenvalue 1. Thus it can be seen that $\nu = \alpha x$ for some $\alpha \neq 0$. Since $\sum_{i=1}^n \nu_i = 1$, it must be true that $\alpha > 0$, which implies that $\nu \geq 0$.

The solution to Eq. (3.4) is given by $\xi(t) = e^{Ct}\xi(0)$. Therefore, it is obvious that $\xi_i(t) \rightarrow \sum_{i=1}^n (\nu_i \xi_i(0)), i = 1, \dots, n$, as $t \rightarrow \infty$. ■

Note that if we replace matrix C with γC in Eq. (3.4), where $\gamma > 0$, we can increase consensus speed by increasing γ . The solution to Eq. (3.4) with this new matrix is given by $\xi = e^{\gamma C t} \xi(0) = e^{C(\gamma t)} \xi(0)$, which converges faster than the original solution if we choose $\gamma > 1$.

Ref. [57] shows that the group of agents \mathcal{A} is consensus reachable if and only if the associated interaction graph \mathcal{G} has a spanning tree. The proof for this claim in [57] is constructive in that the linear update law is based on a communication graph which is the spanning tree of \mathcal{G} . Of course, there may exist other connections in graph \mathcal{G} which are ignored. Ref. [57] only partially answers the question of whether the update law (3.3) accounting for all existing connections achieves consensus asymptotically. The next result provides a complete answer.

Theorem 3.3.2 *The consensus strategy (3.3), achieves consensus asymptotically for \mathcal{A} if and only if the associated (static) interaction graph \mathcal{G} has a spanning tree.*

Proof: (Sufficiency.) Obviously matrix C in Eq. (3.4) associated with graph \mathcal{G} has the same properties as matrix A in Lemma 3.3.1. The fact that graph \mathcal{G} has a spanning tree implies that the directed graph of matrix C has a spanning tree. Therefore, we know that matrix C has exactly one zero eigenvalue and all the others are in the open left half plane. As a result, we know that the update law (3.3) achieves consensus asymptotically for \mathcal{A} according to Lemma 3.3.2.

(Necessity.) Suppose that the consensus strategy (3.3) achieves consensus asymptotically for \mathcal{A} but that \mathcal{G} does not have a spanning tree. Then there exist at least two agents A_i and A_j such that there is no path in \mathcal{G} that contains both A_i and A_j . Therefore it is impossible to bring data between these two agents into consensus which implies that consensus cannot be achieved asymptotically for \mathcal{A} [57]. ■

Note that the linear update law (3.3) only achieves consensus for constant coordination variables, which may not be suitable for applications where the coordination variable evolves dynamically. For example, in the context of leader-following approaches (c.f. [38]), the group leader's trajectory can act as the coordination variable for the whole group.

Dynamic Consensus

Suppose that the information variable on each vehicle is driven by the same time-varying input $u(t)$, which might represent an *a priori* known feedforward signal. The associated consensus scheme is given by

$$\dot{\xi}_i = - \sum_{j=1}^n k_{ij} G_{ji} (\xi_i - \xi_j) + u(t), \quad i = 1, \dots, n. \quad (3.7)$$

Eq. (3.7) can also be written in matrix form as

$$\dot{\xi} = C\xi + Bu(t), \quad (3.8)$$

where C is the matrix associated with graph \mathcal{G} and $B = [1, \dots, 1]^T$. We have the following theorem regarding consensus of the information variables $\xi_i, i = 1, \dots, n$.

Theorem 3.3.3 *The consensus strategy (3.8) achieves consensus asymptotically for \mathcal{A} if and only if the associated interaction graph \mathcal{G} has a spanning tree. Furthermore the information variables satisfy $\|\xi_i(t) - \zeta(t)\| \rightarrow 0$ as $t \rightarrow \infty$, where $\zeta(t)$ is the solution of*

$$\dot{\zeta} = u(t), \quad \zeta(0) = \mu,$$

where μB is equilibrium of the differential equation

$$\dot{\pi} = C\pi, \quad \pi(0) = \xi(0).$$

Proof: (Sufficiency.) The solution to Eq. (3.8) is given by $\xi(t) = \xi_s(t) + \xi_e(t)$, where $\xi_s(t) = e^{Ct}\xi(0)$ and $\xi_e(t) = \int_0^t e^{C(t-\tau)}Bu(\tau)d\tau$ (c.f. [100]). Note that ξ_s represents the zero input solution to Eq. (3.8), that is, solution to $\dot{\xi} = C\xi$. From Theorem 3.3.2, it is obvious that each component of ξ_s satisfies $\xi_{si}(t) \rightarrow \mu$ as $t \rightarrow \infty, i = 1, \dots, n$. Also note that ξ_e represents the zero state solution to Eq. (3.8). We know that $e^{C(t-\tau)}B = B$ since $e^{C(t-\tau)}$ always has row sum equal to 1. Therefore, it can be seen that each component of ξ_e satisfies $\xi_{ei} = \int_0^t u(\tau)d\tau, i = 1, \dots, n$. Combining ξ_s and ξ_e , gives $\|\xi_i(t) - \zeta(t)\| \rightarrow 0$ as $t \rightarrow \infty$.

(Necessity.) The necessary part follows directly from Theorem 3.3.2. ■

Equilibrium Points

We have shown that the linear consensus strategy (3.3) achieves consensus asymptotically for \mathcal{A} if the graph \mathcal{G} has a spanning tree. In addition, $\xi_i(t)$ will converge to $\sum_{i=1}^n (\nu_i \xi_i(0))$ as $t \rightarrow \infty$, where $\sum_{i=1}^n \nu_i = 1$ and $\nu_i \geq 0$. A natural question is whether each initial condition $\xi_i(0)$ will contribute to the final equilibrium point. In the following we provide a partial answer to this question. We assume that graph \mathcal{G} has a spanning tree in this section.

Observe that if there is a node A_k in \mathcal{G} without an incoming link (there is at most one such node in graph \mathcal{G} from Theorem 3.3.2), the linear update law corresponding to this node is given by $\dot{\xi}_k = 0$ from Eq. (3.3), which implies that $\xi_k(t) = \xi_k(0)$ for all t . Therefore, the other nodes must converge to $\xi_k(0)$ for any $k_{ij} > 0$. That is, $\nu_k = 1$ and $\nu_i = 0, \forall i \neq k$.

In general, the initial condition of a node contributes to the equilibrium value if and only if the node has a directed path to all the other nodes in \mathcal{G} . Thus $\nu_i \neq 0$ for any node which has directed paths to all the other nodes in \mathcal{G} and $\nu_i = 0$ otherwise. As a special case, the initial condition of each node in a graph contributes to the final equilibrium point if and only if the graph is strongly connected. The above argument can be explained as follows. If there is no path from node j to node m in \mathcal{G} , it is impossible for $\xi_m(t)$ to be influenced by $\xi_j(0)$. On the other hand, if there is a path from node j to every other node in \mathcal{G} , then $\xi_i(t), \forall i \neq j$, will be influenced by $\xi_j(0)$.

The fact that $\nu_i \geq 0, i = 1, \dots, n$ can also be explained from the following perspective. Assume that $\nu_\ell < 0$ for some ℓ . Consider the case $\xi_\ell(0) > 0$ and $\xi_i(0) = 0, \forall i \neq \ell$. We know that $\xi_i(t)$ will converge to $\sum_{i=1}^n (\nu_i \xi_i(0)) = \nu_\ell \xi_\ell(0)$, which is negative. Following the update law (3.3), $\dot{\xi}_\ell(0) < 0$ if there is any incoming link to A_ℓ and $\dot{\xi}_\ell(0) = 0$ otherwise. In the first situation, $\xi_\ell(t)$ will decrease and $\xi_i(t), \forall i \neq \ell$ cannot decrease since $\dot{\xi}_i(0) \geq 0$, which implies that $\xi_i(t)$ will be synchronized to a value c with $0 \leq c < \xi_\ell(0)$. In the second situation, $\xi_i(t)$ will be synchronized to $\xi_\ell(0)$. Both cases are contradictory to the above result. Therefore, $\nu_i \geq 0, i = 1, \dots, n$.

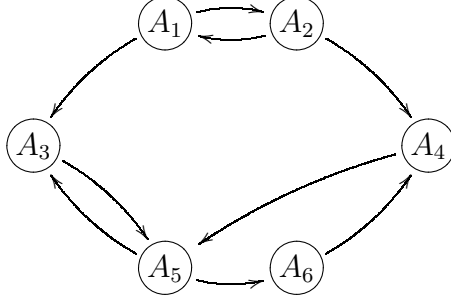


Figure 3.5: Communication topology.

Illustrative Example

In this section, we consider a scenario where six vehicles are to rendezvous at a position along a parameterized trajectory represented by $(r_x(\tau(t)), r_y(s(t)))$. Fig. 3.5 shows the corresponding communication links between these vehicles. Note the existence of a spanning tree.

It is assumed that each vehicle knows the parameterized trajectory. Therefore the parameters τ and s therefore represent the minimum information needed to achieve the coordination objective: i.e., τ and s are the coordination variables. We will instantiate τ and s on each vehicle as τ_i and s_i , $i = 1, \dots, 6$. Here we let $\xi_i = [\tau_i, s_i]^T$, $i = 1, \dots, 6$.

Based on the communication topology shown in Fig. 3.5, the matrix C is given by

$$C = \gamma \begin{bmatrix} -1.5 & 1.5 & 0 & 0 & 0 & 0 \\ 2 & -2 & 0 & 0 & 0 & 0 \\ 0.9 & 0 & -2.8 & 0 & 1.9 & 0 \\ 0 & 1.2 & 0 & -2.5 & 0 & 1.3 \\ 0 & 0 & 1.4 & 1.8 & -3.2 & 0 \\ 0 & 0 & 0 & 0 & 0.7 & -0.7 \end{bmatrix} \otimes I_2,$$

where $\gamma > 0$ is a coefficient, \otimes denotes the Kronecker product, and $k_{ij} > 0$, $(i, j) = 1, \dots, 6$, is chosen arbitrarily. The initial conditions for each instantiation of τ and s are given by $\tau_i = 0.2i - 0.1$ and $s_i = 0.2i$, $i = 1, \dots, 6$.

Fig. 3.6 shows the consensus scenario using update law (3.4) for $\gamma = 1$ and $\gamma = 5$ respectively. We can see that only the initial conditions of A_1 and A_2 affect the

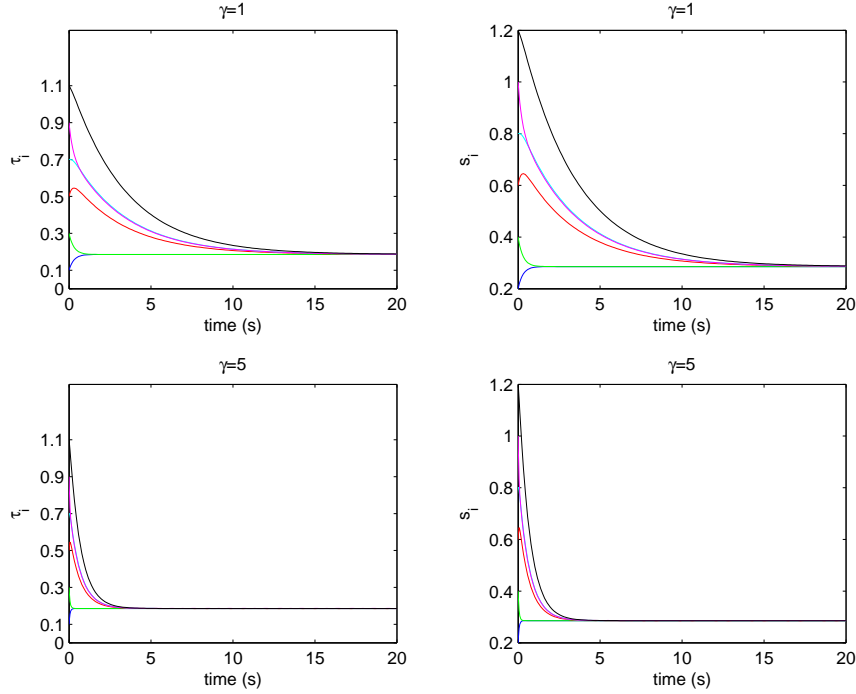


Figure 3.6: Consensus of τ_i and s_i using update law (3.4).

equilibrium value, which is consistent with the communication graph shown in Fig. 3.5, where it can be seen that only A_1 and A_2 have a directed path to all the other nodes. Fig. 3.7 shows the same consensus scenario corresponding to the communication graph formed by deleting the link from A_2 to A_1 in Fig. 3.5. It can be seen that each instantiation of τ and s converges to $\tau_1(0)$ and $s_1(0)$ respectively.

Fig. 3.8 illustrates a dynamic consensus scenario using update law (3.8) for $\gamma = 1$ and $\gamma = 5$ respectively. The common predefined planning schemes for τ and s are given by $\dot{\tau} = \frac{1}{5} |\sin(t)|$ and $\dot{s} = \frac{1}{4} |\cos(t)|$ respectively. Here we let $u(t) = [\frac{1}{5} |\sin(t)|, \frac{1}{4} |\cos(t)|]^T$ in Eq. (3.8). It can be seen that consensus is achieved asymptotically and that both τ_i and s_i follow the appropriate trajectories.

3.3.2 Consensus Using Discrete-Time Update Scheme

Before moving on, we need the following definitions. A stochastic matrix P is called indecomposable and aperiodic (SIA) if $\lim_{n \rightarrow \infty} P^n = \mathbf{1}y^T$, where y is some column

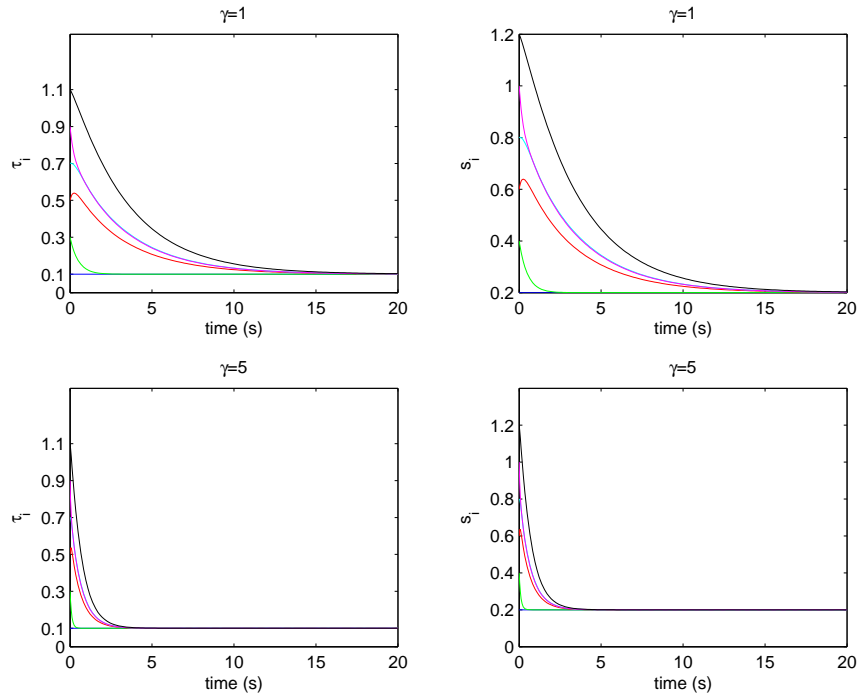


Figure 3.7: Consensus of τ_i and s_i without link from A_2 to A_1 using update law (3.4).

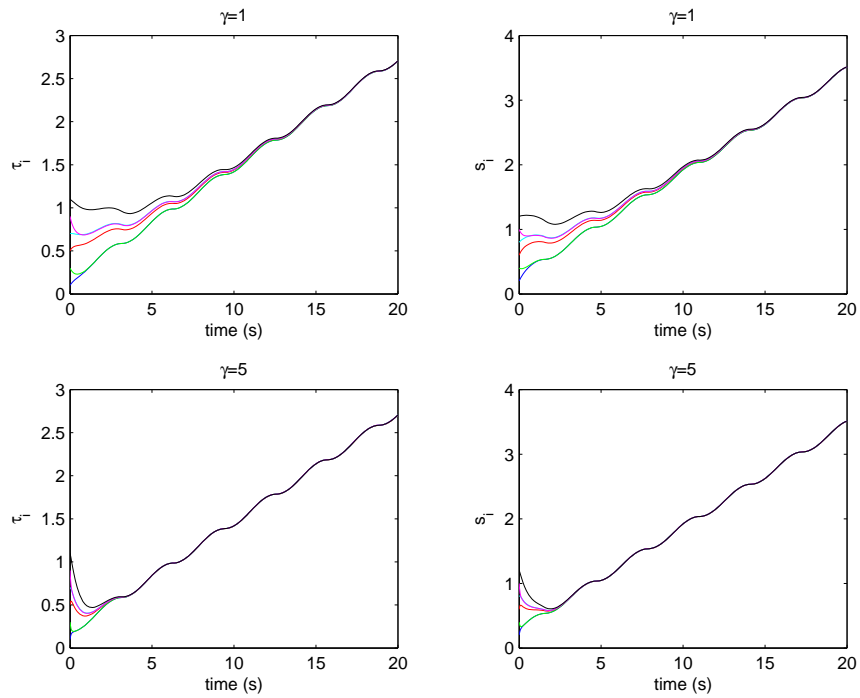


Figure 3.8: Consensus and evolution of τ_i and s_i using update law (3.8).

vector [101]. For nonnegative matrices, $A \geq B$ implies that $A - B$ is a nonnegative matrix. It is easy to verify that if $A \geq \rho B$, for some $\rho > 0$, and the directed graph of B has a spanning tree, then the directed graph of A has a spanning tree.

We need the following lemmas to derive our main results.

Lemma 3.3.3 *If a nonnegative matrix $A = [a_{ij}] \in M_n(\mathbb{R})$ has the same positive constant row sums given by $\mu > 0$, then μ is an eigenvalue of A with an associated eigenvector $\mathbf{1}$ and $\rho(A) = \mu$, where $\rho(\cdot)$ denotes the spectral radius. In addition, the eigenvalue μ of A has algebraic multiplicity equal to one, if and only if the graph associated with A has a spanning tree. Furthermore, if the graph associated with A has a spanning tree and $a_{ii} > 0$, then μ is the unique eigenvalue of maximum modulus.*

Proof: The first statement follows directly from the properties of nonnegative matrices (c.f. [99]).

For the second statement, we need to show both the necessary and sufficient conditions.

(Sufficiency.) If the graph associated with A has a spanning tree, then the graph associated with $B = A - \mu I_n$ also has a spanning tree. We know that $\lambda_i(A) = \lambda_i(B) + \mu$, where $i = 1, \dots, n$, and $\lambda_i(\cdot)$ represents the i^{th} eigenvalue. Noting that B satisfies the conditions in Lemma 3.3.1, we know that zero is an eigenvalue of B with algebraic multiplicity equal to one, which implies that μ is an eigenvalue of A with algebraic multiplicity equal to one.

(Necessity.) If the graph associated with A does not have a spanning tree, we know that $B = A - \mu I_n$ has more than one zero eigenvalue from Lemma 3.3.1, which in turn implies that A has more than one eigenvalue equal to μ .

For the third statement, the Gersgorin disc theorem [99] implies that all the eigenvalues of A are located in the union of the n discs given by

$$\bigcup_{i=1}^n \{z \in \mathbf{C} : |z - a_{ii}| \leq \sum_{j \neq i} |a_{ij}|\},$$

where \mathbf{C} is the set of complex numbers. Noting that $a_{ii} > 0$, it is easy to see that this union is included in a circle given by $\{z \in \mathbf{C} : |z| = \mu\}$ and the circular boundaries of the union

of n discs has only one intersection with the circle at $z = \mu$. Thus we know that $|\lambda| < \mu$ for every eigenvalue of A satisfying $\lambda \neq \mu$. Combining the second statement, we know that μ is the unique eigenvalue of maximum modulus. ■

Corollary 3.3.4 *A stochastic matrix has algebraic multiplicity equal to one for its eigenvalue $\lambda = 1$ if and only if the graph associated with the matrix has a spanning tree. Furthermore, a stochastic matrix with positive diagonal elements has the property that $|\lambda| < 1$ for every eigenvalue not equal to one.*

Lemma 3.3.4 *If $A \in M_n(\mathbb{R})$ and $A \geq 0$, then $\rho(A)$ is an eigenvalue of A and there is a nonnegative vector $x \geq 0$, $x \neq 0$, such that $Ax = \rho(A)x$.*

Proof: See Theorem 8.3.1 in [99]. ■

Lemma 3.3.5 *Let $A = [a_{ij}] \in M_n(\mathbb{R})$ be a stochastic matrix. If A has an eigenvalue $\lambda = 1$ with algebraic multiplicity equal to one, and all the other eigenvalues satisfy $|\lambda| < 1$, then A is SIA, that is, $\lim_{m \rightarrow \infty} A^m \rightarrow \mathbf{1}\nu^T$, where ν satisfies $A^T\nu = \nu$ and $\mathbf{1}^T\nu = 1$. Furthermore, each element of ν is nonnegative.*

Proof: The first part of the lemma follows Lemma 8.2.7 in [99]. For the second part, it is obvious that A^T is also nonnegative and has $\rho(A^T) = 1$ as an eigenvalue with algebraic multiplicity equal to one. Thus Lemma 3.3.4 implies that the eigenspace of A^T associated with eigenvalue $\lambda = 1$ is given by cx , where $c \in \mathbb{C}$, $c \neq 0$, and x is a nonnegative eigenvector. Since ν is also an eigenvector of A^T associated with eigenvalue $\lambda = 1$ and satisfies $\mathbf{1}^T\nu = 1$, it follows that each element of ν must be nonnegative. ■

Next, we show necessary and sufficient condition for consensus of information using discrete-time update scheme (3.1).

Theorem 3.3.5 *With a time-invariant interaction topology and constant weighting factors, the discrete-time update scheme (3.1) achieves consensus asymptotically for \mathcal{A} as $k \rightarrow \infty$ if and only if the associated interaction graph \mathcal{G} has a spanning tree.*

Proof: From Lemma 3.2.1, we need to show that $D^k \rightarrow \mathbf{1}c^T$, where c is a constant column vector.

(Sufficiency.) Obviously D is a stochastic matrix with positive diagonal entries. The fact that graph \mathcal{G} has a spanning tree also implies that the directed graph of D has a spanning tree. Combining Corollary 3.3.4 and Lemma 3.3.5, we know that $\lim_{k \rightarrow \infty} D^k \rightarrow \mathbf{1}\nu^T$, where ν satisfies the properties defined in Lemma 3.3.5.

(Necessity.) If \mathcal{G} does not have a spanning tree, neither does the directed graph of D , which implies, by Corollary 3.3.4, that the algebraic multiplicity of eigenvalue $\lambda = 1$ of D is $m > 1$. Therefore, the Jordan decomposition of D^k has the form $D^k = MJ^kM^{-1}$, where M is full rank and J^k is lower triangular with m diagonal elements equal to one. Therefore, the rank of $\lim_{k \rightarrow \infty} D^k$ is at least $m > 1$ which implies, by Lemma 3.2.1, that \mathcal{A} cannot reach consensus asymptotically. ■

Using discrete-time consensus scheme (3.1), we have similar results for dynamics consensus and equilibrium point analysis. We omit these two parts for simplicity.

3.4 Consensus Under Dynamically Changing Interaction Topologies

We need the following two lemmas. The first lemma is from [35] and the second lemma is originally from [101] and restated in [35].

Lemma 3.4.1 [35] *Let $m \geq 2$ be a positive integer and let P_1, P_2, \dots, P_m be nonnegative $n \times n$ matrices with positive diagonal elements, then*

$$P_1 P_2 \cdots P_m \geq \gamma (P_1 + P_2 + \cdots + P_m),$$

where $\gamma > 0$ can be specified from matrices P_i , $i = 1, \dots, m$.

Lemma 3.4.2 [101] *Let S_1, S_2, \dots, S_k be a finite set of SIA matrices with the property that for each sequence $S_{i_1}, S_{i_2}, \dots, S_{i_j}$ of positive length, the matrix product $S_{i_j} S_{i_{j-1}} \cdots S_{i_1}$ is SIA. Then for each infinite sequence S_{i_1}, S_{i_2}, \dots there exists a column vector y such that*

$$\lim_{j \rightarrow \infty} S_{i_j} S_{i_{j-1}} \cdots S_{i_1} = \mathbf{1}y^T.$$

3.4.1 Consensus Using Discrete-Time Update Scheme

The next lemma sets the stage for showing that under certain conditions, the existence of a spanning tree is sufficient for consensus under dynamically changing interaction topologies using the discrete-time update scheme (3.1).

Lemma 3.4.3 *If the union of a set of directed graphs $\{\mathcal{G}_{i_1}, \mathcal{G}_{i_2}, \dots, \mathcal{G}_{i_m}\} \subset \bar{\mathcal{G}}$ has a spanning tree, then the matrix product $D_{i_m} \cdots D_{i_2} D_{i_1}$ is SIA, where D_{i_j} is a stochastic matrix corresponding to each directed graph \mathcal{G}_{i_j} in Eq. (3.2).*

Proof: From Lemma 3.4.1, we know that $D_{i_m} \cdots D_{i_2} D_{i_1} \geq \gamma \sum_{j=1}^m D_{i_j}$ for some $\gamma > 0$.

Since the union of $\{\mathcal{G}_{i_1}, \mathcal{G}_{i_2}, \dots, \mathcal{G}_{i_m}\}$ has a spanning tree, we know that the directed graph of matrix $\sum_{j=1}^m D_{i_j}$ has a spanning tree, which in turn implies that the directed graph of the matrix product $D_{i_m} \cdots D_{i_2} D_{i_1}$ has a spanning tree. Also the matrix product $D_{i_m} \cdots D_{i_2} D_{i_1}$ is a stochastic matrix with positive diagonal entries since stochastic matrices with positive diagonal entries are closed under matrix multiplication.

Combining Corollary 3.3.4 and Lemma 3.3.5, we know that the matrix product $D_{i_1} D_{i_2} \cdots D_{i_m}$ is SIA. ■

The following theorem extends the discrete-time convergence result of [35].

Theorem 3.4.1 *Let $\mathcal{G}[k] \in \bar{\mathcal{G}}$ be a switching interaction graph at time $t = kT$. Also let $\alpha_{ij}[k] \in \bar{\alpha}$, where $\bar{\alpha}$ is a finite set of arbitrary positive numbers. The discrete-time update scheme (3.1) achieves consensus asymptotically for \mathcal{A} if there exists an infinite sequence of uniformly bounded, non-overlapping time intervals $[k_j T, (k_j + l_j)T)$, $j = 1, 2, \dots$, starting at $k_1 = 0$, with the property that each interval $[(k_j + l_j)T, k_{j+1}T)$ is uniformly bounded and the union of the graphs across each such interval has a spanning tree. Furthermore, if the union of the graphs after some finite time does not have a spanning tree, then consensus cannot be achieved asymptotically for \mathcal{A} .*

Proof: Let \bar{D} denote the set of all possible matrices $D[k]$ under dynamically changing interaction topologies and weighting factors $\alpha_{ij}[k]$. We know that \bar{D} is a finite set since both set $\bar{\mathcal{G}}$ and set $\bar{\alpha}$ are finite.

Consider the j th time interval $[k_j T, k_{j+1}T)$, which includes the time interval $[k_j T, (k_j + l_j)T)$ and must be uniformly bounded since both $[k_j T, (k_j + l_j)T)$ and $[(k_j + l_j)T, k_{j+1}T)$ are uniformly bounded. Also the sequence of time intervals $[k_j T, k_{j+1}T)$, $j = 1, 2, \dots$, are contiguous.

The union of the graphs across $[k_j T, k_{j+1}T)$, denoted as $\bar{\mathcal{G}}[k_j]$, has a spanning tree since the union of the graphs across $[k_j T, (k_j + l_j)T)$ has a spanning tree. Let

$\{D[k_j], D[k_j + 1], \dots, D[k_{j+1} - 1]\}$ be the set of stochastic matrices corresponding to each graph in the union $\bar{\mathcal{G}}[k_j]$. Following Lemma 3.4.3, the matrix product $D[k_{j+1} - 1] \cdots D[k_j + 1]D[k_j]$, $j = 1, 2, \dots$, is SIA. Then by applying Lemma 3.4.2 and mimicking a similar proof for Theorem 2 in [35], the first part can be proved.

If the union of the graphs after some finite time \hat{t} does not have a spanning tree, then during the infinite time interval $[\hat{t}, \infty)$, there exist at least two agents such that there is no path in the union of the graphs that contains these two agents, which then implies that information of these two agents cannot reach consensus. ■

3.4.2 Consensus Using Continuous-Time Update Scheme

In this section, we will focus on demonstrating that under certain conditions, the existence of a spanning tree is also sufficient for consensus under dynamically changing interaction topologies using the continuous-time update scheme. To do so, we need the following lemma.

Lemma 3.4.4 *If the union of the directed graphs $\{\mathcal{G}_{t_1}, \mathcal{G}_{t_2}, \dots, \mathcal{G}_{t_m}\} \subset \bar{\mathcal{G}}$ has a spanning tree and C_{t_i} is the matrix corresponding to each directed graph \mathcal{G}_{t_i} in Eq. (3.4), then the matrix product $e^{C_{t_m}\Delta t_m} \cdots e^{C_{t_2}\Delta t_2} e^{C_{t_1}\Delta t_1}$ is SIA, where $\Delta t_i > 0$ are bounded.*

Proof: From Eq. (3.4), each matrix C_{t_i} satisfies the properties defined in Lemma 3.3.1. Thus each C_{t_i} can be written as the sum of a nonnegative matrix M_{t_i} and $-\eta_{t_i}I_n$, where η_{t_i} is the maximum absolute value of the diagonal entries of C_{t_i} , $i = 1, \dots, m$.

From Lemma 1 in [31], we know that $e^{C_{t_i}\Delta t_i} = e^{-\eta_{t_i}\Delta t_i} e^{M_{t_i}\Delta t_i} \geq \rho_i M_{t_i}$ for some $\rho_i > 0$. Since the union of the directed graphs $\{\mathcal{G}_{t_1}, \mathcal{G}_{t_2}, \dots, \mathcal{G}_{t_m}\}$ has a spanning tree, we know that the union of the directed graphs of M_{t_i} has a spanning tree, which in turn implies that the union of the directed graphs of $e^{C_{t_i}\Delta t_i}$ has a spanning tree. From Lemma 3.4.1, we know that $e^{C_{t_m}\Delta t_m} \cdots e^{C_{t_2}\Delta t_2} e^{C_{t_1}\Delta t_1} \geq \gamma \sum_{i=1}^m e^{C_{t_i}\Delta t_i}$ for some $\gamma > 0$, which implies that the above matrix product also has a spanning tree.

It can also be verified that each matrix $e^{C_{t_i}\Delta t_i}$ is a stochastic matrix with positive diagonal entries, which implies that the above matrix product is also stochastic with positive diagonal entries.

Combining Corollary 3.3.4 and Lemma 3.3.5, we know that the above matrix product is SIA. ■

In this dissertation, we also apply dwell time (c.f. [102, 35]) to the continuous-time update scheme (3.4), which implies that the interaction graph and weighting factors are constrained to change only at discrete times, that is, the matrix $C(t)$ is piecewise constant.

Eq. (3.4) can be rewritten as

$$\dot{\xi}(t) = C(t_i)\xi(t), \quad t \in [t_i, t_i + \tau_i) \quad (3.9)$$

where t_0 is the initial time and t_1, t_2, \dots is an infinite time sequence at which the interaction graph or weighting factors change, resulting in a change in $C(t)$.

Let $\tau_i = t_{i+1} - t_i$ be the dwell time, $i = 0, 1, \dots$. Note that the solution to Eq. (3.9) is given by $\xi(t) = e^{C(t_k)(t-t_k)} e^{C(t_{k-1})\tau_{k-1}} \dots e^{C(t_1)\tau_1} e^{C(t_0)\tau_0} \xi(0)$, where k is the largest nonnegative integer satisfying $t_k \leq t$. Let $\bar{\tau}$ be a finite set of arbitrary positive numbers. Let Υ be an infinite set generated from set $\bar{\tau}$, which is closed under addition, and multiplications by positive integers. We assume that $\tau_i \in \Upsilon, i = 0, 1, \dots$. By choosing the set $\bar{\tau}$ properly, dwell time can be chosen from an infinite set Υ , which somewhat simulates the case when the interaction graph \mathcal{G} changes dynamically over time.

The following theorem extends the continuous-time convergence result in [35].

Theorem 3.4.2 *Let t_1, t_2, \dots be an infinite time sequence at which the interaction graph or weighting factors switch and $\tau_i = t_{i+1} - t_i \in \Upsilon, i = 0, 1, \dots$. Let $\mathcal{G}(t_i) \in \bar{\mathcal{G}}$ be a switching interaction graph at time $t = t_i$ and $\sigma_{ij}(t_i) \in \bar{\sigma}$, where $\bar{\sigma}$ is a finite set of arbitrary positive numbers. The continuous-time update scheme (3.3) achieves consensus asymptotically for \mathcal{A} if there exists an infinite sequence of uniformly bounded, non-overlapping time intervals $[t_{i_j}, t_{i_j+l_j}), j = 1, 2, \dots$, starting at $t_{i_1} = t_0$, with the property that each interval $[t_{i_j+l_j}, t_{i_{j+1}})$ is uniformly bounded and the union of the graphs across each such interval has a spanning tree. Furthermore, if the union of the graphs after some finite time does not have a spanning tree, then consensus cannot be achieved asymptotically for \mathcal{A} .*

Proof: The set of all possible matrices $e^{C(t_i)\tau_i}$, where $\tau_i \in \Upsilon$, under dynamically changing interaction topologies and weighting factors can be chosen or constructed by matrix multiplications from the set $\bar{E} = \{e^{C(t_i)\tau_i}, \tau_i \in \bar{\tau}\}$. Clearly \bar{E} is finite since $\bar{\mathcal{G}}$, $\bar{\sigma}$, and $\bar{\tau}$ are all finite.

Consider the j th time interval $[t_{i_j}, t_{i_{j+1}})$, which includes the time interval $[t_{i_j}, t_{i_j+l_j})$ and must be uniformly bounded since both $[t_{i_j}, t_{i_j+l_j})$ and $[t_{i_j+l_j}, t_{i_{j+1}})$ are uniformly bounded. Also the sequence of time intervals $[t_{i_j}, t_{i_{j+1}})$, $j = 1, 2, \dots$, are contiguous.

The union of the graphs across $[t_{i_j}, t_{i_{j+1}})$, denoted as $\bar{\mathcal{G}}(t_{i_j})$, has a spanning tree since the union of graphs across $[t_{i_j}, t_{i_j+l_j})$ has a spanning tree. Let $\{C(t_{i_j}), C(t_{i_{j+1}}), \dots, C(t_{i_{j+1}-1})\}$ be a set of matrices corresponding to each graph in the union $\bar{\mathcal{G}}(t_{i_j})$. Following Lemma 3.4.4, the matrix product $e^{C(t_{i_{j+1}-1})\tau_{i_{j+1}-1}} \dots e^{C(t_{i_{j+1}})\tau_{i_{j+1}}} e^{C(t_{i_j})\tau_{i_j}}$, $j = 1, 2, \dots$, is SIA. Then, the first part follows from Lemma 3.4.2 and an argument similar to the proof of Theorem 2 in [35].

The second part is similar to that in Theorem 3.4.1. ■

3.4.3 Discussion

The contribution of this section is that the results in [35], which are limited to undirected graphs, are extended to directed graphs. Therefore, unidirectional information exchange is allowed instead of requiring bidirectional information exchange. This will be important in applications where bidirectional communication or sensing is not available.

Ref. [35] shows that consensus of information (the heading of each agent in their context) can be achieved if the union of a collection of graphs is connected frequently enough. This section demonstrates that the same result can be achieved as long as the union of the graphs has a spanning tree, which is a milder requirement than being connected and implies that one half of the information exchange links required in [35] can be removed without adversely affecting the convergence result. In this sense, the results for convergence in [35] can be thought of as a special case of a more general result. Of course, the final achieved equilibrium points will depend on the property of the directed graphs. For example, compared to strongly connected graphs, graphs that are not strongly connected

will reach different final equilibrium points (see [31] for an analysis of the final equilibrium points).

The leader following scenario described in [35] can also be thought of as a special case of our result. If there is one agent in the group which does not have any incoming link, but the union of the interaction graphs has a spanning tree frequently enough, then this agent must be the root of the spanning tree, i.e, the leader. Since consensus is guaranteed, the information state of the other agents asymptotically converges to the information state of the leader. Therefore, the scenario discussed in [35] of being linked to a leader frequently enough is a special case of having a spanning tree, frequently enough, with the leader as the root.

For the continuous model used in [35], the switching times of the interaction graph is constrained to be separated by τ_D time units, where τ_D is a constant dwell time. Our continuous update scheme allows the switching times to be within an infinite set of positive numbers generated by any finite set of positive numbers, which is better suited to simulating the random switching of interaction graphs. Therefore, the continuous scheme in [35] can be thought of a special case of our result by letting $\bar{\tau} = \{\tau_d\}$ and $\Upsilon = \{k\tau_d | k = 1, 2, \dots\}$.

Unlike the update schemes in [35], we do not constrain the weighting factors in our discrete and continuous update schemes, other than to require that they be positive. This provides flexibility to account for relative confidence in information from different agents.

An additional contribution of this section is the proof for properties of nonnegative matrices with the same positive row sums. The Perron-Frobenius Theorem states that if a nonnegative matrix A is irreducible, that is, the directed graph of A is strongly connected, then the spectral radius of A is a simple eigenvalue. We show that the irreducibility condition is too stringent for nonnegative matrices with the same positive row sums. Lemma 3.3.3 explicitly shows that for a nonnegative matrix A with identical positive row sums, the spectral radius of A (the row sum in this case) is a simple eigenvalue if and only if the directed graph of A has a spanning tree. In other words, A may be reducible but retains its spectral radius as a simple eigenvalue. Furthermore, if A has a spanning tree

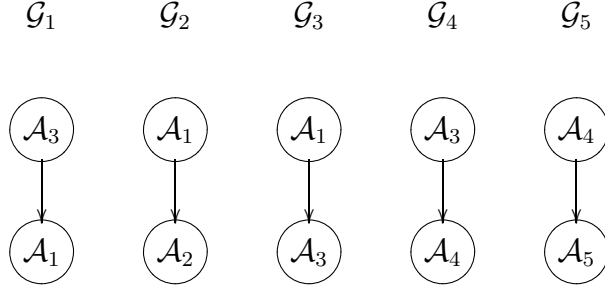


Figure 3.9: Possible interaction topologies for $\mathcal{A} = \{A_i | i = 1, \dots, 5\}$.

and positive diagonal entries, we know that the spectral radius of A is the unique eigenvalue of maximum modulus.

Note that we assume that weighting factors α_{ij} and σ_{ij} are chosen from any finite set of positive numbers for simplicity of proof. In fact, the results of this section are still valid if this assumption is relaxed to $\alpha_{ij} \in [\alpha_L, \alpha_M]$ and $\sigma_{ij} \in [\sigma_L, \sigma_M]$, where α_L , α_M , σ_L , and σ_M are arbitrary positive numbers satisfying $\alpha_L < \alpha_M$ and $\sigma_L < \sigma_M$. The argument is based on the concluding remark in [101], which deals with the case when the set of stochastic matrices is infinite.

3.4.4 Simulation Results

In this section, we simulate information consensus for five agents under dynamically changing interaction topologies using the discrete-time update scheme (3.2) and the continuous-time update scheme (3.9) respectively.

For simplicity, we constrain the possible interaction graphs for these five agents to be within the set $\mathcal{G}_s = \{\mathcal{G}_1, \mathcal{G}_2, \mathcal{G}_3, \mathcal{G}_4, \mathcal{G}_5\}$ as shown in Fig. 3.9, which is obviously a subset of $\bar{\mathcal{G}}$. For the discrete-time update scheme, we assume that the interaction graph switches randomly in \mathcal{G}_s at each time $t = kT$, where $k = 0, 1, 2, \dots$ and T is 0.5 seconds. For the continuous-time update scheme, we assume that the interaction graph switches randomly in \mathcal{G}_s at each random time $t = t_k$, $k = 0, 1, 2, \dots$. The weighting factors in Eqs. (3.2) and (3.9) are chosen arbitrarily a priori for each directed graph in \mathcal{G}_s to satisfy $\alpha_{ij}[k] > 0$ and $\sigma_{ij}(t_k) > 0$, $(i, j) \in \mathcal{I}$ and $k = 0, 1, 2, \dots$.



Figure 3.10: The union of \mathcal{G}_s .

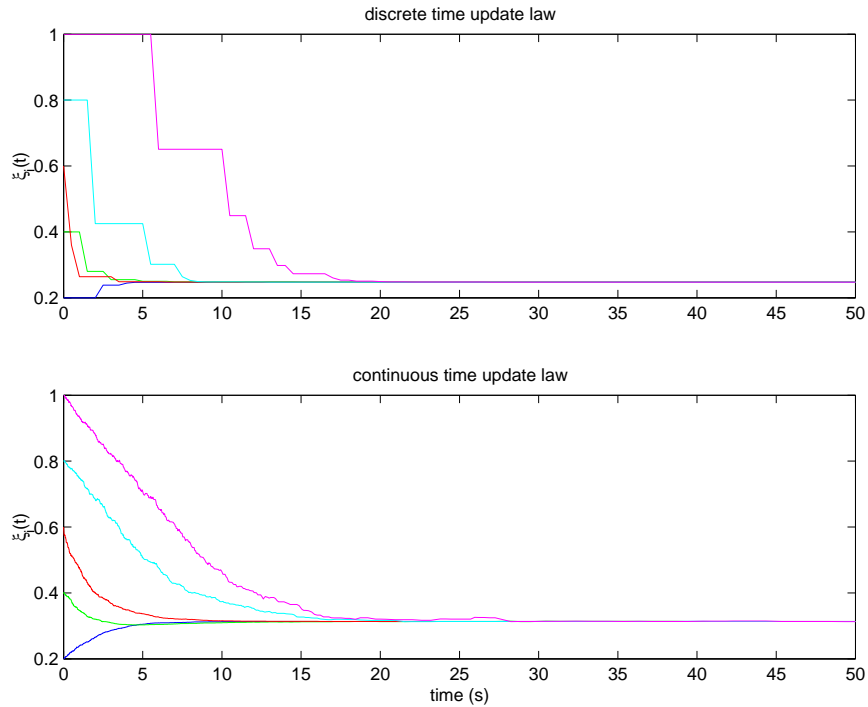


Figure 3.11: Consensus with $\mathcal{G}[k]$ and $\mathcal{G}(t_k)$ randomly switching from \mathcal{G}_s .

Note that each directed graph in \mathcal{G}_s does not have a spanning tree but that the union of these graphs do have a spanning tree is evident from Fig. 3.10. As the switching between graphs in \mathcal{G}_s is random, the condition for consensus will be generically satisfied. Alternatively, it is obvious that the union of these graphs is not connected, which implies that the conditions in [35] are not satisfied. Simulation results show that asymptotic consensus is achieved using both the discrete-time update scheme and the continuous-time update scheme.

The initial information variable was selected arbitrarily as $\xi_i = 0.2 * i$, $i = 1, \dots, 5$. Fig. 3.11 shows the consensus results using both the discrete-time update scheme and the continuous-time update scheme. Note that $\xi_i(t)$, $i = 1, \dots, 5$, reaches consensus for both cases.

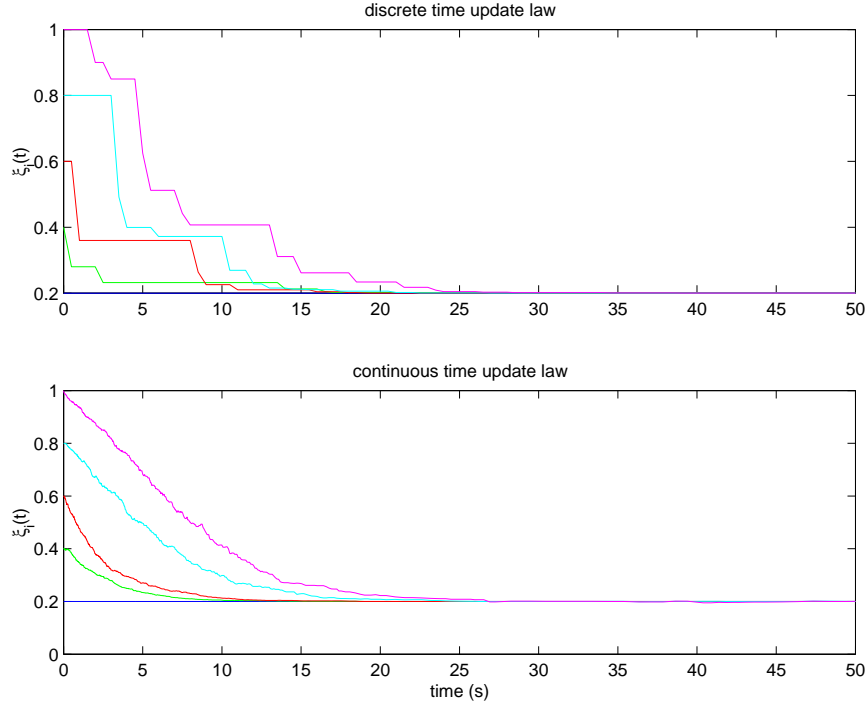


Figure 3.12: Consensus with $\mathcal{G}[k]$ and $\mathcal{G}(t_k)$ randomly switching from \mathcal{G}'_s .

Consider now a leader following scenario where the information graph switches in $\mathcal{G}'_s \triangleq \mathcal{G}_s \setminus \mathcal{G}_1$. As a result, there is no information exchange link from A_3 to A_1 . In this case, the union of the information graphs has a spanning tree, however, unlike the previous case there is no incoming information link to A_1 . Fig. 3.12 shows the consensus results using both the discrete-time update scheme and the continuous-time update scheme. Note that $\xi_i(t)$, $i = 2, \dots, 5$, converges asymptotically to $\xi_1(0)$ as expected. This is similar to the leader following case in [35] except that we do not need the followers to be jointly linked to the leader, that is, the union of the directed graphs is not necessarily connected.

Chapter 4

Multi-agent Formation Control

4.1 Introduction

This chapter presents some new results on spacecraft formation control and multiple robot coordination. One motivation for multi-agent systems is to achieve the same gains for mechanically controlled systems as has been gained in distributed computation. Rather than having a single monolithic (and therefore expensive and complicated) machine do everything, the hope is that many inexpensive, simple machines, can achieve the same, or enhanced functionality, through coordination. In essence, the objective is to replace expensive complicated hardware with software and multiple copies of simple hardware [103].

In Section 4.2, we propose a decentralized architecture for multiple spacecraft formation flying in deep space with formation feedback introduced. In Section 4.3, we propose a constructive satisficing approach to multi-agent formation maneuvers.

4.2 Multiple Spacecraft Formation Flying

In this section, we propose a decentralized formation scheme for spacecraft formation flying in deep space. This scheme is built on the combined strength of decentralized control and the virtual structure approach. By following a decentralized coordination architecture via the virtual structure approach, we introduce decentralized formation control strategies, which are appropriate when a large number of spacecraft are involved and/or stringent inter-spacecraft communication limitations are exerted. In our decentralized scheme, each spacecraft in the formation instantiates a local copy of the formation

control, i.e. the coordination vector under the virtual structure framework. The local instantiation of the coordination vector in each spacecraft is then synchronized by communication with its neighbors following a bidirectional ring topology. The effectiveness of the proposed control strategies is demonstrated through simulation results.

4.2.1 Problem Statement

In this section, we introduce some preliminary notation and properties for spacecraft formation flying including reference frames, unit quaternions, desired states for each spacecraft, and spacecraft dynamics.

Reference Frames

Four coordinate frames are used in this section as shown in Fig. 4.1. Reference frame \mathcal{F}_O is used as an inertial frame. Reference frame \mathcal{F}_F is fixed at the virtual center of the formation, i.e. the virtual structure, as a formation frame. Reference frame \mathcal{F}_i is embedded at the center of mass of each spacecraft as a body frame, which rotates with the spacecraft and represents its orientation. Reference frame \mathcal{F}_i^d represents the desired configuration for each spacecraft. Given any vector p , the representation of p in terms of its components in \mathcal{F}_O , \mathcal{F}_F , and \mathcal{F}_i are represented by $[p]_O$, $[p]_F$, and $[p]_i$ respectively.

Let the direction cosine matrix C_{ab} denote the orientation of the frame \mathcal{F}_a with respect to \mathcal{F}_b , then $[p]_a = C_{ab}[p]_b$, where $[p]_a$ and $[p]_b$ are the coordinate representations of vector p in \mathcal{F}_a and \mathcal{F}_b respectively.

Unit Quaternions

Unit quaternions (c.f. Ref. [104]) are used to represent the attitudes of rigid bodies in this section. A unit quaternion is defined as $q = [\hat{q}^T, \bar{q}]^T$, where $\hat{q} = a \cdot \sin(\frac{\phi}{2})$ and $\bar{q} = \cos(\frac{\phi}{2})$. In this notation, a is a unit vector in the direction of rotation with a coordinate representation $[a_1, a_2, a_3]^T$, called the eigenaxis, and ϕ is the rotation angle about a , called the Euler angle. By definition, a unit quaternion is subject to the constraint that $q^T q = 1$. Note that a unit quaternion is not unique since q and $-q$ represent the same

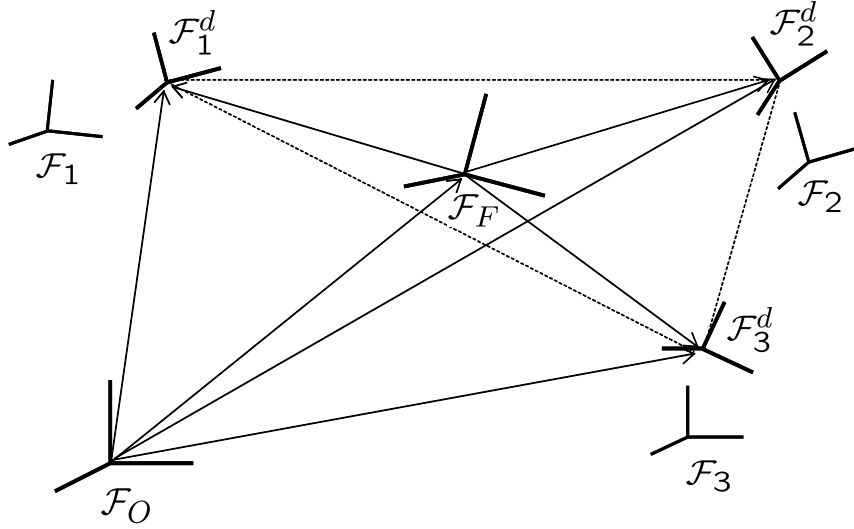


Figure 4.1: Coordinate Frame Geometry.

attitude. However, uniqueness can be achieved by restricting ϕ to the range $0 \leq \phi \leq \pi$ so that $\bar{q} \geq 0$ [105]. In the remainder of the section, we assume that $\bar{q} \geq 0$.

The product of two unit quaternions p and q is defined by

$$qp = \begin{bmatrix} \bar{q}\hat{p} + \bar{p}\hat{q} + \hat{q} \times \hat{p} \\ \bar{q}\bar{p} - \hat{q}^T \hat{p} \end{bmatrix},$$

which is also a unit quaternion. The conjugate of the unit quaternion q is defined by $q^* = [-\hat{q}^T, \bar{q}]^T$. The conjugate of qp is given by $(qp)^* = p^*q^*$. The multiplicative identity quaternion is denoted by $\mathbf{q}_I = [0, 0, 0, 1]^T$, where $qq^* = q^*q = \mathbf{q}_I$ and $q\mathbf{q}_I = \mathbf{q}_Iq = q$. Suppose that q^d and q represent the desired and actual attitude respectively, then the attitude error is given by $q_e = q^{d*}q = [\hat{q}_e^T, \bar{q}_e]^T$, which represents the attitude of the actual reference frame \mathcal{F} with respect to the desired reference frame \mathcal{F}^d .

The relationship between the rotation matrix C_{ab} and the unit quaternion q is given by

$$C_{ab} = (2\bar{q}^2 - 1)I + 2\hat{q}\hat{q}^T - 2\bar{q}\hat{q}^\times,$$

where q represents the attitude of \mathcal{F}_a with respect to \mathcal{F}_b [104].

Given a vector v with coordinate representation $[v_1, v_2, v_3]^T$, the cross-product operator is denoted by [106]

$$v^\times = \begin{bmatrix} 0 & -v_3 & v_2 \\ v_3 & 0 & -v_1 \\ -v_2 & v_1 & 0 \end{bmatrix},$$

which represents the fact that $v \times w = v^\times w$. Also define $\Omega(v)$ as

$$\Omega(v) = \begin{bmatrix} -v^\times & v \\ -v^T & 0 \end{bmatrix}.$$

The Desired States for Each Spacecraft

In the virtual structure approach, the entire desired formation is treated as a single structure called the “virtual structure” with formation frame \mathcal{F}_F located at its virtual center of mass to represent its configuration. The virtual structure then has position r_F , velocity v_F , attitude q_F , and angular velocity ω_F relative to \mathcal{F}_O .

Let r_i, v_i, q_i , and ω_i represent the position, velocity, attitude, and angular velocity of the i th spacecraft relative to the inertial frame \mathcal{F}_O . Similarly, let r_{iF}, v_{iF}, q_{iF} , and ω_{iF} represent the position, velocity, attitude, and angular velocity of the i th spacecraft relative to the formation frame \mathcal{F}_F . A superscript “ d ” is also used to represent the corresponding desired state of each spacecraft relative to either \mathcal{F}_O or \mathcal{F}_F .

Conceptually, we can think that place holders corresponding to each spacecraft are embedded in the virtual structure to represent the desired position and attitude for each spacecraft. As the virtual structure as a whole evolves in time, the place holders trace out trajectories for each corresponding spacecraft to track. As a result, the actual states of the i th place holder represent the desired states of the i th spacecraft. With \mathcal{F}_F as a reference frame, these states can be denoted by $r_{iF}^d, q_{iF}^d, v_{iF}^d$, and ω_{iF}^d .

Generally, $r_{iF}^d, q_{iF}^d, v_{iF}^d$, and ω_{iF}^d can vary with time, which means the desired formation shape is time-varying. However, if we are concerned with formation maneuvers that preserve the overall formation shape, that is, each place holder needs to preserve fixed relative position and orientation in the virtual structure, r_{iF}^d and q_{iF}^d should be constant and

v_{iF}^d and ω_{iF}^d should be zero. This requirement can be loosened to make the formation shape more flexible by allowing the place holders to expand or contract while still keeping fixed relative orientation. We will focus on this scenario in this latter section. Of course, the approach here can be readily extended to the general case.

Let $\lambda_F = [\lambda_1, \lambda_2, \lambda_3]$ where the components represent the expansion/contraction rates of the virtual structure along each \mathcal{F}_F axis. The state of the virtual structure can be defined as $\xi = [r_F^T, v_F^T, q_F^T, \omega_F^T, \lambda_F^T, \dot{\lambda}_F^T]^T$. We note that if each spacecraft has knowledge of ξ , and its own desired position and orientation with respect to the virtual structure, then formation keeping is transformed into an individual tracking problem. Therefore, the vector ξ represents the minimum amount of information needed by each spacecraft to coordinate its motion with the group. Motivated by this reasoning, we will call ξ the *coordination vector*.

Given ξ , the desired states for the i th spacecraft are given by

$$\begin{aligned}
[r_i^d]_O &= [r_F]_O + C_{OF}\Lambda[r_{iF}^d]_F \\
[v_i^d]_O &= [v_F]_O + C_{OF}\dot{\Lambda}[r_{iF}^d]_F + [\omega_F]_O \times (C_{OF}\Lambda[r_{iF}^d]_F) \\
[q_i^d]_O &= [q_F]_O[q_{iF}^d]_F \\
[\omega_i^d]_O &= [\omega_F]_O,
\end{aligned} \tag{4.1}$$

where $C_{OF}(q_F)$ is the rotation matrix of the frame \mathcal{F}_O with respect to \mathcal{F}_F and $\Lambda = \text{diag}(\lambda_F)$. Note that unlike the constant desired states r_{iF}^d , v_{iF}^d , q_{iF}^d , and ω_{iF}^d relative to \mathcal{F}_F , the desired states r_i^d , v_i^d , q_i^d , and ω_i^d relative to \mathcal{F}_O are time-varying since ξ is time-varying. The evolution equations of the desired states are given by

$$\begin{aligned}
[\dot{r}_i^d]_O &= [\dot{v}_i^d]_O \\
[\dot{v}_i^d]_O &= [\dot{v}_F]_O + 2[\omega_F]_O \times (C_{OF}\dot{\Lambda}[r_{iF}^d]_F) \\
&\quad + C_{OF}\ddot{\Lambda}[r_{iF}^d]_F + [\dot{\omega}_F]_O \times (C_{OF}\Lambda[r_{iF}^d]_F) \\
[\dot{q}_i^d]_O &= [\dot{q}_F]_O[q_{iF}^d]_F \\
[\dot{\omega}_i^d]_O &= [\dot{\omega}_F]_O.
\end{aligned} \tag{4.2}$$

Spacecraft Dynamics

The translational dynamics of each spacecraft relative to \mathcal{F}_O are

$$\begin{aligned}\frac{dr_i}{dt_o} &= v_i \\ m_i \frac{dv_i}{dt_o} &= f_i,\end{aligned}\tag{4.3}$$

where m_i and f_i are the mass and control force associated with the i th spacecraft respectively.

The rotational dynamics of each spacecraft relative to \mathcal{F}_O (c.f. Ref. [12]) are

$$\begin{aligned}\frac{d\hat{q}_i}{dt_o} &= -\frac{1}{2}\omega_i \times \hat{q}_i + \frac{1}{2}\bar{q}_i\omega_i \\ \frac{d\bar{q}_i}{dt_o} &= -\frac{1}{2}\omega_i \cdot \hat{q}_i \\ J_i \frac{d\omega_i}{dt_o} &= -\omega_i \times (J_i\omega_i) + \tau_i,\end{aligned}\tag{4.4}$$

where J_i and τ_i are inertia tensor and control torque associated with the i th spacecraft respectively.

4.2.2 Decentralized Architecture via the Virtual Structure Approach

In this section, we propose a decentralized architecture for spacecraft formation flying via the virtual structure approach. In order to demonstrate the salient features of our decentralized scheme, we first introduce previous work on centralized architectures via the virtual structure approach and previous work on general decentralized control architectures.

Previous Work on Centralized Architectures

Ref. [15] introduced the general centralized coordination architecture shown in Fig. 4.2, which is based on the virtual structure approach.

The system \mathbf{G} is a discrete event supervisor, which evolves a series of formation patterns by outputting its current formation pattern y_G . The system \mathbf{F} is the formation control module, which produces and broadcasts the coordination vector ξ . The system \mathbf{K}_i is the local spacecraft controller for the i th spacecraft, which receives the coordination

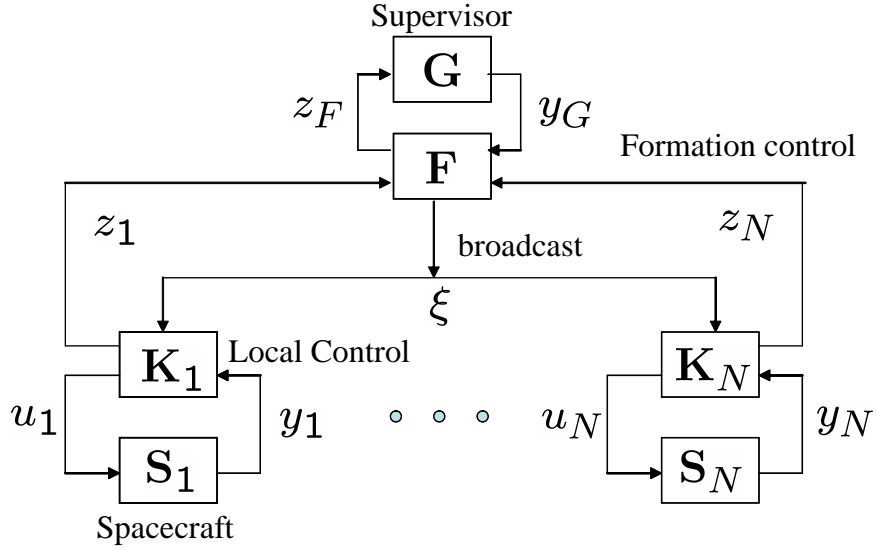


Figure 4.2: The centralized architecture based on the virtual structure approach.

vector ξ from the formation control module, converts ξ to the desired states for the i th spacecraft, and then controls the actual state for the i th spacecraft to track its desired state. The system S_i is the i th spacecraft, with control input u_i representing the control force and torque, and output y_i representing the measurable outputs from the i th spacecraft. In this centralized scheme, G and F are implemented at a centralized location (e.g. spacecraft #1), and then the coordination vector ξ is broadcast to the local controllers of the other spacecraft. Note that there is formation feedback from each local spacecraft controller to the formation control module F through the performance measure z_i . Also, there is formation feedback from F to G through the performance measure z_F [15].

The strength of this centralized scheme is that formation algorithms are fairly easy to realize. The weakness is that heavy communication and computation burden is concentrated on the centralized location, which may degrade the overall system performance. Also the centralized location results in a single point of failure for the whole system.

Previous Work on Decentralized Control

In Ref. [10], a decentralized architecture is proposed for autonomous establishment and maintenance of satellite formations, where each satellite only processes local measurement information and transmission vectors from the other nodes so that a local Kalman filter can be implemented to obtain a local control. It is also shown that the decentralized framework generates a neighboring optimal control if the planned maneuvers and trajectories are themselves optimal.

In Ref. [72], a decentralized control is implemented using a bidirectional ring topology, where each robot only needs position information of its two neighbors. A formation pattern is defined to be a set composed of the desired locations for each robot, i.e.

$$P = \{h_1^d, \dots, h_N^d\},$$

where N is the number of mobile robots in the formation. Two competing objectives are considered. The first objective is to move the robots to their final destinations. The second objective is to maintain formation during the transition. The goal of the control law for each robot is to drive the total tracking error and formation error of the group to zero. Similarly, in Ref. [73], three objectives are considered for the synchronized multiple spacecraft rotation problem. The first objective is to rotate each spacecraft to zero attitude error. The second objective is to maintain formation throughout the maneuver. The third objective is to rotate the spacecraft about a defined axis of rotation.

Decentralized Architecture

In this section, instead of using a set of desired locations for each agent as a formation pattern, we take advantage of the virtual structure approach to define the formation pattern by $P = \xi^d$, where $\xi^d = [r_F^{dT}, v_F^{dT}, q_F^{dT}, \omega_F^{dT}, \lambda_F^{dT}, \dot{\lambda}_F^{dT}]^T$ is the desired constant coordination vector representing the desired states of the virtual structure. We will assume piecewise rigid formations which implies that $v_F^d = \omega_F^d = \dot{\lambda}_F^d \equiv 0$. By specifying the formation pattern for the group, the movements of each spacecraft can be completely defined. Through a sequence of formation patterns $P^{(k)} = \xi^{d(k)}$, $k = 1, \dots, K$, the group can achieve a class of formation maneuver goals. In Ref. [72], the formation pattern is

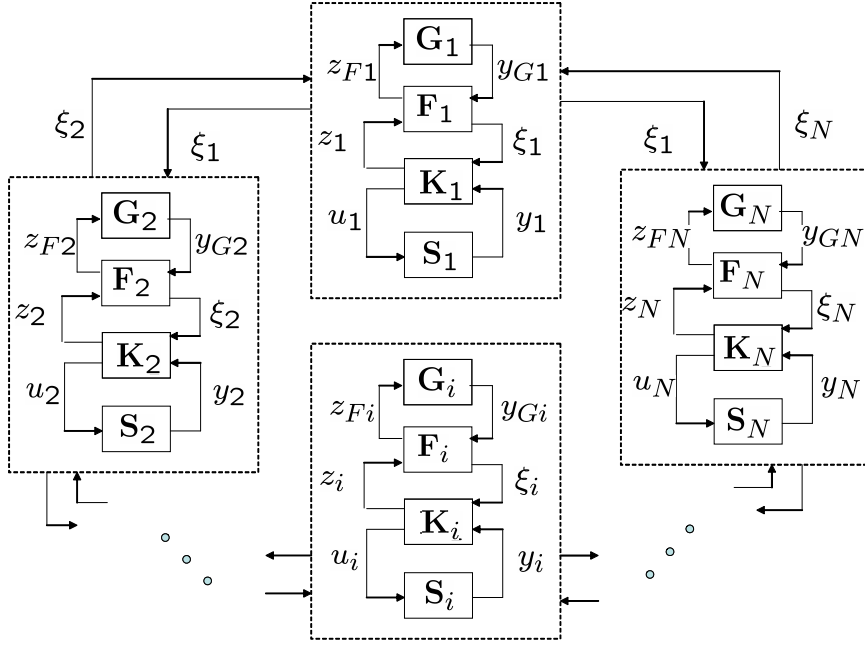


Figure 4.3: The decentralized architecture via the virtual structure approach.

defined in such a way that each vehicle only knows its final location in the formation while its trajectory throughout the maneuver is not specified. Here the formation pattern is defined such that each spacecraft will track a trajectory specified by the state of the virtual structure, while preserving a certain formation shape. From this point of view, collision avoidance is handled more efficiently than in Ref. [72].

In our decentralized architecture, each spacecraft in the formation instantiates a local copy of the coordination vector. We use $\xi_i = [r_{Fi}^T, v_{Fi}^T, q_{Fi}^T, \omega_{Fi}^T, \lambda_{Fi}^T, \dot{\lambda}_{Fi}^T]^T$ to represent the coordination vector instantiated in the i th spacecraft corresponding to the coordination vector ξ defined in the third subsection of Sec. 4.2.1. A bidirectional ring topology is used to communicate the coordination vector instantiation instead of the position or attitude information among each spacecraft. A decentralized architecture via the virtual structure approach is shown in Fig. 4.3.

In this case, instead of implementing the discrete event supervisor and formation control module at a centralized location, each spacecraft has a local copy of the discrete event supervisor G and formation control module F , denoted by G_i and F_i for the

i th spacecraft respectively. As in Fig. 4.2, \mathbf{K}_i and \mathbf{S}_i represent the i th local spacecraft controller and the i th spacecraft respectively.

Before the group maneuver starts, a sequence of formation patterns has been preset in each discrete event supervisor \mathbf{G}_i . The goal of \mathbf{G}_i is to transition through the sequence of formation patterns so that a class of group maneuver goals can be accomplished sequentially. Certain mechanisms need to be applied to coordinate and synchronize the group starting time, e.g., simple semaphores. When the group maneuver starts, each discrete event supervisor \mathbf{G}_i outputs the current formation pattern $y_{G_i} = \xi^{d(1)}$, to the formation control module \mathbf{F}_i . Each formation control module \mathbf{F}_i implements a coordination vector instantiation ξ_i . The goal of \mathbf{F}_i is to evolve ξ_i to its current desired formation pattern $\xi^{d(k)}$ and synchronize ξ_i with coordination vector instantiations implemented on other spacecraft. Here we use a bidirectional ring topology, which means that the coordination vector ξ_i instantiated in the i th spacecraft is synchronized with its two neighbors, that is, instantiations ξ_{i-1} and ξ_{i+1} implemented in the $(i-1)$ th and the $(i+1)$ th spacecraft respectively. Communications between the i th spacecraft and the $(i-1)$ th and $(i+1)$ th spacecraft needs to be established to transmit and receive the coordination vector instantiations. The formation control module \mathbf{F}_i then sends its coordination vector instantiation ξ_i to the local spacecraft controller \mathbf{K}_i . Based on ξ_i , the local controller \mathbf{K}_i can derive the desired states and the corresponding derivatives for the i th spacecraft from Eqs. (4.1) and (4.2). A local controller \mathbf{K}_i is designed to guarantee that the i th spacecraft tracks its desired states asymptotically. Formation feedback is also included from the i th spacecraft controller \mathbf{K}_i to the i th formation control module \mathbf{F}_i through the performance measure z_i indicating the i th spacecraft's tracking performance. Accordingly, as we will see in Sec. 4.2.3, the control law for ξ_i implemented in \mathbf{F}_i depends on the performance measure z_i , the current desired formation pattern $y_{G_i} = \xi^{d(k)}$, and the corresponding coordination vector instantiations ξ_{i-1} and ξ_{i+1} from the i th spacecraft's neighbors. Of course, formation feedback can also be included from other spacecraft to the i th formation control module \mathbf{F}_i at the cost of additional communication. Formation feedback from the i th formation control module \mathbf{F}_i to the i th discrete event supervisor \mathbf{G}_i is also included through the performance measure z_{F_i} , which indicates how far the i th instantiation ξ_i is from its current maneuver goal $\xi^{d(k)}$

and synchronization performance between ξ_i and its neighbors. Like the coordination and synchronization of the first group maneuver starting time, similar mechanisms can be applied to indicate the accomplishment of the current formation pattern and coordinate and synchronize the starting time for the next formation pattern among spacecraft. Then the same procedure described above repeats so that a sequence of formation patterns can be achieved.

Compared with the architecture in Ref. [10], which is based on a fully interconnected network, the architecture proposed here imposes fewer communication requirements. Even if the compression of data transmission is realized in Ref. [10], each vehicle still needs extensive data transmitted from all the other vehicles, which causes additional inter-vehicle communications especially when a large number of vehicles are involved. The architecture proposed here only requires communication between adjacent neighbors during the maneuver.

The communication requirement for each spacecraft during the maneuver can be estimated as follows. We know that r_{Fi} , v_{Fi} , ω_{Fi} , λ_{Fi} , and $\dot{\lambda}_{Fi}$ all have 3 components and q_{Fi} has 4 components. Thus the coordination vector ξ_i has 19 components. Assume that each component is encoded as B bits and the sample rate of the system is given by L Hz. By communicating with its two adjacent neighbors, the required bandwidth for each spacecraft can be estimated as $38BL$ bits/sec. Note that this is the case when group translation, group rotation, and group expansion/contraction are all involved. If only one group maneuver is involved, the bandwidth can be further reduced to almost one third of the above bandwidth estimate.

Compared to its centralized alternative, there is no master in the loop and each spacecraft evolves in a parallel manner so that a single point of failure existing in any centralized implementation can be eliminated and the total system performance will not degrade catastrophically under failure. As a result, the decentralized implementation offers more flexibility, reliability, and robustness than the corresponding centralized alternative. The weakness is that each local instantiation must be synchronized, which accounts for additional complexity and inter-vehicle communications to the whole system. Due to the ring topology and the implementation of the coordination vector, information exchange

among spacecraft can be reduced in the above decentralized architecture. Therefore, this weakness can be somewhat mitigated although the disadvantage of increased inter-vehicle communication requirements is a typical concern for decentralized systems. Of course, there may exist discrepancies between the starting time of each instantiation of the coordination vector dynamics. This starting time discrepancy can be mitigated through the control law for each coordination vector, which will synchronize neighboring coordination vector instantiations. Also, there may exist time delay when neighboring spacecraft exchange information. This issue is not modelled in the above decentralized architecture and needs to be addressed in future work.

4.2.3 Decentralized Formation Control Strategies

Two major tasks need to be carried out in the decentralized formation control scheme via the virtual structure approach. One is to propose suitable control laws for each spacecraft to track its desired states defined by the virtual structure. The other is to control and synchronize each virtual structure instantiation to achieve the desired formation patterns in a decentralized manner. In the first and second subsection of Sec. 4.2.3, we present control strategies for each spacecraft and each virtual structure instantiation respectively. In the third subsection of Sec. 4.2.3, we provide convergence analysis for the system composed of the coupled dynamics of N spacecraft and N coordination vector instantiations.

Formation Control Strategies for Each Spacecraft

For the i th spacecraft, define $X_i = [r_i^T, v_i^T, q_i^T, \omega_i^T]^T$ and $X_i^d = [r_i^{dT}, v_i^{dT}, q_i^{dT}, \omega_i^{dT}]^T$ as the actual state and desired state respectively. Define $\tilde{X}_i = X_i - X_i^d = [\tilde{r}_i^T, \tilde{v}_i^T, \tilde{q}_i^T, \tilde{\omega}_i^T]^T$ as the error state for the i th spacecraft.

We know that the desired states for each spacecraft also satisfy the translational and rotational dynamics (4.3) and (4.4) respectively, that is,

$$\begin{aligned}
\frac{dr_i^d}{dt_o} &= v_i^d \\
m_i \frac{dv_i^d}{dt_o} &= f_i^d \\
\frac{d\hat{q}_i^d}{dt_o} &= -\frac{1}{2}\omega_i^d \times \hat{q}_i^d + \frac{1}{2}\bar{q}_i^d \omega_i^d \\
\frac{d\bar{q}_i^d}{dt_o} &= -\frac{1}{2}\omega_i^d \cdot \hat{q}_i^d \\
J_i \frac{d\omega_i^d}{dt_o} &= -\omega_i^d \times (J_i \omega_i^d) + \tau_i^d.
\end{aligned} \tag{4.5}$$

This is valid since the desired states for each spacecraft are the same as the actual states for each corresponding place holder, which satisfies the translational and rotational dynamics.

The proposed control force for the i th spacecraft is given by

$$f_i = m_i(\dot{v}_i^d - K_{ri}(r_i - r_i^d) - K_{vi}(v_i - v_i^d)), \tag{4.6}$$

where m_i is the mass of the i th spacecraft, and K_{ri} and K_{vi} are symmetric positive definite matrices.

The proposed control torque for the i th spacecraft is given by

$$\tau_i = J_i \dot{\omega}_i^d + \frac{1}{2}\omega_i \times J_i(\omega_i + \omega_i^d) - k_{qi} \widehat{q}_i^{d*} q_i - K_{\omega_i}(\omega_i - \omega_i^d), \tag{4.7}$$

where J_i is the moment of inertia of the i th spacecraft, k_{qi} is a positive scalar, K_{ω_i} is a symmetric positive definite matrix, and \hat{q} represents the vector part of the quaternion.

Note that Eqs. (4.6) and (4.7) require both X_i^d and \dot{X}_i^d which are obtained from ξ_i and $\dot{\xi}_i$ using Eqs. (4.1) and (4.2).

Formation Control Strategies for Each Virtual Structure Instantiation

As in the third subsection of Sec. 4.2.2, ξ_i is the i th coordination vector instantiation and $\xi^{d(k)}$ is the current desired constant goal for the coordination vector instantiations, i.e. the current formation pattern. For notation simplicity, we hereafter use ξ^d instead of $\xi^{d(k)}$ to represent a certain formation pattern to be achieved. Define

$$\tilde{\xi}_i = \xi_i - \xi^d = [\tilde{r}_{Fi}^T, \tilde{v}_{Fi}^T, \tilde{q}_{Fi}^T, \tilde{\omega}_{Fi}^T, \tilde{\lambda}_{Fi}^T, \tilde{\dot{\lambda}}_{Fi}^T]^T$$

as the error state for the i th coordination vector instantiation. There are two objectives for the instantiation of the coordination vector implemented in each spacecraft. The first objective is to reach its desired constant goal ξ^d defined by the formation pattern set. The second objective is to synchronize each instantiation, i.e., $\xi_1 = \xi_2 = \dots = \xi_N$. Following the idea introduced in Ref. [72, 73], where behavior-based strategies are used to realize goal seeking and formation keeping for each agent, we apply behavior-based strategies to synchronize the coordination vector instantiations during the maneuver as well as evolve it to its desired goal at the end of the maneuver.

Define E_G as the goal seeking error to represent the total error between the current instantiation ξ_i and the desired goal ξ^d :

$$E_G(t) = \sum_{i=1}^N \|\xi_i - \xi^d\|^2.$$

Also define E_S as the synchronization error to represent the total synchronization error between neighboring instantiations:

$$E_S(t) = \sum_{i=1}^N \|\xi_i - \xi_{i+1}\|^2,$$

where the summation index i is defined modulo N , i.e., $\xi_{N+1} = \xi_1$ and $\xi_0 = \xi_N$. Defining $E(t) = E_G(t) + E_S(t)$, then the control objective is to drive $E(t)$ to zero asymptotically.

Since the coordination vector represents the states of the virtual structure, we suppose that the i th coordination vector instantiation satisfies the following rigid body dynamics

$$\begin{pmatrix} \dot{r}_{Fi} \\ m_F \dot{v}_{Fi} \\ \dot{q}_{Fi} \\ J_F \dot{\omega}_{Fi} \\ \dot{\lambda}_{Fi} \\ \ddot{\lambda}_{Fi} \end{pmatrix} = \begin{pmatrix} v_{Fi} \\ f_{Fi} \\ \frac{1}{2} \Omega(\omega_{Fi}) q_{Fi} \\ -\omega_{Fi} \times J_F \omega_{Fi} + \tau_{Fi} \\ \dot{\lambda}_{Fi} \\ \nu_{Fi} \end{pmatrix}, \quad (4.8)$$

where m_F and J_F are the virtual mass and virtual inertia of the virtual structure, f_{Fi} and τ_{Fi} are the virtual force and virtual torque exerted on the i th implementation of the virtual structure, and ν_{Fi} is the virtual control effort used to expand or contract the formation.

The tracking performance for the i th spacecraft is defined as $e_{Ti} = e(X_i, X_i^d)$, where $e(X_i, X_i^d) > 0$ when $X_i \neq X_i^d$ and $e(X_i, X_i^d) = 0$ when $X_i = X_i^d$. In the sequel, we choose $e_{Ti} = \|\tilde{X}_i\|^2$. Define $\Gamma_{Gi} = D_G + K_F e_{Ti}$ to incorporate formation feedback from the i th spacecraft to the i th coordination vector implementation, where D_G and K_F are symmetric positive definite matrices. Obviously, Γ_{Gi} is also a positive definite matrix. If we let $K_F = 0$, there is no formation feedback.

The proposed control force f_{Fi} is given by

$$\begin{aligned} f_{Fi} = & m_F(-K_G(r_{Fi} - r_F^d) - \Gamma_{Gi}v_{Fi} \\ & - K_S(r_{Fi} - r_{F(i+1)}) - D_S(v_{Fi} - v_{F(i+1)}) \\ & - K_S(r_{Fi} - r_{F(i-1)}) - D_S(v_{Fi} - v_{F(i-1)})), \end{aligned} \quad (4.9)$$

where K_G is a symmetric positive definite matrix, and K_S and D_S are symmetric positive semi-definite matrices.

The proposed control torque τ_{Fi} is given by

$$\begin{aligned} \tau_{Fi} = & -k_G \widehat{q_F^{d*}} q_{Fi} - \Gamma_{Gi} \omega_{Fi} \\ & - k_S \widehat{q_{F(i+1)}^*} q_{Fi} - D_S(\omega_{Fi} - \omega_{F(i+1)}) \\ & - k_S \widehat{q_{F(i-1)}^*} q_{Fi} - D_S(\omega_{Fi} - \omega_{F(i-1)}), \end{aligned} \quad (4.10)$$

where $k_G > 0$ and $k_S \geq 0$ are scalars, Γ_{Gi} follows the same definition as above, D_S is a symmetric positive semi-definite matrix, and \hat{q} represents the vector part of the quaternion.

Similar to Eq. (4.9), the proposed control effort ν_{Fi} is given by

$$\begin{aligned} \nu_{Fi} = & -K_G(\lambda_{Fi} - \lambda_F^d) - \Gamma_{Gi} \dot{\lambda}_{Fi} \\ & - K_S(\lambda_{Fi} - \lambda_{F(i+1)}) - D_S(\dot{\lambda}_{Fi} - \dot{\lambda}_{F(i+1)}) \\ & - K_S(\lambda_{Fi} - \lambda_{F(i-1)}) - D_S(\dot{\lambda}_{Fi} - \dot{\lambda}_{F(i-1)}), \end{aligned} \quad (4.11)$$

where K_G is a symmetric positive definite matrix, Γ_{Gi} follows the same definition as above, and K_S and D_S are symmetric positive semi-definite matrices.

Note that the matrices in Eqs. (4.9), (4.10), and (4.11) can be chosen differently based on specific requirements to change the weights of translation, rotation, and expansion/contraction effects. In Eqs. (4.9), (4.10), and (4.11), the first two terms are used to

drive $E_G \rightarrow 0$, the third and fourth terms are used to synchronize the i th and $(i + 1)$ th coordination vector instantiations, and the fifth and sixth terms are used to synchronize the i th and $(i - 1)$ th coordination vector instantiations. The second term, that is, the formation feedback term is also used to slow down the i th virtual structure implementation when the i th spacecraft has a large tracking error. This strategy needs each spacecraft to know its neighboring coordination vector instantiations, which can be accomplished by nearest neighbor communication. From Eqs. (4.9), (4.10), and (4.11), we can also see that besides ξ_{i-1} , ξ_i , and ξ_{i+1} the control laws for the i th coordination vector instantiation also require the current constant formation pattern ξ^d and \tilde{X}_i through the formation feedback gain matrix Γ_{Gi} .

Convergence Analysis

The following Lemmas will be used to prove our main theorem.

Lemma 4.2.1 *If both the unit quaternion and angular velocity pairs (q_s, ω_s) and (q_p, ω_p) satisfy the rotational dynamics (4.4) with moment of inertia J and with control torque τ_s and τ_p respectively, $\delta\omega = \omega_s - \omega_p$ and $\delta q = q_s - q_p$ with $\delta\hat{q} = \hat{q}_s - \hat{q}_p$ and $\delta\bar{q} = \bar{q}_s - \bar{q}_p$, and $V_1 = \delta\bar{q}^2 + \delta\hat{q} \cdot \delta\hat{q}$ and $V_2 = \frac{1}{2}\delta\omega \cdot J\delta\omega$, then $\dot{V}_1 = \delta\omega \cdot \widehat{q_p^* q_s}$ and $\dot{V}_2 = \delta\omega \cdot (\tau_s - \tau_p - \frac{1}{2}(\omega_s \times J\delta\omega))$.*

Proof: Identical to the proof for attitude control in Ref. [12] by replacing q_i with q_p , ω_i with ω_p , q_i^d with q_s , and ω_i^d with ω_s . ■

For a vector x , we simply use $x^T x$ or $\|x\|^2$ to represent the vector dot product $x \cdot x$ hereafter.

Lemma 4.2.2 *If $A \in \mathbb{R}^{k \times k}$ and $B \in \mathbb{R}^{l \times l}$ are symmetric positive semi-definite matrices, then $A \otimes B$ is positive semi-definite, where \otimes denotes the Kronecker product. Moreover, if both A and B are symmetric positive definite, then so is $A \otimes B$.*

Proof: See Ref. [107]. ■

Lemma 4.2.3 *If C is a circulant matrix with the first row given by $[2, -1, 0, \dots, 0, -1] \in \mathbb{R}^N$, then $C \in \mathbb{R}^{N \times N}$ is symmetric positive semi-definite. Let $P \in \mathbb{R}^{p \times p}$ and $Z =$*

$[z_1^T, \dots, z_N^T]^T$, where $z_i \in \mathbb{R}^p$. If the terms $P(z_i - z_{i-1}) + P(z_i - z_{i+1})$ are stacked in a column vector, the resulting vector can be written as $(C \otimes P)Z$.

Proof: See Ref. [72]. ■

From Eqs. (4.3), (4.4), (4.6), and (4.7), the dynamics for the i th spacecraft can be represented by $\dot{\tilde{X}}_i = f(\tilde{X}_i, \xi_i)$, where $f(\cdot, \cdot)$ can be determined from those equations. From Eqs. (4.8), (4.9), (4.10), and (4.11), the dynamics for the i th coordination vector instantiation can be represented by $\dot{\xi}_i = g(\xi_{i-1}, \xi_i, \xi_{i+1}, \tilde{X}_i)$, where $g(\cdot, \cdot, \cdot, \cdot)$ can also be determined from those equations. Therefore, the coupled dynamics of the whole system composed of N spacecraft and N coordination vector instantiations are time-invariant with states \tilde{X}_i and ξ_i , $i = 1, \dots, N$. LaSalle's invariance principle will be used to prove the main theorem for convergence of the whole system.

Theorem 4.2.1 *If the control laws for each spacecraft are given by (4.6) and (4.7), and the control laws for each coordination vector instantiation are given by (4.9), (4.10) and (4.11), then $\sum_{i=1}^N e_{Ti} + E(t) \rightarrow 0$ asymptotically.*

Proof: For the whole system consisting of N spacecraft and N coordination vector instantiations, consider the Lyapunov function candidate:

$$V = V_{sp} + V_{Ft} + V_{Fr} + V_{Fe}, \quad (4.12)$$

where

$$\begin{aligned}
V_{sp} &= \sum_{i=1}^N \left(\frac{1}{2} \tilde{r}_i^T K_{r_i} \tilde{r}_i + \frac{1}{2} \tilde{v}_i^T \tilde{v}_i + k_{q_i} \tilde{q}_i^T \tilde{q}_i + \frac{1}{2} \tilde{\omega}_i^T J_i \tilde{\omega}_i \right), \\
V_{Ft} &= \frac{1}{2} \sum_{i=1}^N (r_{Fi} - r_{F(i+1)})^T K_S (r_{Fi} - r_{F(i+1)}) \\
&\quad + \frac{1}{2} \sum_{i=1}^N (\tilde{r}_{Fi}^T K_G \tilde{r}_{Fi} + v_{Fi}^T v_{Fi}), \\
V_{Fr} &= \sum_{i=1}^N k_S (q_{Fi} - q_{F(i+1)})^T (q_{Fi} - q_{F(i+1)}) \\
&\quad + \sum_{i=1}^N \left(k_G \tilde{q}_{Fi}^T \tilde{q}_{Fi} + \frac{1}{2} \omega_{Fi}^T J_F \omega_{Fi} \right), \\
V_{Fe} &= \frac{1}{2} \sum_{i=1}^N (\lambda_{Fi} - \lambda_{F(i+1)})^T K_S (\lambda_{Fi} - \lambda_{F(i+1)}) \\
&\quad + \frac{1}{2} \sum_{i=1}^N (\tilde{\lambda}_{Fi}^T K_G \tilde{\lambda}_{Fi} + \dot{\lambda}_{Fi}^T \dot{\lambda}_{Fi}).
\end{aligned}$$

With the proposed control force (4.6) for each spacecraft, the second equation in the translational dynamics (4.3) for the i th spacecraft can be rewritten as $\dot{\tilde{v}}_i = -K_{r_i} \tilde{r}_i - K_{v_i} \tilde{v}_i$. Applying Lemma 4.2.1, the derivative of V_{sp} is

$$\begin{aligned}
\dot{V}_{sp} &= \sum_{i=1}^N (-\tilde{v}_i^T K_{v_i} \tilde{v}_i) \\
&\quad + \sum_{i=1}^N \tilde{\omega}_i^T \left(k_{q_i} \widehat{q}_i^{d*} \tilde{q}_i + \tau_i - \tau_i^d - \frac{1}{2} (\omega_i \times J_i \tilde{\omega}_i) \right).
\end{aligned}$$

From Eq. (4.5), $\tau_i^d = J_i \dot{\omega}_i^d + \omega_i^d \times (J_i \omega_i^d)$. With the proposed control torque (4.7) for each spacecraft, after some manipulation, we know that

$$\dot{V}_{sp} = \sum_{i=1}^N (-\tilde{v}_i^T K_{v_i} \tilde{v}_i - \tilde{\omega}_i^T K_{\omega_i} \tilde{\omega}_i) \leq 0. \quad (4.13)$$

Differentiating V_{Ft} , we can get

$$\begin{aligned}
\dot{V}_{Ft} &= \sum_{i=1}^N v_{Fi}^T (K_S (r_{Fi} - r_{F(i+1)}) \\
&\quad + K_S (r_{Fi} - r_{F(i-1)}) + K_G \tilde{r}_{Fi} + \frac{f_{Fi}}{m_F}).
\end{aligned}$$

With the proposed control force (4.9) for each coordination vector instantiation,

$$\begin{aligned}\dot{V}_{Ft} = & - \sum_{i=1}^N (v_{Fi}^T \Gamma_{Gi} v_{Fi} \\ & + (v_{Fi} - v_{F(i+1)})^T D_S (v_{Fi} - v_{F(i+1)})) \leq 0.\end{aligned}\quad (4.14)$$

Applying Lemma 4.2.1, the derivative of V_{Fr} is

$$\begin{aligned}\dot{V}_{Fr} = & \sum_{i=1}^N (\omega_{Fi} - \omega_{F(i+1)})^T k_S q_{F(i+1)}^* \widehat{q_{Fi}} \\ & + \sum_{i=1}^N \omega_{Fi}^T (k_G \widehat{q_{Fi}^{d*}} + \tau_{Fi} - \frac{1}{2} \omega_{Fi} \times J_F \omega_{Fi}).\end{aligned}$$

After some manipulation,

$$\dot{V}_{Fr} = \sum_{i=1}^N \omega_{Fi}^T (k_S q_{F(i+1)}^* \widehat{q_{Fi}} - k_S q_{Fi}^* \widehat{q_{F(i-1)}} + k_G \widehat{q_{Fi}^{d*}} + \tau_{Fi}).$$

With the proposed control torque (4.10) for each coordination vector instantiation,

$$\begin{aligned}\dot{V}_{Fr} = & - \sum_{i=1}^N (\omega_{Fi}^T \Gamma_{Gi} \omega_{Fi} \\ & + (\omega_{Fi} - \omega_{F(i+1)})^T D_S (\omega_{Fi} - \omega_{F(i+1)})) \leq 0.\end{aligned}\quad (4.15)$$

Similar to \dot{V}_{Ft} , with the proposed control effort (4.11) for each coordination vector instantiation, the derivative of V_{Fe} is

$$\begin{aligned}\dot{V}_{Fe} = & - \sum_{i=1}^N (\dot{\lambda}_{Fi}^T \Gamma_{Gi} \dot{\lambda}_{Fi} \\ & + (\dot{\lambda}_{Fi} - \dot{\lambda}_{F(i+1)})^T D_S (\dot{\lambda}_{Fi} - \dot{\lambda}_{F(i+1)})) \leq 0.\end{aligned}\quad (4.16)$$

From Eqs. (4.13), (4.14), (4.15), and (4.16), it is obvious that $\dot{V} = \dot{V}_{sp} + \dot{V}_{Ft} + \dot{V}_{Fr} + \dot{V}_{Fe} \leq 0$. Let $\Sigma = \{(\tilde{X}_1, \dots, \tilde{X}_N, \tilde{\xi}_1, \dots, \tilde{\xi}_N) | \dot{V} = 0\}$, and let $\bar{\Sigma}$ be the largest invariant set in Σ . On $\bar{\Sigma}$, $\dot{V} \equiv 0$, i.e. $\dot{V}_{sp} = \dot{V}_{Ft} = \dot{V}_{Fr} = \dot{V}_{Fe} \equiv 0$, which implies that $\tilde{v}_i \equiv 0$, $\tilde{\omega}_i \equiv 0$, $v_{Fi} \equiv 0$, $\omega_{Fi} \equiv 0$, $\dot{\lambda}_{Fi} \equiv 0$, $i = 1, \dots, N$.

Since $\tilde{v}_i \equiv 0$, we know that $\tilde{r}_i = 0$ from Eqs. (4.3) and (4.6). Since $\tilde{\omega}_i \equiv 0$, we also know that $\widehat{q_i^{d*}} = 0$ from Eqs. (4.4) and (4.7), which then implies that $q_i = q_i^d$, i.e. $\tilde{q}_i = 0$.

Then following $v_{Fi} \equiv 0$, from Eq. (4.9) and the second equation in Eq. (4.8), it can be seen that

$$\begin{aligned} & K_G \tilde{r}_{Fi} + K_S(r_{Fi} - r_{F(i+1)}) \\ & + K_S(r_{Fi} - r_{F(i-1)}) = 0, \quad i = 1, \dots, N, \end{aligned}$$

which is equivalent to

$$\begin{aligned} & K_G \tilde{r}_{Fi} + K_S(\tilde{r}_{Fi} - \tilde{r}_{F(i+1)}) \\ & + K_S(\tilde{r}_{Fi} - \tilde{r}_{F(i-1)}) = 0, \quad i = 1, \dots, N. \end{aligned} \quad (4.17)$$

From Lemma 4.2.3, Eq. (4.17) can also be written as $(I_N \otimes K_G + C \otimes K_S)\tilde{r}_F = 0$, where $\tilde{r}_F = [\tilde{r}_{F1}^T, \dots, \tilde{r}_{FN}^T]^T$, I_N is an $N \times N$ identity matrix, and C is the circulant matrix defined in Lemma 4.2.3. Based on Lemma 4.2.2 and 4.2.3, $I_N \otimes K_G$ is positive definite and $C \otimes K_S$ is positive semi-definite. Thus we know that $\tilde{r}_F = 0$.

Following a similar procedure as above, we can also show that $\tilde{\lambda}_{Fi} = 0$ since $\dot{\lambda}_{Fi} \equiv 0$.

Also following $\omega_{Fi} \equiv 0$, from Eq. (4.10) and the fourth equation in Eq. (4.8), we know that

$$\begin{aligned} & \widehat{k_G q_F^{d*} q_{Fi}} + \widehat{k_S q_{F(i+1)}^* q_{Fi}} + \widehat{k_S q_{F(i-1)}^* q_{Fi}} = 0, \\ & i = 1, \dots, N. \end{aligned} \quad (4.18)$$

Since the quaternion multiplication is associative, we know that $q_{F(i+1)}^* q_{Fi} = q_{F(i+1)}^* \mathbf{q_I} q_{Fi} = q_{F(i+1)}^* (q_F^d q_F^{d*}) q_{Fi} = (q_{F(i+1)}^* q_F^d) (q_F^{d*} q_{Fi})$, where $\mathbf{q_I}$ is the multiplicative identity quaternion defined in the second subsection of Sec. 4.2.1. Therefore, Eq. (4.18) is equivalent to

$$\begin{aligned} & \widehat{k_G q_F^{d*} q_{Fi}} + \widehat{k_S (q_{F(i+1)}^* q_F^d) (q_F^{d*} q_{Fi})} \\ & + \widehat{k_S (q_{F(i-1)}^* q_F^d) (q_F^{d*} q_{Fi})} = 0, \quad i = 1, \dots, N. \end{aligned} \quad (4.19)$$

Following Ref. [73] and applying the property of the unit quaternion, Eq. (4.19) can be written as $\widehat{p_i (q_F^{d*} q_{Fi})} = 0$, where $p_i = k_G \mathbf{q_I} + k_S (q_F^{d*} q_{F(i+1)}) + k_S (q_F^{d*} q_{F(i-1)})$.

Compared with Eq. (7) in Ref. [73], Eq. (4.19) has the same form when we treat q_i as $q_F^{d*} q_{Fi}$ and k_F as k_S and delete $k_e \widehat{q_{iR}}$ term in Eq. (7) in Ref. [73]. It can be verified

that their proof for $\widehat{q}_i = 0$ is still valid when $k_e \widehat{q}_{iR}$ term is omitted, which is only used to guarantee the rotation of the spacecraft about a defined axis.

Then following the result $\widehat{q}_i = 0$ in Ref. [73], we can show that $\widehat{q_{F_i}^{d*}} = 0$, which implies that $q_{F_i} = q_{F_i}^d$, i.e. $\tilde{q}_{F_i} = 0$.

Therefore, by LaSalle's invariance principle, $\|\tilde{X}_i\| \rightarrow 0$, $\|\tilde{\xi}_i\| \rightarrow 0$, and $\|\xi_i - \xi_{i+1}\| \rightarrow 0$, $i = 1, \dots, N$. Accordingly, $\sum_{i=1}^N e_{T_i} + E(t) \rightarrow 0$ asymptotically. ■

From Theorem 4.2.1, we can see that each virtual structure instantiation will achieve its final goal asymptotically and each spacecraft will also track its desired state specified by the virtual structure asymptotically during the maneuver. Therefore, the formation maneuver can be achieved asymptotically.

Discussion

Note that different performance measure functions $e(\cdot, \cdot)$ may be chosen to measure formation maintenance. For example, $e(\tilde{X}_i) = \tilde{X}_i^T P \tilde{X}_i$, where P is symmetric positive definite. Matrix P can be designed to adjust the relative weights of translational and rotational formation error based on certain requirements. The motivation for the design of the nonlinear gain matrices Γ_{G_i} is to meet the following requirements. When a spacecraft is out of its desired configuration, that is, e_{T_i} is large, its coordination vector instantiation will slow down or even stop, allowing the spacecraft to regain formation. When a spacecraft is maintaining its desired configuration, that is, e_{T_i} is small, its coordination vector instantiation will keep moving toward its final goal at a reasonable speed. By this design, each coordination vector instantiation will be aimed at performing reasonably fast formation maneuvers as well as preserving tight formation shape during the maneuver even in the case of control saturation, disturbances, and malfunctions. In this section, we choose a candidate for such gain matrices as $\Gamma_{G_i} = D_G + K_F e_{T_i}$, where $D_G = D_G^T > 0$ is the gain matrix which corresponds to the nominal formation speed when the formation is preserved tightly, and $K_F = K_F^T > 0$ is the formation gain matrix which weights the performance measure e_{T_i} . Of course, other choices are also feasible. In the case of $K_F = 0$, no formation feedback is introduced. We will see that formation gain matrix with larger entries

result in better formation maintenance but slower convergence speed. We can see that

$$\begin{aligned} e_{Ti} \rightarrow 0 &\Rightarrow \Gamma_{Gi} \rightarrow D_G \\ e_{Ti} \rightarrow \infty &\Rightarrow \Gamma_{Gi} \rightarrow \infty. \end{aligned}$$

As a result, nonlinear gains slow down or speed up the coordination vector instantiation based on how far out of the desired configuration each spacecraft is.

Since PD-like control laws are used for each spacecraft and each coordination vector instantiation, the transient specifications for each spacecraft and each coordination vector instantiation can be satisfied by designing corresponding gain matrices in the control laws following the design procedure for the coefficients of a second-order system. For a second order system $s^2 + k_1s + k_2 = 0$, if we define rise time t_r and damping ratio ζ , then natural frequency ω_n is approximately $1.8/t_r$. Therefore, if we let $k_2 = \omega_n^2 = (1.8/t_r)^2$ and $k_1 = 2\zeta\omega_n = 2\zeta(1.8/t_r)$, the transient specifications for the system are satisfied. We can design K_{ri} , k_{qi} , K_G , and k_G according to k_2 , and design K_{vi} , $K_{\omega i}$, and D_G according to k_1 . For example, K_{ri} and K_{vi} can be defined as k_2I_3 and k_1I_3 respectively, where I_3 is a 3×3 identity matrix.

An illustrative example is shown as follows. Let $K_G = I_3$ and $K_S = D_S = 0$ in Eq. (4.9). Note that the translational dynamics of the i th coordination vector instantiation can be rewritten as $\ddot{\tilde{r}}_{Fi} + \Gamma_{Gi}\dot{\tilde{r}}_{Fi} + K_G\tilde{r}_{Fi} = 0$, where $\tilde{r}_{Fi} = r_{Fi} - r_{Fi}^d = [\tilde{r}_{Fxi}, \tilde{r}_{Fyi}, \tilde{r}_{Fzi}]^T$. Fig. 4.4 shows a plot of \tilde{r}_{Fxi} for different choices of matrix Γ_{Gi} . We can see that the dynamics of the i th coordination vector instantiation evolve more slowly as the elements of Γ_{Gi} are increased to be sufficiently large. That is, it takes longer time for the i th coordination vector instantiation to achieve its desired states. When $\Gamma_{Gi} \rightarrow \infty$, the coordination vector instantiation will stop evolving.

Moreover, for each spacecraft, if we define a translational tracking error for the i th spacecraft as $E_{ti} = \frac{1}{2}\tilde{r}_i^T K_{ri}\tilde{r}_i + \frac{1}{2}\|\tilde{v}_i\|^2$, E_{ti} decreases during the maneuver and $\tilde{r}_i^T K_{ri}\tilde{r}_i$ is bounded by $2E_{ti}(0) - \|\tilde{v}_i\|^2$ following the proof for \dot{V}_{sp} . Similarly if we define a rotational tracking error as $E_{ri} = k_{qi}\|\tilde{q}_i\|^2 + \frac{1}{2}\tilde{\omega}_i^T J_i \tilde{\omega}_i$, E_{ri} decreases during the maneuver and $\|\tilde{q}_i\|^2$ is bounded by $\frac{1}{k_{qi}}(E_{ri}(0) - \frac{1}{2}\tilde{\omega}_i^T J_i \tilde{\omega}_i)$. For each coordination vector instantiation, following the proof for \dot{V}_{Ft} , \dot{V}_{Fr} , and \dot{V}_{Fe} , we know that V_{Ft} , V_{Fr} , and V_{Fe} are bounded by $V_{Ft}(0)$,

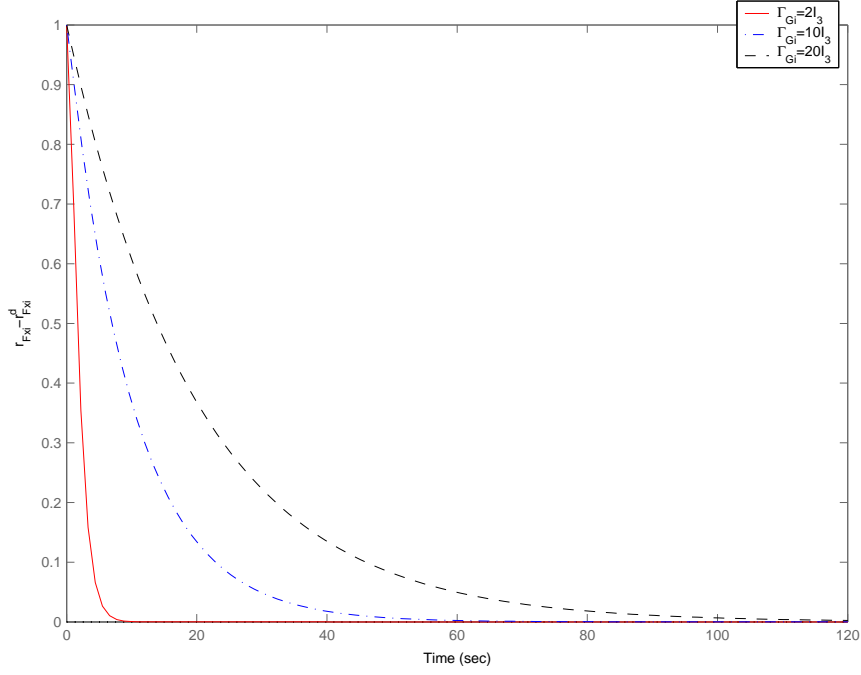


Figure 4.4: Plot of \tilde{r}_{Fxi} with initial conditions $\tilde{r}_{Fxi} = 1$ and $\dot{\tilde{r}}_{Fxi} = 0$ for different choices of Γ_{Gi} .

$V_{Fr}(0)$, and $V_{Fe}(0)$ respectively. Therefore, $\sum_{i=1}^N (r_{Fi} - r_{F(i+1)})^T K_S (r_{Fi} - r_{F(i+1)}) \leq 2V_{Fr}(0)$, $\sum_{i=1}^N \tilde{r}_{Fi}^T K_G \tilde{r}_{Fi} \leq 2V_{Fe}(0)$, $\sum_{i=1}^N \|q_{Fi} - q_{F(i+1)}\|^2 \leq \frac{1}{k_S} V_{Fr}(0)$, $\sum_{i=1}^N \|\tilde{q}_{Fi}\|^2 \leq \frac{1}{k_G} V_{Fe}(0)$, $\sum_{i=1}^N (\lambda_{Fi} - \lambda_{F(i+1)})^T K_S (\lambda_{Fi} - \lambda_{F(i+1)}) \leq 2V_{Fr}(0)$, and $\sum_{i=1}^N \tilde{\lambda}_{Fi}^T K_G \tilde{\lambda}_{Fi} \leq 2V_{Fe}(0)$.

4.2.4 Simulation Results

In this section, we consider a scenario with nine spacecraft. In the scenario, a mothership spacecraft with mass equal to 1500 Kg is located one kilometer away from a plane where eight daughter spacecraft each with mass 150 Kg are distributed equally along a circle with a diameter one kilometer in the plane. The configuration of the nine spacecraft is shown in Fig. 4.5. We assume that the nine spacecraft evolve like a rigid structure, that is, the formation shape is preserved and each spacecraft preserves a fixed relative orientation within the formation throughout the formation maneuvers.

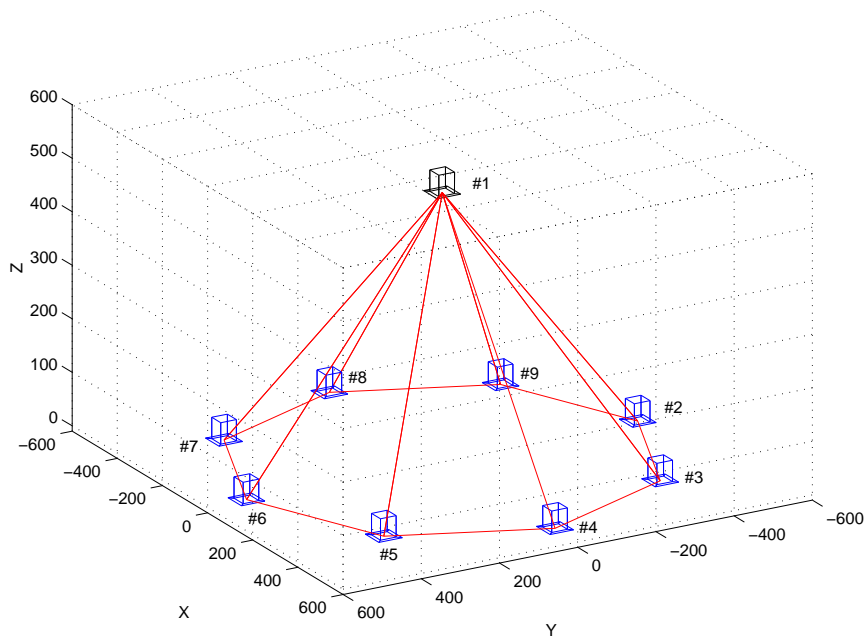


Figure 4.5: The geometric configuration of nine spacecraft.

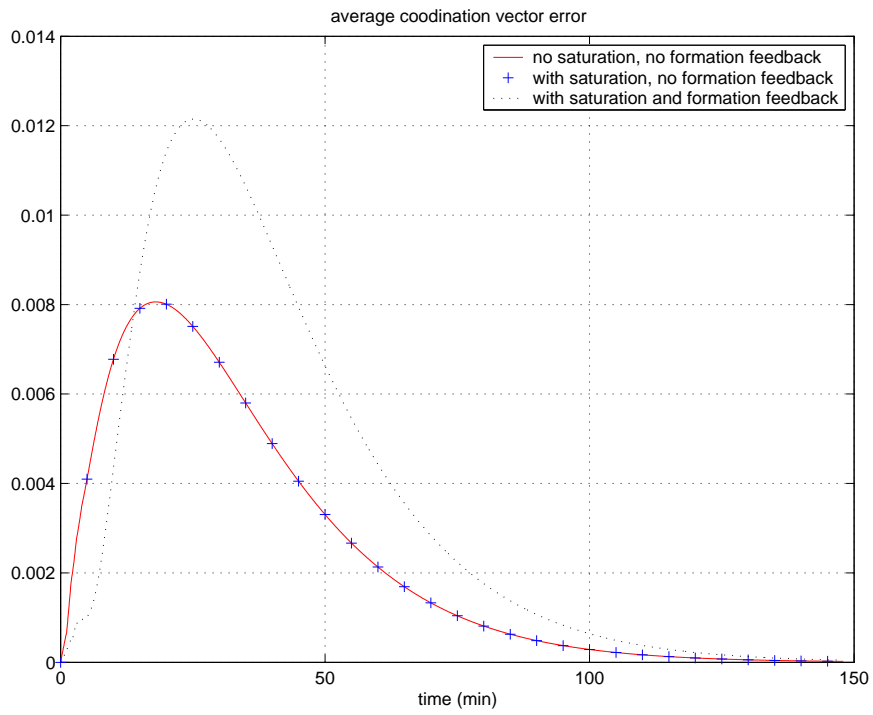


Figure 4.6: The average coordination error of the coordination vector instantiations.

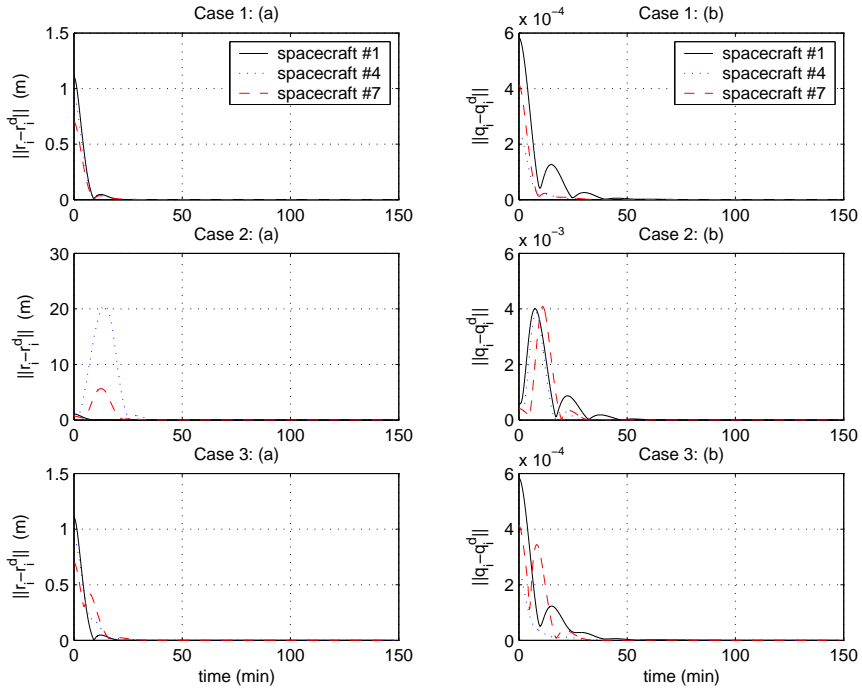


Figure 4.7: The absolute position and attitude tracking errors.

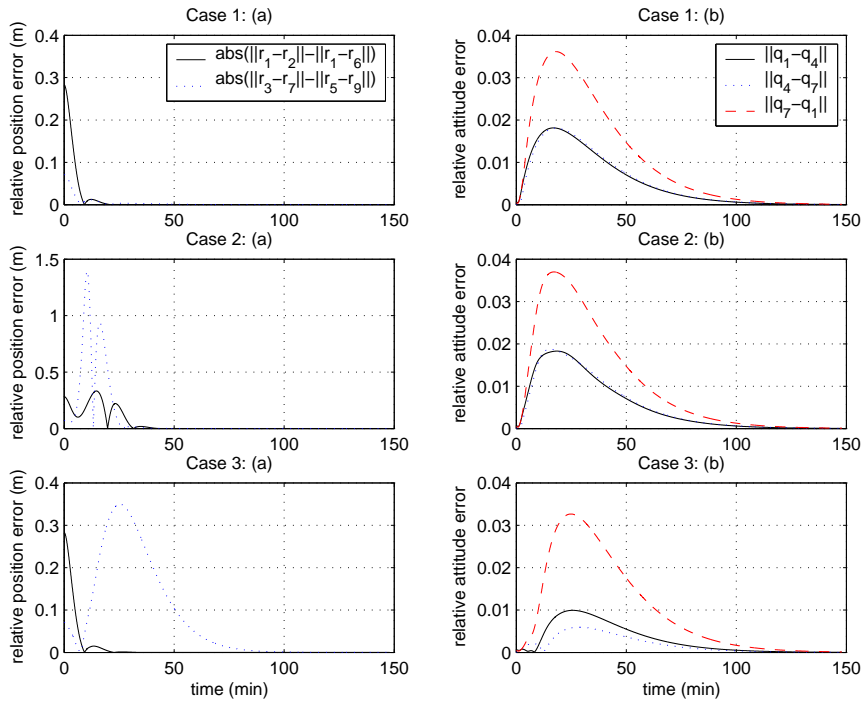


Figure 4.8: The relative position and attitude errors.

We simulate a scenario when the nine spacecraft start from rest with some initial position and attitude errors and then perform a group rotation of 45 degrees about the inertial z axis. Here we assume that each place holder in the formation has the same orientation, that is, q_{iF}^d is the same for each spacecraft. In simulation, we instantiate a local copy of the coordination vector ξ in each spacecraft and synchronize them using the control strategy introduced in the second subsection of Sec. 4.2.3. To show the robustness of the control strategy, we start the coordination vector implementation in each spacecraft at a different time instance and introduce a different sample time varying from 0.4 seconds to 0.6 seconds for each coordination vector instantiation. Various communication delays are also added among spacecraft. Three cases will be compared in this section. These include cases without actuator saturation and formation feedback (case 1), with actuator saturation but without formation feedback (case 2), with both actuator saturation and formation feedback (case 3). In fact, there is another case without actuator saturation but with formation feedback (case 4). Since there is little difference between this case and case 1, we will not include this case in this section. Here we assume that the control force and control torque for spacecraft #1 are saturated at $|f_x|, |f_y|, |f_z| = 2$ N and $|\tau_x|, |\tau_y|, |\tau_z| = 0.0006$ Nm respectively, and the control force and control torque for all the other spacecraft are saturated at $|f_x|, |f_y|, |f_z| = 1$ N and $|\tau_x|, |\tau_y|, |\tau_z| = 0.0003$ Nm respectively.

In this section, the average coordination error is defined as $\frac{1}{N} \sum_{i=1}^N \|\xi_i - \bar{\xi}\|$, where $\bar{\xi} = \frac{1}{N} \sum_{i=1}^N \xi_i$. The average coordination error in these three cases is plotted in Fig. 4.6. We can see that each instantiation of the coordination vector is synchronized asymptotically in all these cases. Also, the average coordination error is large during the initial time interval since each local instantiation starts at a different time instance. Case 1 and 2 are identical since the actuator saturation for each spacecraft does not affect the dynamics of the virtual structure when there is no formation feedback from each spacecraft to its coordination vector instantiation. The maximum average coordination error in case 3 is larger than that in the other two cases since formation feedback is introduced for each coordination vector instantiation, which may add some dissimilarities between different instantiations.

In Fig. 4.7, we plot the absolute position and attitude tracking errors for spacecraft #1, #4, and #7 in these three cases. The position tracking error is defined as $\|r_i - r_i^d\|$ while the attitude tracking error is defined as $\|q_i - q_i^d\|$. We can see the tracking errors in each case will decrease to zero asymptotically by using the control law given in the first subsection of Sec. 4.2.3. The absolute position and attitude tracking errors in case 2 are much larger than those in the other two cases due to the actuator saturation. In case 3, with formation feedback, the absolute position and attitude tracking errors are similar to those in case 1 even if there is actuator saturation. When we increase the entries in the gain matrix K_F to increase formation feedback, the absolute tracking errors can be decreased further but the system convergence time will become longer correspondingly.

In Fig. 4.8, we plot the relative position and attitude errors between some spacecraft in these three cases. Based on the configuration, the desired relative distance between spacecraft #1 and #2 and the desired relative distance between spacecraft #1 and #6 should be equal. The desired relative distance between spacecraft #3 and #7 and the desired relative distance between spacecraft #5 and #9 should also be equal. We plot $|\|r_1 - r_2\| - \|r_1 - r_6\||$ and $|\|r_3 - r_7\| - \|r_5 - r_9\||$ in part (a) as examples to see how well the formation shape is preserved. The desired relative attitude between each spacecraft should be equal based on our previous assumption. We plot $\|q_1 - q_4\|$, $\|q_4 - q_7\|$, and $\|q_7 - q_1\|$ in part (b) as examples to see how well the relative orientation relationships between these spacecraft are preserved. Similarly, the relative position tracking errors in case 2 are larger than those in the other two cases due to the control force saturation. In case 3, with formation feedback, the relative position errors are smaller than those in case 2. The relative attitude errors in case 3 are even smaller than those in the other two cases due to the formation feedback.

In Fig. 4.9, we plot the control effort for spacecraft #1 in these three cases. We can see that both the control force and control torque approach zero asymptotically. We can also see that τ_z saturates in case 2 during the initial time period while this saturation is mitigated with formation feedback introduced in case 3.

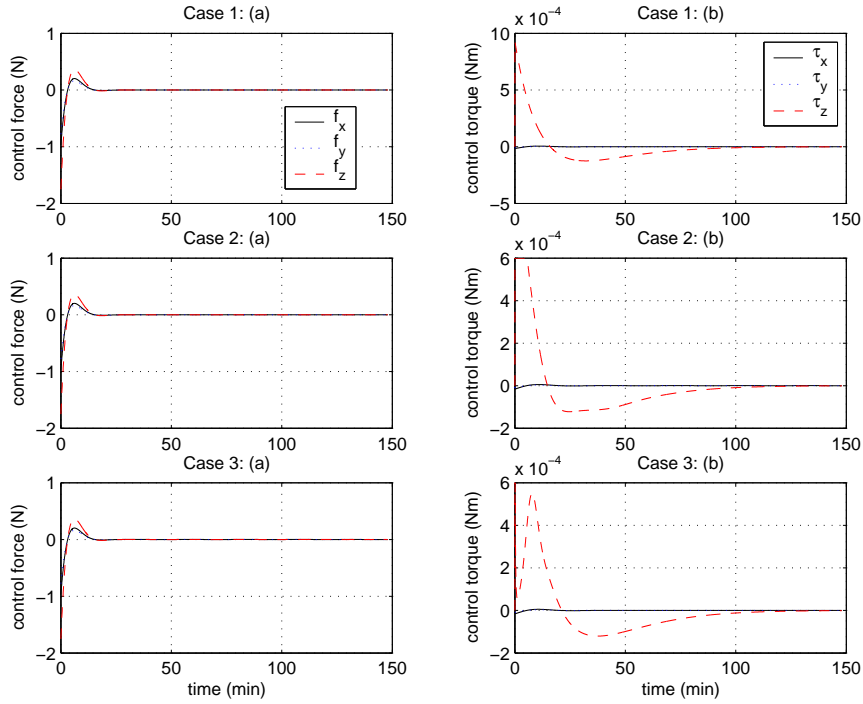


Figure 4.9: The control effort for spacecraft #1.

4.3 Satisficing Approach to Multi-agent Coordinated Control

In this section, we address the problem of multi-agent formation maneuvers by combining the group CLF approach [108] with the satisficing control paradigm [30]. As a result, the application of satisficing controls is extended from regulation problems to multi-agent coordination. We show that under certain conditions a group of satisficing control laws chosen from the robustly satisficing set can guarantee bounded formation keeping error, finite completion time, and reasonable formation velocity as well as inverse optimality and desirable stability margins. This technique is applied to a group of nonholonomic robots in experimental study as a proof of concept.

4.3.1 Satisficing Theory

As models for each individual agent, we will consider only affine nonlinear systems of the form

$$\dot{x} = f(x) + g(x)u, \quad (4.20)$$

where $x \in \mathbb{R}^n$, $f: \mathbb{R}^n \rightarrow \mathbb{R}^n$, $g: \mathbb{R}^n \rightarrow \mathbb{R}^{n \times m}$ and $u \in \mathbb{R}^m$. We will assume throughout the section that f and g are locally Lipschitz functions. A continuously differentiable function $V: \mathbb{R}^n \rightarrow \mathbb{R}$ is said to be a control Lyapunov function (CLF) for the system if V is positive definite, radially unbounded, and if $\inf_u \frac{\partial V}{\partial x}(f + gu) < 0$, for all $x \neq 0$.

The basic idea of satisficing is to define two utility functions that quantify the benefits and costs of an action. At a state x , the benefits of choosing a control u are given by the ‘‘selectability’’ function $p_s(u, x)$. Similarly, at a state x , the costs associated with choosing u are given by the ‘‘rejectability’’ function $p_r(u, x)$. The ‘‘satisficing’’ set is those options for which selectability exceeds rejectability: i.e., $S_b(x) = \{u : p_s(u, x) > \frac{1}{b}p_r(u, x)\}$ where $b(x)$ is a (possibly state-dependent) parameter that can be used to control the size of the set.

As in [30], we will associate the notion of selectability with stability, and the notion of rejectability with instantaneous cost. In particular, let $p_s(u, x) = -\frac{\partial V}{\partial x}(f + gu)$, where V is a known CLF. Obviously, only stabilizing controls will make $p_s(u, x)$ positive. We choose the rejectability criteria to be $p_r(u, x) = l(x) + u^T R(x)u$, where $R(x) = R(x)^T > 0$ is a positive definite matrix function whose elements are locally Lipschitz and $l: \mathbb{R}^n \rightarrow \mathbb{R}$ is a locally Lipschitz non-negative function. For these choices the satisficing set becomes

$$S_b(x) = \left\{ u \in \mathbb{R}^m : -\frac{\partial V}{\partial x}(f + gu) > \frac{1}{b}[l(x) + u^T R(x)u] \right\}. \quad (4.21)$$

Note if the value of b is too small, S_b might be empty. To ensure that the satisficing set is always nonempty we define:

$$\underline{b}(x) \triangleq \begin{cases} \frac{l}{-\frac{\partial V}{\partial x}f}, & \text{if } \frac{\partial V}{\partial x}g = 0 \\ \frac{2\frac{\partial V}{\partial x}f + 2\sqrt{\frac{(\frac{\partial V}{\partial x}f)^2 + l\frac{\partial V}{\partial x}gR^{-1}g^T(\frac{\partial V}{\partial x})^T}}{\frac{\partial V}{\partial x}gR^{-1}g^T(\frac{\partial V}{\partial x})^T}}, & \text{otherwise} \end{cases}. \quad (4.22)$$

From Lemma 5 in [30], we know that for each $x \neq 0$, $\underline{b}(x) \geq 0$, and $b > \underline{b}(x)$ implies that $S_b(x) \neq \emptyset$.

Letting

$$\alpha_1(x, b) \triangleq \frac{1}{2} b R^{-1} g^T \left(\frac{\partial V}{\partial x} \right)^T \quad (4.23)$$

$$\alpha_2(x, b) \triangleq R^{-1/2} \sqrt{\frac{1}{4} b^2 \frac{\partial V}{\partial x} g R^{-1} g^T \left(\frac{\partial V}{\partial x} \right)^T - l - b \frac{\partial V}{\partial x} f}, \quad (4.24)$$

the subscript b on S can be eliminated (S is the union of the sets S_b over all $b > \underline{b}$), and the *satisficing set* for $x \neq 0$, can be characterized as

$$S(x) = \{ -\alpha_1(x, b) + \alpha_2(x, b) \nu : b > \underline{b}(x), \|\nu\| < 1 \},$$

where $\nu \in \mathbb{R}^m$. We know that $S(x)$ is nonempty for $x \neq 0$, and the satisficing set can be parameterized by the two selection functions $b(x) \in \mathbb{R}$ and $\nu(x) \in \mathbb{R}^m$.

The mapping $k : \mathbb{R}^n \rightarrow \mathbb{R}^m$ is called a *satisficing control* if $k(0) = 0$, $k(x) \in S(x)$ for each $x \in \mathbb{R}^n \setminus \{0\}$, and k is locally Lipschitz on $\mathbb{R}^n \setminus \{0\}$. It is shown in [30] that if $k(x)$ is a satisficing control then the closed loop system $\dot{x} = f + gk$ is uniformly asymptotically stable. It is also shown in [30] that if V is a CLF, $\nu : \mathbb{R}^n \rightarrow \mathbb{R}^m$ is locally Lipschitz on $\mathbb{R}^n \setminus \{0\}$ and satisfies $\|\nu(x)\| < 1$, and $b : \mathbb{R}^n \rightarrow \mathbb{R}^+$ is locally Lipschitz on $\mathbb{R}^n \setminus \{0\}$ and satisfies $\underline{b}(x) < b(x)$, then

$$k(x) = \begin{cases} 0, & \text{if } x = 0 \\ -\alpha_1(x, b(x)) + \alpha_2(x, b(x)) \nu(x), & \text{otherwise} \end{cases} \quad (4.25)$$

is a satisficing control.

In [30], the *robust satisficing set*, denoted $S_R(x)$, is defined as

$$\begin{aligned} S_R(x) &= \{ u \in S(x) : \frac{\partial V}{\partial x} g R^{-1/2} \nu \leq 0 \} \\ &= \{ -\alpha_1(x, b) + \alpha_2(x, b) \nu : \\ &\quad b > \underline{b}(x), \|\nu\| < 1, \frac{\partial V}{\partial x} g R^{-1/2} \nu \leq 0 \}. \end{aligned}$$

The mapping $k_R : \mathbb{R}^n \rightarrow \mathbb{R}^m$ is called a *robustly satisficing control* if $k_R(0) = 0$, $k_R(x) \in S_R(x)$ for each $x \in \mathbb{R}^n \setminus \{0\}$, and k_R is locally Lipschitz on $\mathbb{R}^n \setminus \{0\}$. It is shown in [30]

that if k_R is a robustly satisficing control, then it has stability margins equal to $(-\frac{1}{2}, \infty)$ and it is inverse-optimal. It is also shown in [30] that Eq. (4.25) is a robustly satisficing control if $\frac{\partial V}{\partial x} g R^{-1/2} \nu \leq 0$ is also satisfied besides all the other conditions for a satisficing control.

4.3.2 Satisficing Control for Formation Maneuvers

Suppose each agent's dynamics can be described as

$$\dot{x}_i = f_i(x_i) + g_i(x_i)u_i, \quad i = 1, \dots, N, \quad (4.26)$$

where f_i and g_i are locally Lipschitz functions, $x_i \in \mathbb{R}^{n_i}$, and $u_i \in \mathbb{R}^{m_i}$.

In this section we apply the virtual leader/virtual structure approach (c.f. [3, 15, 70, 109]). We define a virtual leader or virtual center of the virtual structure, which in turn defines the rest of the formation, that is, defines the desired state for each agent. Let $x_0(s(t))$ denote the parameterized state of the virtual leader or the virtual center of the virtual structure, where s is a parameter that incorporates error feedback into the whole system through its evolution [109]. Let $x_i^d(s(t))$ represent the desired state of the i th agent, which can be defined from $x_0(s(t))$. Our goal is to construct a group of controllers that guarantee multi-agent coordination in the sense of the framework developed in [108].

Since we have CLF-based techniques developed for the regulation problem, an intuitive way to tackle tracking is to transform it to a regulation problem. Letting $\tilde{x}_i = x_i - x_i^d$ we have that

$$\dot{\tilde{x}}_i = f_i(\tilde{x}_i + x_i^d) - \dot{x}_i^d + g_i(\tilde{x}_i + x_i^d)u_i. \quad (4.27)$$

It is clear that system (4.27) is a time-varying system since x_i^d and \dot{x}_i^d are functions of time. Under certain circumstances it is relatively straightforward to find a CLF $V_i(x_i, x_i^*)$ to regulate $x_i \rightarrow x_i^*$ asymptotically when x_i^* is a constant desired state. Accordingly, we know that $\dot{V}_i = \frac{\partial V_i}{\partial x_i} \dot{x}_i < 0, \forall x_i \neq x_i^*$. If $x_i^d(s(t))$ is a smooth desired state, we can replace x_i^* in the CLF $V_i(x_i, x_i^*)$ with $x_i^d(s(t))$ to obtain $V_i(x_i, x_i^d(s(t)))$. If $V_i(x_i, x_i^d(s(t)))$ is smooth and $\frac{\partial V_i}{\partial x_i} \dot{x}_i < 0, \forall x_i \neq x_i^d(s)$, for each specific $s \in [s_1, s_2]$, we can view $V_i(x_i, x_i^d(s(t)))$ as a pointwise (in s) CLF to regulate x_i to $x_i^d(s)$ in a pointwise fashion. We have the following definition to formally define a pointwise CLF.

Definition 4.3.1 A continuously differentiable function $V_i : \mathbb{R}^{n_i} \times \mathbb{R}^{n_i} \rightarrow \mathbb{R}$ is a pointwise control Lyapunov function (pCLF) for system (4.26) if it is positive definite, radially unbounded, and satisfies

$$\inf_{u_i \in \mathbb{R}^{m_i}} \left\{ \frac{\partial V_i(x_i, x_i^d(s))}{\partial x_i} [f_i(x_i) + g_i(x_i)u_i] \right\} < 0, \quad (4.28)$$

$\forall x_i \neq x_i^d(s)$ and each constant $s \in [s_1, s_2]$.

Hereafter we assume that a pointwise CLF can be found for a smooth parameterized desired trajectory $x_i^d(s)$, that is, $V_i(x_i, x_i^d(s)) = 0$ at $x_i = x_i^d(s)$ for each $s \in [s_1, s_2]$. We also assume that $V_i(x_i, x_i^d(s)) \rightarrow \infty$ if $\|x_i - x_i^d(s)\| \rightarrow \infty$ for any $s \in [s_1, s_2]$. Note that $\dot{V}_i = \frac{\partial V_i}{\partial x_i} \dot{x}_i + \frac{\partial V_i}{\partial s} \dot{s}$. Although \dot{V}_i is not necessarily negative, we can use satisficing control to guarantee that $\frac{\partial V_i}{\partial x_i} \dot{x}_i < 0$, a property which is necessary for our later result.

Following the definition in [108], we define a formation measure function as

$$F(x, s) = \sum_{i=1}^N \beta_i V_i(x_i(t), x_i^d(s)), \quad (4.29)$$

where V_i is the pointwise CLF for each agent and $\beta_i > 0$, to represent the tracking performance. The formation is defined to be preserved if $F(x, s) \leq F_U$, where F_U is an upper bound on the formation measure function $F(x, s)$.

Following [108], let \dot{s} be given by

$$\dot{s} = \begin{cases} \min \left\{ \frac{v_0}{\delta + \left\| \frac{\partial x_0(s)}{\partial s} \right\|}, \frac{-\frac{\partial F}{\partial x} \dot{x}}{\delta + \left| \frac{\partial F}{\partial s} \right|} \left(\frac{\sigma(F_U)}{\sigma(F(x, s))} \right) \right\}, & s_1 \leq s < s_2 \\ 0, & s = s_2 \end{cases}, \quad (4.30)$$

where $\delta > 0$ is a small positive constant, v_0 is the nominal velocity for the formation, and $\sigma(\cdot)$ is a class \mathcal{K} function. Therefore, formation maneuvers are performed in two steps. First, when $s_1 \leq s < s_2$, the formation is preserved within some boundary given by F_U . Second, when $s = s_2$, each agent is regulated to a constant desired state given by $x_i^d(s_2)$ and reaches (eventually) its final goal.

Lemma 4.3.1 If \dot{s} is given by Eq. (4.30), then $F(x(t_0), s(t_0)) \leq F_U$ implies that $F(x(t), s(t)) \leq F_U, \forall t \geq t_0$. Furthermore, given a class \mathcal{K} function $\sigma_i(\cdot)$, if $s \in [s_1, s_2]$ and there is

a control $u_i(x_i, s)$ and an arbitrary constant $\mu_i > 0$ such that $\frac{-\frac{\partial V_i}{\partial x_i} \dot{x}_i}{\sigma_i(V_i(x_i, x_i^d(s)))} \geq \mu_i$ and $\frac{-\frac{\partial V_i}{\partial x_i} \dot{x}_i}{\sigma_i(V_i(x_i, x_i^d(s)))} \rightarrow \infty$ as $V_i \rightarrow 0$, $i = 1, \dots, N$, then s will reach s_2 within finite time and $\left\| \frac{dx_0}{dt} \right\| \approx v_0$ for $F(x, s) \ll F_U$ and $\delta v_0 \ll \left\| \frac{\partial x_0(s)}{\partial s} \right\|$.

Proof: see [108]. ■

The satisficing control framework for time-invariant systems can be used to find a class of valid control laws. We extend satisficing control from the regulation problems to the pointwise time-varying regulation problems. Let $V_i(x_i, x_i^d(s))$ be the pointwise CLF for each specific $s \in [s_1, s_2]$, which will be used to regulate x_i to $x_i^d(s)$. Also let $l_i(x_i, x_i^d(s)) = \sigma_i(V_i(x_i, x_i^d(s)))$. We use $\frac{\partial V_i(x_i, x_i^d(s))}{\partial x_i}$ and $l_i(x_i, x_i^d(s))$ to replace $\frac{\partial V}{\partial x}$ and l in Eqs. (4.22), (4.23), and (4.24) respectively to obtain $b_i(x_i, x_i^d(s))$, $\alpha_1(x_i, b_i)$, and $\alpha_2(x_i, b_i)$. A robustly satisficing control for the i th agent in the formation is now given by

$$u_i(x_i, s) = -\alpha_1(x_i, b_i) + \alpha_2(x_i, b_i)\nu_i, \quad (4.31)$$

where $\nu_i: \mathbb{R}^n \times \mathbb{R}^n \rightarrow \mathbb{R}^{m_i}$ is locally Lipschitz on $\mathbb{R}^n \setminus \{x_i^d(s)\}$ and satisfies $\|\nu_i(x_i, x_i^d(s))\| < 1$, $\frac{\partial V_i}{\partial x_i} g_i R_i^{-1/2} \nu_i \leq 0$, and $b_i: \mathbb{R}^n \times \mathbb{R}^n \rightarrow \mathbb{R}^+$ is locally Lipschitz on $\mathbb{R}^n \setminus \{x_i^d(s)\}$ and satisfies $\underline{b}_i(x_i, x_i^d(s)) < b_i(x_i, x_i^d(s))$. Therefore, we know that the control law (4.31) guarantees inverse optimality and desirable stability margins from a pointwise perspective.

The following theorem shows that the class of robustly satisficing controllers satisfy the conditions of Lemma 4.3.1.

Theorem 4.3.2 *If $s \in [s_1, s_2]$, \dot{s} is given by Eq. (4.30), and $u_i(x_i, s)$ is given by Eq. (4.31) with $\sigma_i(\cdot)$ chosen properly, then the robustly satisficing control law (4.31) satisfies all desired properties for a feasible control law specified in Lemma 4.3.1. Moreover, the control law (4.31) guarantees that $F(x, s) < F_U$ for all $t > T$ for arbitrary $F(x(s(t_0)), s(t_0))$, where T is some finite constant.*

Proof: For the first part of the proof, it can be verified that $F(x, s)$ is ultimately bounded due to the fact that $\dot{F}(x, s) < 0$ if $F(x(t), s(t)) \geq F_U$ following the definition of \dot{s} . Therefore, we know that $\|x_i - x_i^d(s)\|$ is bounded. Since $s \in [s_1, s_2]$ and $x_i^d(s)$ is smooth, it is straightforward to see that $\|x_i^d\|$ is bounded, which implies that $\|x_i\|$ is also bounded. Noting that $l_i = \sigma_i(V_i) > 0$, $\forall x_i \neq x_i^d(s)$, we get that \underline{b}_i is locally Lipschitz on $\mathbb{R}^n \setminus \{x_i^d(s)\}$

following Lemma 6 in [30]. When $x_i \rightarrow x_i^d(s)$, function $\sigma_i(\cdot)$ can be chosen such that $l_i = \sigma_i(V_i(x_i, x_i^d(s)))$ has a sufficiently high order to guarantee that

$$\lim_{x_i \rightarrow x_i^d(s)} -\frac{\sigma_i(V_i)}{\frac{\partial V_i}{\partial x_i} f_i}$$

and

$$\lim_{x_i \rightarrow x_i^d(s)} \frac{2\frac{\partial V_i}{\partial x_i} f_i + 2\sqrt{(\frac{\partial V_i}{\partial x_i} f_i)^2 + l_i \frac{\partial V_i}{\partial x_i} g_i R_i^{-1} g_i^T (\frac{\partial V_i}{\partial x_i})^T}}{\frac{\partial V_i}{\partial x_i} g_i R_i^{-1} g_i^T (\frac{\partial V_i}{\partial x_i})^T}$$

are bounded. Combining all the above arguments, we know that \underline{b}_i is bounded, $\forall x_i \neq x_i^d(s)$. Accordingly, an upper bounded b_i can be chosen to be above the bounded \underline{b}_i , e.g. $b_i = \underline{b}_i + \kappa_i$, where κ_i is any positive constant. In the following, we suppose that $0 < b_i < L_i$, where L_i is a positive constant.

Following Eq. (4.21), we know that

$$\begin{aligned} & -\frac{\partial V_i}{\partial x_i} \dot{x}_i > \frac{1}{b_i} (l_i + u_i^T R_i u_i) \\ \implies & -\frac{\partial V_i}{\partial x_i} \dot{x}_i > \frac{1}{b_i} (\sigma_i(V_i) + u_i^T R_i u_i) \\ \implies & -\frac{\partial V_i}{\partial x_i} \dot{x}_i > \frac{\sigma_i(V_i)}{b_i} \\ \implies & \frac{-\frac{\partial V_i}{\partial x_i} \dot{x}_i}{\sigma_i(V_i)} > \frac{1}{L_i}. \end{aligned}$$

Note again that $\sigma_i(\cdot)$ can be chosen to have a higher order such that $\frac{-\frac{\partial V_i}{\partial x_i} \dot{x}_i}{\sigma_i(V_i)} \rightarrow \infty$ as $V_i \rightarrow 0$ (see Lemma II.2 in [6] for an example of selection). As a result, the desired properties for a feasible control law in Lemma 4.3.1 are satisfied correspondingly.

For the second part of the proof, note that $\frac{\partial F}{\partial s} = \sum_{i=1}^N \beta_i \frac{\partial V_i}{\partial x_i^d} \frac{\partial x_i^d}{\partial s}$. Since $s \in [s_1, s_2]$, $x_i^d(s)$ is smooth, and both $\|x_i^d\|$ and $\|x_i\|$ are bounded, we get that $\|\frac{\partial V_i}{\partial x_i^d}\|$ and $\|\frac{\partial x_i^d}{\partial s}\|$ are also bounded. Therefore, $|\frac{\partial F}{\partial s}|$ is bounded. In the following we suppose that $|\frac{\partial F}{\partial s}| < B$, where B is a positive upper bound.

If $F(x, s) \geq F_U$ at any time t , we can get

$$1 - \frac{\frac{\partial F}{\partial s}}{\delta + |\frac{\partial F}{\partial s}|} \left(\frac{\sigma(F_U)}{\sigma(F(x, s))} \right) > \frac{\delta}{B + \delta} = M. \quad (4.32)$$

Since $u_i(x_i, s)$ is a satisficing control, from Eq. (4.21), we know that

$$\begin{aligned}\frac{\partial F}{\partial x} \dot{x}_i &= \sum_{i=1}^N \beta_i \frac{\partial V_i}{\partial x_i} \dot{x}_i \\ &\leq - \sum_{i=1}^N \frac{\beta_i (l_i(x_i, x_i^d) + u_i^T R_i u_i)}{b_i(x_i, x_i^d)}.\end{aligned}$$

Note that

$$\begin{aligned}\dot{F}(x, s) &= \frac{\partial F}{\partial x} \dot{x} + \frac{\partial F}{\partial s} \dot{s}(x, s) \\ &\leq \frac{\partial F}{\partial x} \dot{x} + \frac{\partial F}{\partial s} \frac{-\frac{\partial F}{\partial x} \dot{x}}{\delta + |\frac{\partial F}{\partial s}|} \left(\frac{\sigma(F_U)}{\sigma(F(x, s))} \right) \\ &= \frac{\partial F}{\partial x} \dot{x} \left[1 - \frac{\frac{\partial F}{\partial s}}{\delta + |\frac{\partial F}{\partial s}|} \left(\frac{\sigma(F_U)}{\sigma(F(x, s))} \right) \right] \\ &\leq - \sum_{i=1}^N \frac{\beta_i (l_i(x_i, x_i^d) + u_i^T R_i^T u_i)}{b_i(x_i, x_i^d)} M \\ &\leq - \sum_{i=1}^N \frac{\beta_i l_i(x_i, x_i^d)}{L_i} M.\end{aligned}\tag{4.33}$$

Let $W_3(x, s) = \sum_{i=1}^N \frac{\beta_i l_i(x_i, x_i^d)}{L_i} M$, then $W_3(x, s) > 0, \forall x_i \neq x_i^d$. From Theorem 3.8 in [110], F will keep decreasing until $F(x, s) < F_U$. Here we assume that F will keep decreasing until $F(x, s) < F_U$ before s reaches s_2 . If not, we know that

$$\frac{\partial F}{\partial x} \dot{x} = \sum_{i=1}^N \beta_i \frac{\partial V_i}{\partial x_i} \dot{x}_i < 0$$

when $s = s_2$. In this case, F will keep decreasing to zero.

If $F(x, s) < F_U$ at some time t_1 , we assume that $F(x, s)$ will increase and exceed F_U at some time. Suppose it reaches the upper bound F_U at some time t_2 , where $t_2 > t_1$. We know that $\dot{F}(s(t_2), x(t_2)) < 0$ from Eq. (4.33), that is, once $F(x, s)$ reaches F_U from below, it will decrease immediately and cannot exceed F_U . Therefore, $F(x, s) < F_U$ within finite time for arbitrary initial formation error. ■

From the above proof, we note that the upperbound F_U is not necessarily a constant throughout the formation maneuvers. We can set F_U as a function of time, for example, a decreasing staircase function or an exponentially decreasing function and so on based on the requirement for formation keeping. By choosing a smaller F_U , the formation will evolve correspondingly more slowly.

4.3.3 Application Example

In this section we use robustly satisficing controllers to perform formation maneuvers for a group of nonholonomic robots. The kinematic equations for these robots are:

$$\begin{aligned}\dot{x}_i &= v_i \cos(\phi_i) \\ \dot{y}_i &= v_i \sin(\phi_i) \\ \dot{\phi}_i &= \omega_i,\end{aligned}$$

where (x_i, y_i) is the Cartesian position of the i th robot, ϕ_i is the orientation of the i th robot, and (v_i, ω_i) is the control input. The translational motion of the robot in the direction perpendicular to the drive axis is restricted, which is known as the nonholonomic constraint. A common technique is to use feedback linearization [111] to simplify the dynamics for a fixed point off the center of the wheel axis which can be denoted as (x_{hi}, y_{hi}) . The disadvantage of doing this is that the angular information about the robot is lost. The off axis position is given by the equations

$$\begin{aligned}x_{hi} &= x_i + L_i \cos(\phi_i) \\ y_{hi} &= y_i + L_i \sin(\phi_i).\end{aligned}$$

Thus the output dynamics are

$$\begin{pmatrix} \dot{x}_{hi} \\ \dot{y}_{hi} \end{pmatrix} = R(\phi_i) \begin{pmatrix} v_i \\ L_i \omega_i \end{pmatrix},$$

where $R(\cdot)$ is the rotation matrix. Setting v_i and $L_i \omega_i$ in the control to

$$\begin{pmatrix} v_i \\ L_i \omega_i \end{pmatrix} = R(-\phi_i) \begin{pmatrix} u_{xi} \\ u_{yi} \end{pmatrix},$$

we obtain

$$\begin{pmatrix} \dot{x}_{hi} \\ \dot{y}_{hi} \end{pmatrix} = \begin{pmatrix} u_{xi} \\ u_{yi} \end{pmatrix}.$$

It is obvious that $f_i(z_i) = 0$, $g_i(z_i) = \text{diag}\{1, 1\}$, where $z_i = [x_{hi}, y_{hi}]^T$, and $u_i = (u_{xi}, u_{yi})$. Let $V_i = \frac{1}{2}(x_{hi} - x_{hi}^d)^2 + \frac{1}{2}(y_{hi} - y_{hi}^d)^2$, which is a valid (pointwise in s)

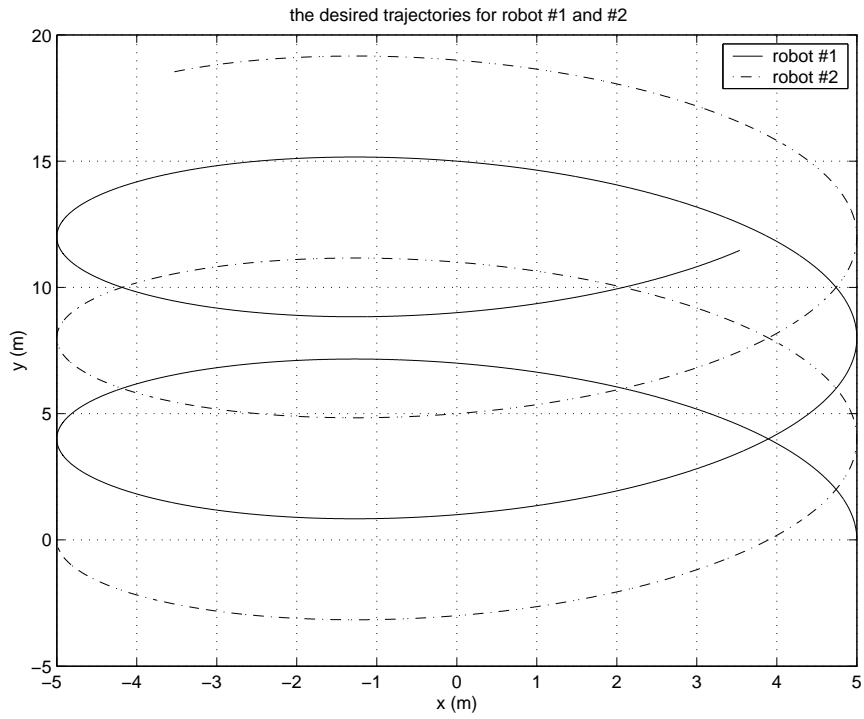


Figure 4.10: The desired trajectories for robot #1 and #2.

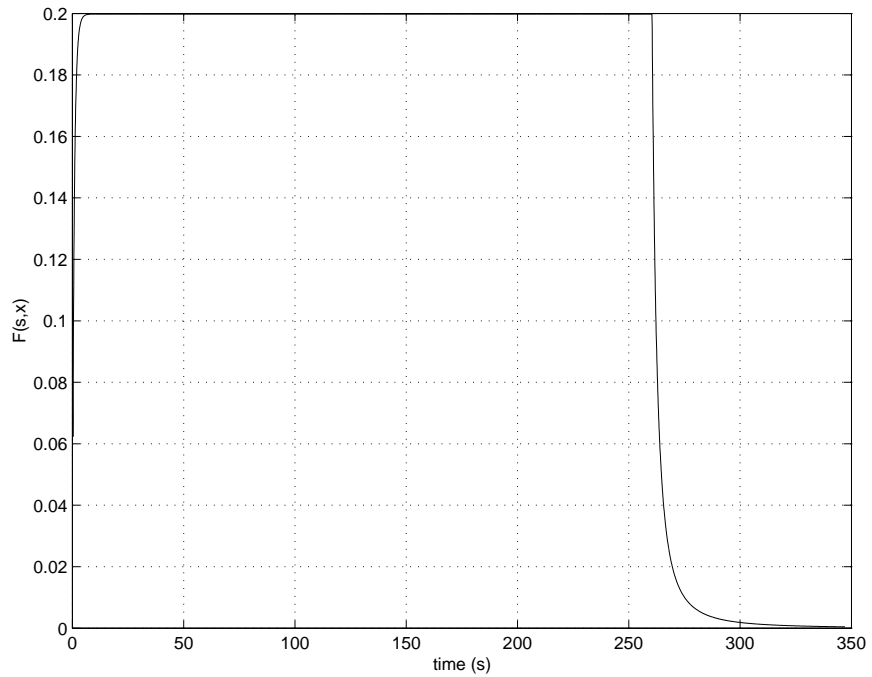


Figure 4.11: The formation function $F(x, s)$ with $F(x(t_0), s(t_0)) = 0.1$.

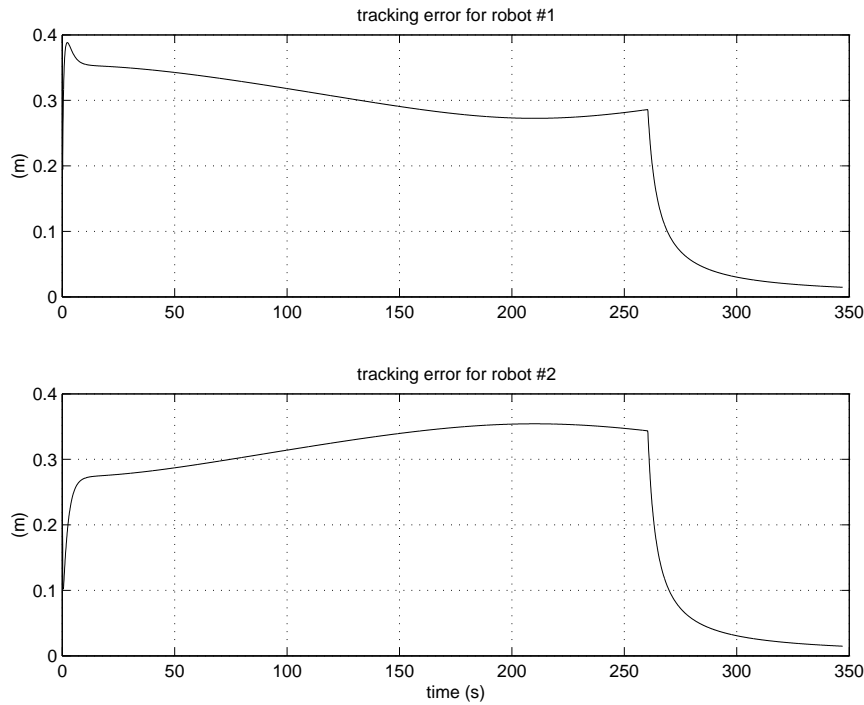


Figure 4.12: The tracking errors for robot #1 and #2 with $F(x(t_0), s(t_0)) = 0.1$.

CLF for the i th robot. Define $F(x, s) = 2 \sum_{i=1}^N V_i(x_{hi}, x_{hi}^d(s))$ as the formation measure function. Let $\sigma_i(V_i) = V_i^2$ and use robustly satisficing control for the robots. Although we use a very simple model here, the general idea of using robustly satisficing control for formation maneuvers is feasible for any affine nonlinear system for which a pointwise CLF can be found.

We will simulate two robots moving in a spiral formation. Set $F_U = 0.2$ and let $s \in [0, 5]$. The desired distance between these two robots is 10 meters. The center of the line connecting the desired positions of the two robots, i.e., the virtual center of the formation, tracks a trajectory (x_{h0}, y_{h0}) given by $(0, s)$. Also the line connecting the desired positions of the two robots rotates about its center counterclockwise with an angle given by $\omega_0 s$. The desired states for the two robots are (x_{hi}^d, y_{hi}^d) which are given by $(5 \cos(\omega_0 s), s + 5 \sin(\omega_0 s))$ and $(-5 \cos(\omega_0 s), s - 5 \sin(\omega_0 s))$ respectively. The two robots start from rest with some initial errors.

In Fig. 4.10, we plot the desired trajectories for robot #1 and #2. The actual trajectories almost coincide with the desired ones. To see the pattern clearly, we let $s \in [0, 15]$. In Fig. 4.11, we plot $F(x, s)$ when the initial formation error is below the upper bound F_U . We can see that the formation error is always bounded by F_U . The tracking errors for robot #1 and #2 in this case are shown in Fig. 4.12. In Fig. 4.13, we plot $F(x, s)$ when the initial formation error is above the upper bound F_U . We can see that even if the initial formation error is above the upper bound, $F(x, s)$ decreases quickly until it is bounded by F_U . The tracking errors for robot #1 and #2 in this case are shown in Fig. 4.14. From Fig. 4.11 and Fig. 4.13, we can see that $F \approx F_U$ when the multi-agent system is far away from its final goal. But when $s = s_2$, $F(x, s)$ will decrease to zero so that each agent can be regulated to its final state. From Fig. 4.11 and Fig. 4.13, we can also see that the completion time for s to reach s_2 , which is 5 in this example, is about 261 seconds. Therefore, the system has finite completion time.

Hardware tests are conducted in a 4.5 meters by 4.5 meters testbed in BYU MAGICC Laboratory. To show the effectiveness of the control laws, two robots will perform a spiral formation with various desired distances during the maneuver. An overhead vision system mounted on the ceiling is used to measure the positions and orientations of the two robots. Fig. 4.15 shows the mobile robots used in the experiment. Fig. 4.16 shows the desired and actual distance between the two robots during the maneuver with $F_U = 0.1$. It can be seen that formation is preserved well during the maneuver. Fig. 4.17 shows the corresponding formation measure function. Note that $F(x, s)$ decreases and stays below F_U for initial formation errors above F_U .

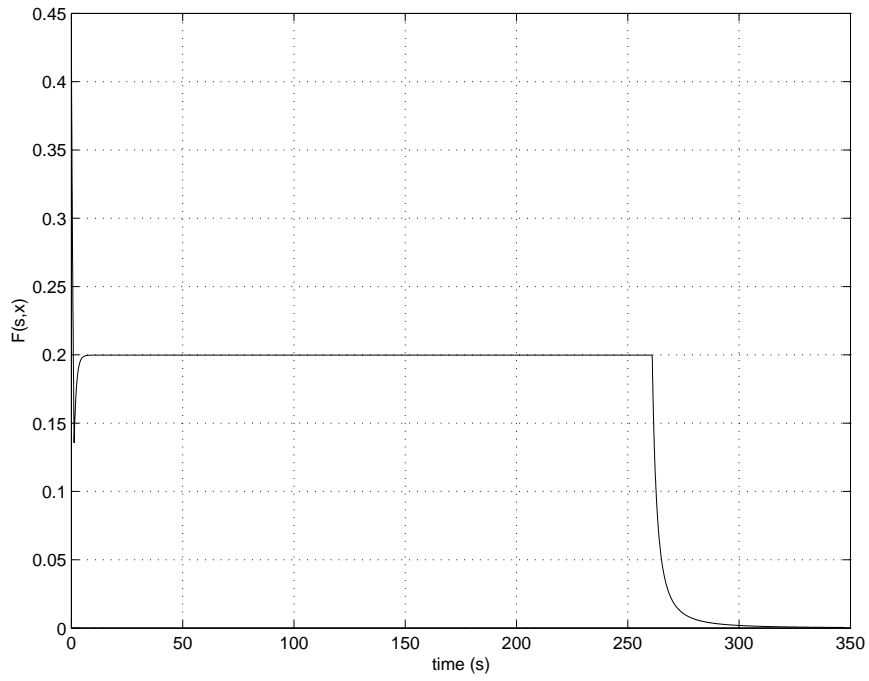


Figure 4.13: The formation function $F(x, s)$ with $F(x(t_0), s(t_0)) = 0.43$.

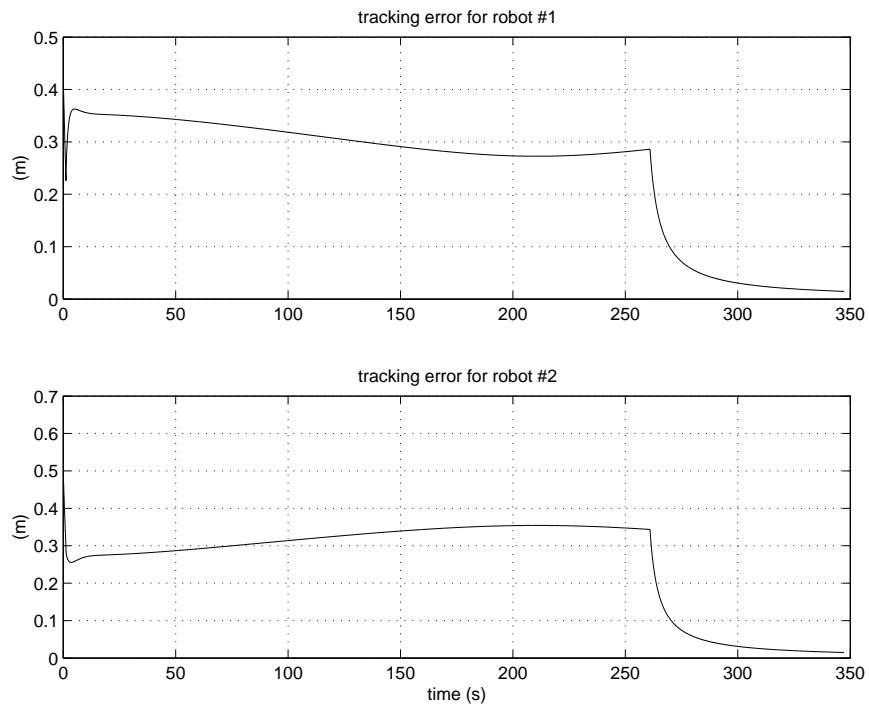


Figure 4.14: The tracking errors for robot #1 and #2 with $F(x(t_0), s(t_0)) = 0.43$.



Figure 4.15: Canister robots used in the experiment.

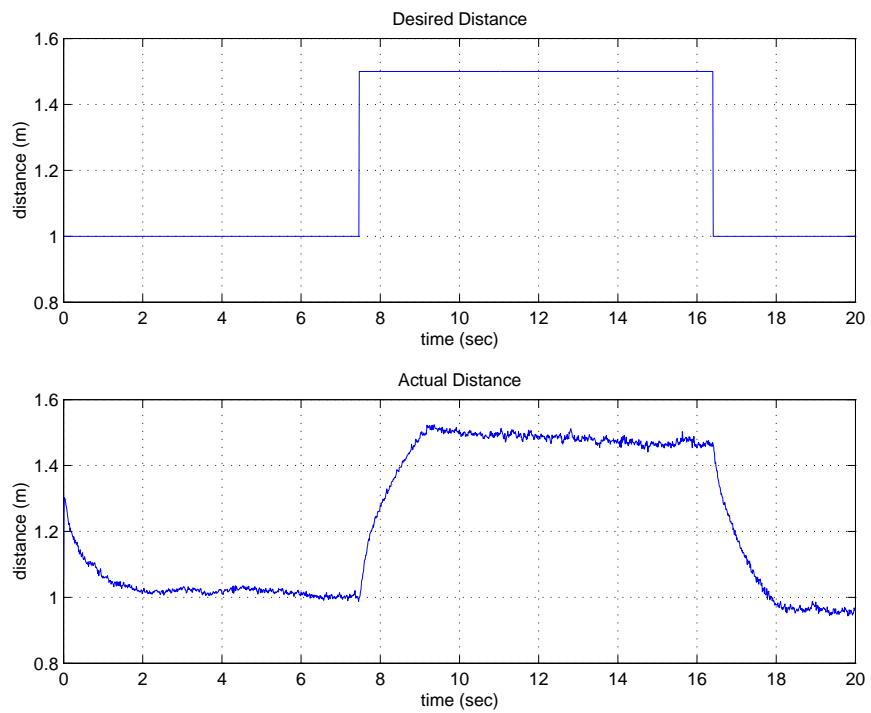


Figure 4.16: The commanded desired distance and actual distance between the two robots with $F_U = 0.1$.

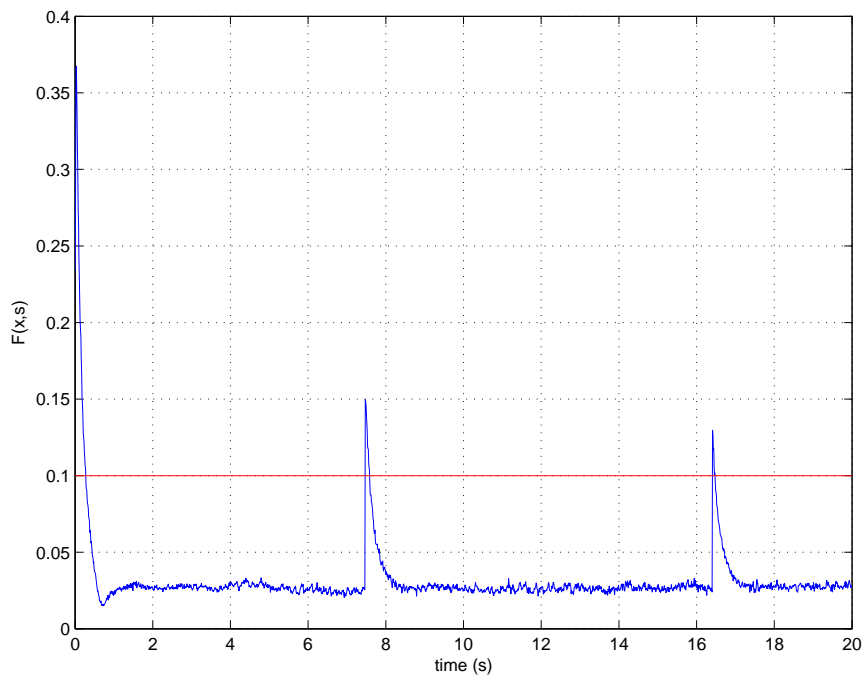


Figure 4.17: Formation measure function $F(x, s)$ with $F_U = 0.1$.

Chapter 5

Trajectory Tracking Control with Input Constraints

5.1 Introduction

This chapter presents some new results on trajectory tracking control strategies. Although we discuss trajectory tracking control in the context of cooperative control, e.g. trajectory tracking in cooperative timing missions [96, 27], these control strategies can be applied to general scenarios.

In Section 5.2, we consider the problem of constrained nonlinear tracking control for small fixed-wing unmanned air vehicles (UAVs). An input-to-state control Lyapunov function (ISS-CLF) based technique is used to design nonlinear tracking controllers for UAVs with velocity and heading rate constraints. In Section 5.3.2, we apply the same design strategies to tracking control of nonholonomic mobile robots with input constraints similar to those of fixed-wing UAVs. Experimental results of the nonlinear tracking controllers for a nonholonomic mobile robot are presented as a proof of concept.

5.2 Trajectory Tracking for UAVs with Velocity and Heading Rate Constraints

The inherent properties of fixed-wing UAVs impose the input constraints of positive minimum velocity due to the stall conditions of the aircraft, bounded maximum velocity, and saturated heading rate. Unmanned air vehicles equipped with low-level altitude-hold, velocity-hold, and heading-hold autopilots can be modelled by kinematic equations of motion that are similar to those of nonholonomic mobile robots. However, existing approaches for mobile robots (c.f. [77, 78, 85, 84]) are not directly applicable to our problem

since negative velocities are allowed in these approaches. This section deals with the issue of tracking control for UAV kinematic models with physically motivated heading rate and velocity constraints. We approach the problem using constrained CLFs. While our approach is designed for UAVs in particular, it is also valid for mobile robot kinematic models with similar input constraints.

We take the following approach to UAV trajectory tracking. We first propose a time-varying, constrained CLF for the UAV kinematic model. Following [30], the CLF is used to define a state-dependent, time-varying set of “feasible” control values from which different controllers can be instantiated. Selection from this feasible control set, guarantees accurate tracking as well as satisfaction of the saturation constraints. As noted in [30], different control strategies can be derived by selection from the feasible control set according to some auxiliary performance index. This approach introduces a great deal of flexibility to the tracking control problem. In this section we propose a simple selection scheme based on saturation functions. The motivation for this selection scheme is computational simplicity. It is worthwhile to mention that the existing CLF-based universal formulas introduced in [95, 94] are not feasible in the UAV case due to its special input constraints, that is, controls are constrained to lie in a rectangle.

The salient features of our approach are as follows: First, under the proposed tracking CLF framework with input constraints, we allow the reference velocity and angular velocity to be piecewise continuous while other approaches to tracking control (e.g. [85, 84]) constrain them to be uniformly continuous in order to apply Barbalat’s lemma. Second, using different selection schemes, our approach can be used to derive a variety of other trajectory tracking strategies. Finally, it is computationally simple and can be implemented on off-the-shelf inexpensive microcontrollers. To illustrate the effectiveness of the controller, we apply our approach to a UAV scenario, where the UAV is assigned to transition through several opportunities in the presence of dynamic hazards. Instead of following simple paths composed of straight lines and circles (e.g. [85, 84]), the UAV tracks a trajectory generated dynamically from the trajectory generator described in [112], which responds the current, possibly time-varying, opportunity/hazard scenario presented to the UAV.

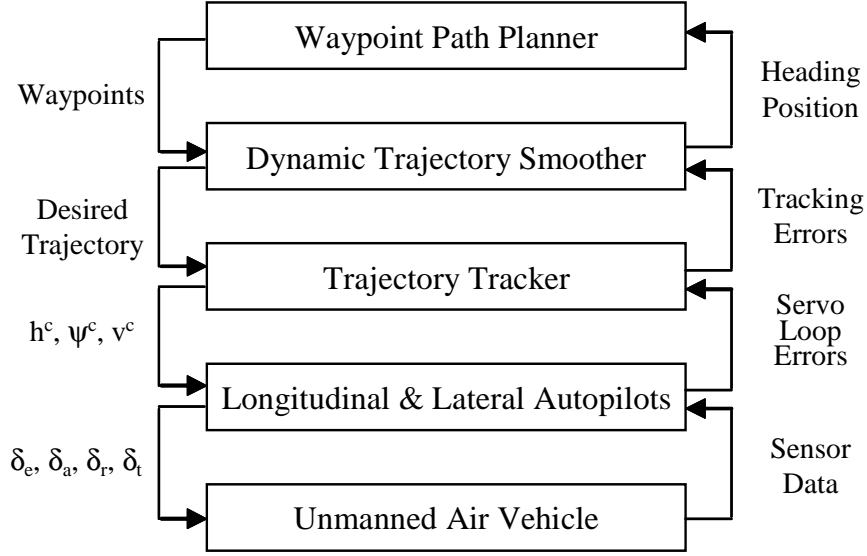


Figure 5.1: System architecture.

5.2.1 Problem Statement

As shown in Fig. 5.1, the overall system architecture considered in this section consists of five layers [45]: Waypoint Path Planner (WPP), Dynamic Trajectory Smoother (DTS), Trajectory Tracker (TT), Longitudinal and Lateral Autopilots, and the UAV.

The WPP generates waypoint paths (straight-line segments) that change in accordance with the dynamic environment consisting of the location of the UAV, the targets, and the dynamically changing threats. The DTS smoothes through these waypoints and produces a feasible time-parameterized desired trajectory, that is, the desired position $(x_r(t), y_r(t))$, heading $\psi_r(t)$, and altitude $h_r(t)$. The TT outputs the velocity command v^c , heading command ψ^c , and altitude command h^c to the autopilots based on the desired trajectory. The autopilots then use these commands to control the elevator, δ_e , aileron, δ_a , rudder δ_r , and throttle δ_t , of the UAV [45]. In this section we focus on the trajectory tracker.

With the UAV equipped with standard autopilots, the resulting UAV/autopilot models are assumed to be first order for heading and Mach hold, and second order for altitude hold [80]. Letting (x, y) , ψ , v , and h denote the inertial position, heading angle, velocity, and altitude of the UAV respectively, the kinematic equations of motion are given by

$$\begin{aligned}
\dot{x} &= v \cos(\psi) \\
\dot{y} &= v \sin(\psi) \\
\dot{\psi} &= \alpha_\psi(\psi^c - \psi) \\
\dot{v} &= \alpha_v(v^c - v), \\
\ddot{h} &= -\alpha_h \dot{h} + \alpha_h(h^c - h),
\end{aligned} \tag{5.1}$$

where ψ^c , v^c , and h^c are the commanded heading angle, velocity, and altitude to the autopilots, and α_* are positive constants [80].

Assuming that α_v is large, v converges to v^c quickly relative to the time-scale of the other dynamics, the first four equations in Eq. (5.1) reduce to

$$\begin{aligned}
\dot{x} &= v^c \cos(\psi) \\
\dot{y} &= v^c \sin(\psi) \\
\dot{\psi} &= \alpha_\psi(\psi^c - \psi).
\end{aligned} \tag{5.2}$$

In the remainder of the section, we assume that the altitude controller follows the design presented in [27], and focus on the design of the velocity and heading controller based on Eq. (5.2). Letting $\psi^c = \psi + \frac{1}{\alpha_\psi}\omega^c$, Eq. (5.2) becomes

$$\begin{aligned}
\dot{x} &= v^c \cos(\psi) \\
\dot{y} &= v^c \sin(\psi) \\
\dot{\psi} &= \omega^c.
\end{aligned} \tag{5.3}$$

The dynamics of the UAV impose the following input constraints

$$\begin{aligned}
\mathcal{U}_1 = \{v^c, \omega^c | 0 < v_{min} \leq v^c \leq v_{max}, \\
-\omega_{max} \leq \omega^c \leq \omega_{max}\}.
\end{aligned} \tag{5.4}$$

Note that if $v_{min} = -v_{max}$, then Eq. (5.3) is the same as the kinematic model for a mobile robot with similar input constraints.

We will assume that the desired reference trajectory $(x_r, y_r, \psi_r, v_r, \omega_r)$ produced by the DTS satisfies

$$\begin{aligned}\dot{x}_r &= v_r \cos(\psi_r) \\ \dot{y}_r &= v_r \sin(\psi_r) \\ \dot{\psi}_r &= \omega_r,\end{aligned}$$

where v_r and ω_r are piecewise continuous and satisfy the constraints

$$\begin{aligned}v_{min} + \epsilon_v &\leq v_r \leq v_{max} - \epsilon_v \\ -\omega_{max} + \epsilon_\omega &\leq \omega_r \leq \omega_{max} - \epsilon_\omega,\end{aligned}\tag{5.5}$$

where ϵ_v and ϵ_ω are positive control parameters. The inclusion of ϵ_* in the constraints of the reference trajectory generator, guarantees that there is sufficient control authority to track the trajectory. We will see that as ϵ_* approach zero, the feasible control set vanishes. The control objective is to find feasible control inputs v^c and ω^c such that $|x_r - x| + |y_r - y| + |\psi_r - \psi| \rightarrow 0$ as $t \rightarrow \infty$.

Transforming the tracking errors expressed in the inertial frame to the UAV frame, the error coordinates [113] can be denoted as

$$\begin{bmatrix} x_e \\ y_e \\ \psi_e \end{bmatrix} = \begin{bmatrix} \cos(\psi) & \sin(\psi) & 0 \\ -\sin(\psi) & \cos(\psi) & 0 \\ 0 & 0 & 1 \end{bmatrix} \begin{bmatrix} x_r - x \\ y_r - y \\ \psi_r - \psi \end{bmatrix}.\tag{5.6}$$

Accordingly, the tracking error model can be represented as

$$\begin{aligned}\dot{x}_e &= \omega^c y_e - v^c + v_r \cos(\psi_e) \\ \dot{y}_e &= -\omega^c x_e + v_r \sin(\psi_e) \\ \dot{\psi}_e &= \omega_r - \omega^c.\end{aligned}\tag{5.7}$$

Following [84], Eq. (5.7) can be simplified as

$$\begin{aligned}\dot{x}_0 &= u_0 \\ \dot{x}_1 &= (\omega_r - u_0)x_2 + v_r \sin(x_0) \\ \dot{x}_2 &= -(\omega_r - u_0)x_1 + u_1,\end{aligned}\tag{5.8}$$

where

$$(x_0, x_1, x_2) \triangleq (\psi_e, y_e, -x_e) \quad (5.9)$$

and $u_0 \triangleq \omega_r - \omega^c$ and $u_1 \triangleq v^c - v_r \cos(x_0)$.

The input constraints under the transformation become

$$\mathcal{U}_2 = \{u_0, u_1 | \underline{\omega} \leq u_0 \leq \bar{\omega}, \underline{v} \leq u_1 \leq \bar{v}\}, \quad (5.10)$$

where $\underline{\omega} \triangleq \omega_r - \omega_{max}$, $\bar{\omega} \triangleq \omega_r + \omega_{max}$, $\underline{v} \triangleq v_{min} - v_r \cos(x_0)$, and $\bar{v} \triangleq v_{max} - v_r \cos(x_0)$ are time-varying.

Obviously, Eqs. (5.6) and (5.9) are invertible transformations, which means $(x_0, x_1, x_2) = (0, 0, 0)$ is equivalent to $(x_e, y_e, \psi_e) = (0, 0, 0)$, or in other words $(x_r, y_r, \psi_r) = (x, y, \psi)$. Therefore, the original tracking control objective is converted to a stabilization objective. That is, our goal is to find feasible control inputs u_0 and u_1 to stabilize x_0 , x_1 , and x_2 .

Note from Eq. (5.8) that when both x_0 and x_2 go to zero, that x_1 becomes uncontrollable. To avoid this situation we introduce another change of variables. Let $\bar{x}_0 = mx_0 + \frac{x_1}{\pi_1}$, where $m > 0$ and $\pi_1 \triangleq \sqrt{x_1^2 + x_2^2 + 1}$. Accordingly, $x_0 = \frac{\bar{x}_0}{m} - \frac{x_1}{m\pi_1}$. Obviously, $(\bar{x}_0, x_1, x_2) = (0, 0, 0)$ is equivalent to $(x_0, x_1, x_2) = (0, 0, 0)$. Therefore it is sufficient to find control inputs u_0 and u_1 to stabilize \bar{x}_0 , x_1 , and x_2 . With the same input constraints (5.10), Eq. (5.8) can be rewritten as

$$\dot{x} = f_1(t, x) + g_1(t, x)[u_0, u_1]^T, \quad (5.11)$$

where $x = [\bar{x}_0, x_1, x_2]^T$,

$$f_1(t, x) = \begin{bmatrix} \frac{x_2}{\pi_1} \omega_r + \frac{1+x_2^2}{\pi_1^3} v_r \sin\left(\frac{\bar{x}_0}{m} - \frac{x_1}{m\pi_1}\right) \\ x_2 \omega_r + v_r \sin\left(\frac{\bar{x}_0}{m} - \frac{x_1}{m\pi_1}\right) \\ -\omega_r x_1 \end{bmatrix}$$

and

$$g_1(t, x) = \begin{bmatrix} m - \frac{x_2}{\pi_1} & -\frac{x_1 x_2}{\pi_1^3} \\ -x_2 & 0 \\ x_1 & 1 \end{bmatrix}.$$

5.2.2 CLF for Tracking Control with Saturation Constraints

In this section, we find a valid CLF for UAV trajectory tracking with input constraints. Consider the following class of affine nonlinear time-varying systems

$$\dot{x} = f(t, x) + g(t, x)u, \quad (5.12)$$

where $x \in \mathbb{R}^n$, $u \in \mathbb{R}^m$, and $f : \mathbb{R}_+ \times \mathbb{R}^n \rightarrow \mathbb{R}^n$ and $g : \mathbb{R}_+ \times \mathbb{R}^n \rightarrow \mathbb{R}^{n \times m}$ are locally Lipschitz in x and piecewise continuous in t .

Definition 5.2.1 (see [87]) *A continuously differentiable function $V : \mathbb{R}_+ \times \mathbb{R}^n \rightarrow \mathbb{R}$ is a control Lyapunov function (CLF) for system (5.12) with input constraints $u \in \mathcal{U} \subset \mathbb{R}^m$ if it is positive-definite, decrescent, radially unbounded in x , and satisfies*

$$\inf_{u \in \mathcal{U}} \left\{ \frac{\partial V}{\partial t} + \frac{\partial V}{\partial x} (f(t, x) + g(t, x)u) \right\} \leq -W(x), \quad (5.13)$$

$\forall x \neq 0$ and $\forall t \geq 0$ where $W(x)$ is a continuous positive-definite function.

In order to find a CLF with bounded input constraints, we prefer the partial derivative of V to be bounded. Accordingly, we have the following lemma.

Lemma 5.2.1 *If $P(x) = \sqrt{x^T x + 1} - 1$, then $P(x)$ is continuously differentiable, radially unbounded, positive-definite, and $\left\| \frac{\partial P}{\partial x} \right\| \leq 1$.*

Proof: Trivial. ■

Lemma 5.2.1 will be used to construct a CLF for system (5.11). The following lemma defines a continuous positive-definite function that will be used in the construction of the CLF.

Lemma 5.2.2 *Let*

$$W(x) = \gamma_0 \left(\frac{\bar{x}_0}{\pi_2} \right)^2 + \gamma_1 k_1 (v_{\min} + \epsilon_v) \frac{x_1}{\pi_1} \sin \left(\frac{x_1}{m\pi_1} \right) + \gamma_2 \left(k_1 - \frac{1}{2} \right) \left(\frac{x_2}{\pi_1} \right)^2 \left[(v_{\min} + \epsilon_v) \cos \left(\frac{x_1}{m\pi_1} \right) - v_{\min} \right], \quad (5.14)$$

where $\pi_2 \triangleq \sqrt{\bar{x}_0^2 + 1}$. If $k_1 > \frac{1}{2}$, $\gamma_i > 0$, and $m > 2 / \cos^{-1} \left(\frac{v_{\min}}{v_{\min} + \epsilon_v} \right)$, then $W(x)$ is continuous and positive-definite.

Proof: Since W is a composition of continuous functions, it is continuous. The first term in Eq. (5.14) is clearly positive and zero if and only if $\bar{x}_0 = 0$. The second term in Eq. (5.14) is nonnegative if $\left| \frac{x_1}{m\pi_1} \right| < \pi$. But since

$$\left| \frac{x_1}{m\pi_1} \right| < \frac{1}{m} < \cos^{-1} \left(\frac{v_{\min}}{v_{\min} + \epsilon_v} \right) / 2 < \pi/4, \quad (5.15)$$

the second term is positive and zero if and only if $x_1 = 0$. Since

$$\begin{aligned} \left| \frac{x_1}{m\pi_1} \right| &< \cos^{-1} \left(\frac{v_{\min}}{v_{\min} + \epsilon_v} \right) / 2 < \cos^{-1} \left(\frac{v_{\min}}{v_{\min} + \epsilon_v} \right) \\ \implies \cos \left(\frac{x_1}{m\pi_1} \right) &> \frac{v_{\min}}{v_{\min} + \epsilon_v} \\ \iff (v_{\min} + \epsilon_v) \cos \left(\frac{x_1}{m\pi_1} \right) - v_{\min} &> 0, \end{aligned} \quad (5.16)$$

the third term in Eq. (5.14) is positive and zero if and only if $x_2 = 0$. ■

The following theorem defines a valid CLF for UAV trajectory tracking with input constraints.

Theorem 5.2.2 *The function*

$$\begin{aligned} V &= P(\bar{x}_0) + k_1 P \begin{pmatrix} x_1 \\ x_2 \end{pmatrix} \\ &= \sqrt{\bar{x}_0^2 + 1} + k_1 \sqrt{x_1^2 + x_2^2 + 1} - (1 + k_1) \end{aligned}$$

satisfies $\inf_{u \in \mathcal{U}_2} \left\{ \frac{\partial V}{\partial x} (f_1 + g_1 u) \right\} \leq -W(x)$, that is, V is a CLF for system (5.11) with input constraints (5.10), if $W(x)$ is given by Lemma 5.2.2, $0 < \gamma_1 < 1$, $0 < \gamma_2 < 1$ and

$$m > \max \left\{ M_0, 1 + \frac{d_2}{\epsilon_\omega} \right\},$$

where

$$M_0 \triangleq \max \left\{ \frac{2}{\cos^{-1} \left(\frac{v_{\min}}{v_{\min} + \epsilon_v} \right)}, 1 + \sqrt{2} \frac{d_1}{\epsilon_\omega} \right\} \quad (5.17)$$

$$\begin{aligned} d_1 \triangleq & \left(k_1 + \frac{1}{2} \right) [2v_{\max} - \epsilon_v] + \gamma_2 \left(k_1 - \frac{1}{2} \right) \epsilon_v \\ & + k_1 [(v_{\max} - \epsilon_v) + \gamma_1 (v_{\min} + \epsilon_v)] \\ & + (\omega_{\max} - \epsilon_\omega) + (v_{\max} - \epsilon_v) + \gamma_0 \end{aligned} \quad (5.18)$$

$$\begin{aligned} d_2 \triangleq & (v_{\max} - \epsilon_v) \left[\sqrt{2} \left(k_1 - \frac{1}{2} \right) \frac{M_2}{M_0} + \sqrt{2} k_1 \frac{M_1}{M_0} + 1 \right] \\ & + (\omega_{\max} - \epsilon_\omega) + \gamma_0 \end{aligned} \quad (5.19)$$

and

$$M_1 \triangleq \sup_{\substack{0 < |\alpha| < 1/M_0 \\ |\beta| < 1/M_0}} \left| \frac{\sin(\alpha - \beta) + \sin(\beta)}{\alpha} \right| \quad (5.20)$$

$$M_2 \triangleq \sup_{\substack{0 < |\alpha| < 1/M_0 \\ |\beta| < 1/M_0}} \left| \frac{\cos(\beta) - \cos(\alpha - \beta)}{\alpha} \right|. \quad (5.21)$$

Proof: Obviously V is positive-definite, decrescent, and radially unbounded, therefore it remains to show that $\dot{V} + W_3 \leq 0$ for all x .

Differentiating V and setting $u_0 = -\epsilon_\omega \text{sign}(\bar{x}_0)$, we obtain the following expression after some algebraic manipulation:

$$\begin{aligned} \dot{V} + W_3(x) = & -\epsilon_\omega \frac{|\bar{x}_0|}{\pi_2} \left(m - \frac{x_2}{\pi_1} \right) \\ & + \sigma_1 u_1 + \sigma_2 + \sigma_3 + \sigma_4 \end{aligned} \quad (5.22)$$

where

$$\begin{aligned} \sigma_1 &= \left(k_1 - \frac{\bar{x}_0 x_1}{\pi_2 \pi_1^2} \right) \left(\frac{x_2}{\pi_1} \right) \\ \sigma_2 &= \gamma_2 \left(k_1 - \frac{1}{2} \right) \left(\frac{x_2}{\pi_1} \right)^2 \left[(v_{\min} + \epsilon_v) \cos \left(\frac{x_1}{m \pi_1} \right) - v_{\min} \right] \\ \sigma_3 &= k_1 \left(\frac{x_1}{\pi_1} \right) \left[v_r \sin \left(\frac{\bar{x}_0}{m} - \frac{x_1}{m \pi_1} \right) + \gamma_1 (v_{\min} + \epsilon_v) \sin \left(\frac{x_1}{m \pi_1} \right) \right] \\ \sigma_4 &= \left(\frac{\bar{x}_0}{\pi_2} \right) \left[\frac{x_2}{\pi_1} \omega_r + \frac{1 + x_2^2}{\pi_1^3} v_r \sin \left(\frac{\bar{x}_0}{m} - \frac{x_1}{m \pi_1} \right) + \gamma_0 \left(\frac{\bar{x}_0}{\pi_2} \right) \right]. \end{aligned}$$

Three cases will be considered with respect to \bar{x}_0 .

Case 1: $|\bar{x}_0| \geq 1$.

Since $|\bar{x}_0/\pi_2| < 1$, $|x_1/\pi_1^2| < 1/2$, and $|\frac{x_2}{\pi_1}| < 1$, we know that $|\sigma_1| \leq (k_1 + 1/2)$. Note that

$$\begin{aligned}\sigma_1 u_1 &\leq (k_1 + 1/2)(2v_{\max} - \epsilon_v) \\ \sigma_2 &\leq \gamma_2(k_1 - 1/2)\epsilon_v \\ \sigma_3 &\leq k_1 [(v_{\max} - \epsilon_v) + \gamma_1(v_{\min} + \epsilon_v)] \\ \sigma_4 &\leq (\omega_{\max} - \epsilon_\omega) + (v_{\max} - \epsilon_v) + \gamma_0.\end{aligned}$$

Since $m > 1 + \sqrt{2}d_1/\epsilon_\omega$, we get that

$$\begin{aligned}\dot{V} + W_3 &\leq -\epsilon_\omega \frac{|\bar{x}_0|}{\pi_2} (m - 1) + d_1 \\ &\leq -\frac{\epsilon_\omega}{\sqrt{2}} (m - 1) + d_1 < 0,\end{aligned}$$

where the second inequality comes from $\frac{|\bar{x}_0|}{\pi_2} \geq 1/\sqrt{2}$ since $|\bar{x}_0| \geq 1$.

Case 2: $0 < |\bar{x}_0| < 1$.

Eq. (5.22) can be arranged as

$$\dot{V} + W_3 = \frac{|\bar{x}_0|}{\pi_2} \left\{ -\epsilon_\omega \left(m - \frac{x_2}{\pi_1}\right) + \frac{\pi_2}{|\bar{x}_0|} [\sigma_1 u_1 + \sigma_2 + \sigma_3 + \sigma_4] \right\}.$$

We will show that

$$d_2 \geq \frac{\pi_2}{|\bar{x}_0|} (\sigma_1 u_1 + \sigma_2) + \frac{\pi_2}{|\bar{x}_0|} \sigma_3 + \frac{\pi_2}{|\bar{x}_0|} \sigma_4, \quad (5.23)$$

which implies that $m > 1 + d_2/\epsilon_\omega$ guarantees that $\dot{V} + W_3 \leq 0$.

Set

$$u_1 = \begin{cases} v_{\min} - v_r \cos\left(\frac{\bar{x}_0}{m} - \frac{x_1}{m\pi_1}\right), & x_2 \geq 0 \\ v_{\max} - v_r \cos\left(\frac{\bar{x}_0}{m} - \frac{x_1}{m\pi_1}\right), & x_2 < 0. \end{cases} \quad (5.24)$$

For the first term in Eq. (5.23), consider the following two cases with regard to

x_2 .

(1): $x_2 \geq 0$.

Noting that $(x_2/\pi_1)^2 \leq |x_2|/\pi_1$ and

$$\begin{aligned} \left| \frac{\bar{x}_0}{m} - \frac{x_1}{m\pi_1} \right| &< 2/m < \cos^{-1} \left(\frac{v_{\min}}{v_{\min} + \epsilon_v} \right) \\ \implies v_{\min} - v_r \cos \left(\frac{\bar{x}_0}{m} - \frac{x_1}{m\pi_1} \right) &< 0, \end{aligned} \quad (5.25)$$

$$\begin{aligned} \left| \frac{\bar{x}_0 x_1}{\pi_2 \pi_1^2} \right| &< \frac{1}{2} \\ \implies \left(k_1 - \frac{\bar{x}_0 x_1}{\pi_2 \pi_1^2} \right) &> \left(k_1 - \frac{1}{2} \right), \end{aligned} \quad (5.26)$$

$$\begin{aligned} \cos \left(\frac{x_1}{m\pi_1} \right) &> 0 \\ \implies (v_{\min} + \epsilon_v) \cos \left(\frac{x_1}{m\pi_1} \right) - v_{\min} &\leq v_r \cos \left(\frac{x_1}{m\pi_1} \right) - v_{\min}, \end{aligned} \quad (5.27)$$

the first term in Eq. (5.23) can be bounded as follows:

$$\begin{aligned} &\frac{\pi_2}{|\bar{x}_0|} (\sigma_1 u_1 + \sigma_2) \\ &= \frac{\pi_2}{|\bar{x}_0|} \left\{ \left(k_1 - \frac{\bar{x}_0 x_1}{\pi_2 \pi_1^2} \right) \left(\frac{|x_2|}{\pi_1} \right) \left[v_{\min} - v_r \cos \left(\frac{\bar{x}_0}{m} - \frac{x_1}{m\pi_1} \right) \right] \right. \\ &\quad \left. + \gamma_2 \left(k_1 - 1/2 \right) \left(\frac{x_2}{\pi_1} \right)^2 \left[(v_{\min} + \epsilon_v) \cos \left(\frac{x_1}{m\pi_1} \right) - v_{\min} \right] \right\} \\ &\leq \frac{\pi_2}{|\bar{x}_0|} \left\{ \left(k_1 - 1/2 \right) \left(\frac{|x_2|}{\pi_1} \right) \left[v_{\min} - v_r \cos \left(\frac{\bar{x}_0}{m} - \frac{x_1}{m\pi_1} \right) \right] \right. \\ &\quad \left. + \left(k_1 - 1/2 \right) \left(\frac{|x_2|}{\pi_1} \right) \left[v_r \cos \left(\frac{x_1}{m\pi_1} \right) - v_{\min} \right] \right\} \\ &\leq \pi_2 \left(k_1 - \frac{1}{2} \right) v_r \frac{1}{m} \left| \frac{\cos \left(\frac{x_1}{m\pi_1} \right) - \cos \left(\frac{\bar{x}_0}{m} - \frac{x_1}{m\pi_1} \right)}{|\bar{x}_0|/m} \right| \\ &\leq \sqrt{2} \left(k_1 - 1/2 \right) (v_{\max} - \epsilon_v) \frac{1}{M_0} M_2, \end{aligned}$$

where the last inequality comes from $1/m < 1/M_0$, $\pi_2 < \sqrt{2}$ since $0 < |\bar{x}_0| < 1$, and Eq. (5.21) by letting $\alpha = \bar{x}_0/m$ and $\beta = x_1/m\pi_1$.

(2): $x_2 < 0$.

Noting that $v_{\max} - v_r \cos \left(\frac{\bar{x}_0}{m} - \frac{x_1}{m\pi_1} \right) \geq \epsilon_v$ and $(v_{\min} + \epsilon_v) \cos \left(\frac{x_1}{m\pi_1} \right) - v_{\min} \leq \epsilon_v$, we get that

$$\frac{\pi_2}{|\bar{x}_0|} (\sigma_1 u_1 + \sigma_2)$$

$$\begin{aligned}
&= \frac{\pi_2}{|\bar{x}_0|} \left\{ \left(k_1 - \frac{\bar{x}_0 x_1}{\pi_2 \pi_1^2} \right) \left(-\frac{|x_2|}{\pi_1} \right) \left[v_{\max} - v_r \cos \left(\frac{\bar{x}_0}{m} - \frac{x_1}{m\pi_1} \right) \right] \right. \\
&\quad \left. + \gamma_2 (k_1 - 1/2) \left(\frac{x_2}{\pi_1} \right)^2 \left[(v_{\min} + \epsilon_v) \cos \left(\frac{x_1}{m\pi_1} \right) - v_{\min} \right] \right\} \\
&\leq \frac{\pi_2}{|\bar{x}_0|} \left\{ \left(k_1 - \frac{1}{2} \right) \left(-\frac{|x_2|}{\pi_1} \right) \epsilon_v + \gamma_2 (k_1 - \frac{1}{2}) \left(\frac{|x_2|}{\pi_1} \right) \epsilon_v \right\} \leq 0.
\end{aligned}$$

The second term in Eq. (5.23) can be bounded as follows:

$$\begin{aligned}
&\frac{\pi_2}{|\bar{x}_0|} \sigma_3 \\
&\leq \frac{\pi_2}{|\bar{x}_0|} \left[k_1 v_r \left(\frac{x_1}{\pi_1} \right) \sin \left(\frac{\bar{x}_0}{m} - \frac{x_1}{m\pi_1} \right) \right. \\
&\quad \left. + k_1 v_r \left(\frac{x_1}{\pi_1} \right) \sin \left(\frac{x_1}{m\pi_1} \right) \right] \\
&\leq \pi_2 k_1 v_r \left| \frac{x_1}{\pi_1} \right| \frac{1}{m} \left| \frac{\sin \left(\frac{\bar{x}_0}{m} - \frac{x_1}{m\pi_1} \right) + \sin \left(\frac{x_1}{m\pi_1} \right)}{|\bar{x}_0|/m} \right| \\
&\leq \sqrt{2} k_1 (v_{\max} - \epsilon_v) \frac{1}{M_0} M_1,
\end{aligned}$$

where the first inequality comes from $\frac{x_1}{\pi_1} \sin \left(\frac{x_1}{m\pi_1} \right) \geq 0$ according to (5.15), and the last inequality comes from $\pi_2 < \sqrt{2}$, $1/m < 1/M_0$, and Eq. (5.20) by letting $\alpha = \bar{x}_0/m$ and $\beta = x_1/m\pi_1$.

The third term in Eq. (5.23) can be bounded as follows:

$$\begin{aligned}
&\frac{\pi_2}{|\bar{x}_0|} \sigma_4 \\
&= \frac{\pi_2}{|\bar{x}_0|} \frac{\bar{x}_0}{\pi_2} \left[\frac{x_2}{\pi_2} \omega_r + \frac{1 + x_2^2}{\pi_1^3} v_r \sin \left(\frac{\bar{x}_0}{m} - \frac{x_1}{m\pi_1} \right) + \gamma_0 \frac{\bar{x}_0}{\pi_2} \right] \\
&\leq \left| \frac{x_2}{\pi_1} \omega_r \right| + \left| \frac{1 + x_2^2}{\pi_1^3} v_r \sin \left(\frac{\bar{x}_0}{m} - \frac{x_1}{m\pi_1} \right) \right| + \gamma_0 \left| \frac{\bar{x}_0}{\pi_2} \right| \\
&\leq (\omega_{\max} - \epsilon_\omega) + (v_{\max} - \epsilon_v) + \gamma_0.
\end{aligned}$$

Combining these expressions gives the desired result.

Case 3: $\bar{x}_0 = 0$.

In this case we have $\dot{V} + W_3 = \sigma_1(u_1 + \sigma_2) + \sigma_3$. For σ_3 we have

$$\begin{aligned}\sigma_3 &= k_1 \left(\frac{x_1}{\pi_1} \right) \sin \left(\frac{x_1}{m\pi_1} \right) [\gamma_1(v_{\min} + \epsilon_v) - v_r] \\ &\leq k_1 \left(\frac{x_1}{\pi_1} \right) \sin \left(\frac{x_1}{m\pi_1} \right) v_r(\gamma_1 - 1) \leq 0.\end{aligned}$$

From Eq. (5.24),

$$u_1 = \begin{cases} v_{\min} - v_r \cos \left(\frac{x_1}{m\pi_1} \right), & x_2 \geq 0 \\ v_{\max} - v_r \cos \left(\frac{x_1}{m\pi_1} \right), & x_2 < 0. \end{cases} \quad (5.28)$$

Consider the following two cases with regard to x_2 .

(1): $x_2 \geq 0$.

Similar to Case 2, we get that

$$\begin{aligned}&\sigma_1 u_1 + \sigma_2 \\ &= k_1 \left(\frac{|x_2|}{\pi_1} \right) \left[v_{\min} - v_r \cos \left(\frac{x_1}{m\pi_1} \right) \right] \\ &\quad + \gamma_2(k_1 - 1/2) \left(\frac{x_2}{\pi_1} \right)^2 [(v_{\min} + \epsilon_v) \cos \left(\frac{x_1}{m\pi_1} \right) - v_{\min}] \\ &\leq k_1 \left(\frac{|x_2|}{\pi_1} \right) \left[v_{\min} - v_r \cos \left(\frac{x_1}{m\pi_1} \right) \right] \\ &\quad + \gamma_2 k_1 \left(\frac{|x_2|}{\pi_1} \right) [v_r \cos \left(\frac{x_1}{m\pi_1} \right) - v_{\min}] \\ &= (\gamma_2 - 1) k_1 \left(\frac{|x_2|}{\pi_1} \right) \left[v_r \cos \left(\frac{x_1}{m\pi_1} \right) - v_{\min} \right],\end{aligned}$$

which is nonpositive since $0 < \gamma_2 < 1$ and $m > 1/\cos^{-1}(v_{\min}/(v_{\min} + \epsilon_v))$.

(2): $x_2 < 0$.

Similar to Case 2, we get that

$$\begin{aligned}&\sigma_1 u_1 + \sigma_2 \\ &= k_1 \left(-\frac{|x_2|}{\pi_1} \right) [v_{\max} - v_r \cos \left(\frac{x_1}{m\pi_1} \right)] \\ &\quad + \gamma_2(k_1 - 1/2) \left(\frac{x_2}{\pi_1} \right)^2 [(v_{\min} + \epsilon_v) \cos \left(\frac{x_1}{m\pi_1} \right) - v_{\min}] \\ &\leq k_1 \left(-\frac{|x_2|}{\pi_1} \right) \epsilon_v + \gamma_2 k_1 \left(\frac{|x_2|}{\pi_1} \right) \epsilon_v\end{aligned}$$

$$\leq (\gamma_2 - 1)k_1 \left(\frac{|x_2|}{\pi_1} \right) \epsilon_v,$$

which is also nonpositive. ■

It is straightforward to show that M_1 and M_2 in Eqs. (5.20) and (5.21) are bounded as $|\alpha|$ approaches both 0 and $1/M_0$. Therefore M_1 and M_2 are finite and can be found by straightforward optimization techniques.

Theorem 5.2.2 demonstrates that V is a valid CLF for system (5.11) under saturation constraints (5.10). Note that a very conservative upper bound is found for m in each case for simplicity of the proof. In reality, m can be much smaller than the upper bound specified above.

5.2.3 Nonlinear Tracking Control based on CLF

With the CLF given in Theorem 5.2.2, our goal in this section is to find a family of feasible tracking control laws based on this CLF.

Define the feasible control set as

$$\mathcal{F}(t, x) = \{u \in \mathcal{U}_2 \mid \frac{\partial V}{\partial x} g_1(t, x)u + \frac{\partial V}{\partial x} f_1(t, x) \leq -W(x)\},$$

where V is given in Theorem 5.2.2 and $W(x)$ is given in Lemma 5.2.2. Note that the fact that V is a constrained CLF for system (5.11) guarantees that $\mathcal{F}(t, x)$ is nonempty for any t and x .

Fig. 5.2 shows the feasible control set at some time $t = \hat{t}$. The line denoted by $\frac{\partial V}{\partial x} g_1 u + \frac{\partial V}{\partial x} f_1 + W = 0$ separates the 2-D control space into two halves, where the half plane $\frac{\partial V}{\partial x} g_1 u + \frac{\partial V}{\partial x} f_1 + W \leq 0$ (the entire right plane in Fig. 5.2) represents the unconstrained stabilizing control values. The input constraints (5.10) produce a time-varying rectangle in the $u_0 - u_1$ plane. The shaded area represents the stabilizing controls which also satisfy input constraints (5.10), that is, the feasible control set $\mathcal{F}(t, x)$.

We have the following theorem.

Theorem 5.2.3 *If the time-varying feedback control law $k(t, x)$ satisfies*

1. $k(t, 0) = 0$,

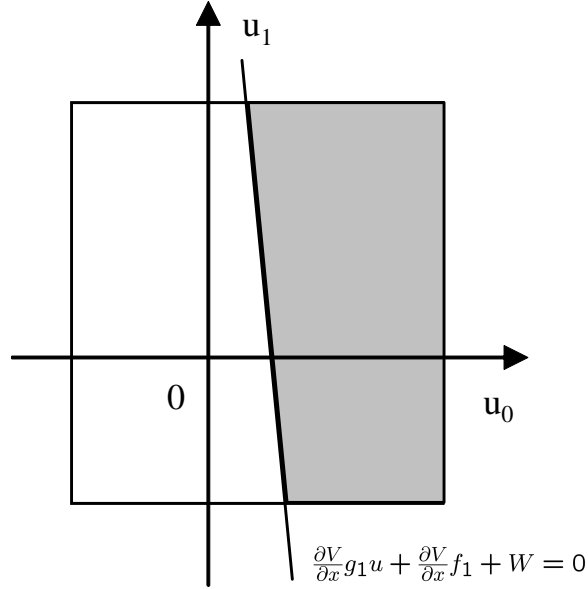


Figure 5.2: The feasible control set $\mathcal{F}(t, x)$ at some time $t = \hat{t}$.

2. $k(t, x) \in \mathcal{F}(t, x), \quad \forall x \neq 0,$

3. $k(t, x)$ is locally Lipschitz in x and piecewise continuous in $t, \quad \forall x \neq 0$ and $\forall t \geq 0,$

then this control solves the tracking problem with input constraints, that is, $|x_r - x| + |y_r - y| + |\psi_r - \psi| \rightarrow 0$ as $t \rightarrow \infty$.

Proof: see [30]. ■

There are an infinite number of possibilities for selecting a feedback strategy that satisfies Theorem 5.2.3. In this section we will investigate the performance of an aggressive selection scheme that chooses the maximum allowable u_0 and u_1 outside of a region close to the origin. This scheme can be interpreted as a high-gain scheme with saturation. Define a saturation function as

$$\text{sat}(a, b, c) = \begin{cases} b, & a < b \\ a, & b \leq a \leq c, \\ c, & a > c \end{cases}$$

where it is assumed that $b < c$.

Define

$$M_3 \triangleq \max\{0, \sup_{\substack{0 < |\alpha| < 1 \\ |\beta| < 1 \\ 0 < \vartheta \leq 1}} (\alpha^2 + 1) \frac{\rho_1}{\alpha^2}\} \quad (5.29)$$

$$M_4 \triangleq \max\{0, \sup_{\substack{0 < \alpha < 1 \\ |\beta| < 1}} (\alpha^2 + 1) \frac{\rho_2}{\alpha^2}\} \quad (5.30)$$

$$M_5 \triangleq \max\{0, \sup_{0 < |\alpha| < 1} (\alpha^2 + 1) \frac{\rho_3}{\alpha^2}\}, \quad (5.31)$$

where

$$\begin{aligned} \rho_1 &= \left(k_1 \beta + \frac{\alpha}{\sqrt{\alpha^2 + 1}} \vartheta \right) \sin\left(\frac{\alpha - \beta}{m}\right) + k_1 \gamma_1 \beta \sin\left(\frac{\beta}{m}\right) \\ \rho_2 &= \frac{|\alpha|}{\sqrt{\alpha^2 + 1}} (\omega_{max} - \epsilon_\omega) \\ &\quad + \left(k_1 - \frac{1}{2}\right) \left[v_{min} - (v_{min} + \epsilon_v) \cos\left(\frac{\alpha - \beta}{m}\right) \right] \\ &\quad + \gamma_2 \left(k_1 - \frac{1}{2}\right) \left[(v_{min} + \epsilon_v) \cos\left(\frac{\beta}{m}\right) - v_{min} \right] \\ \rho_3 &= \frac{|\alpha|}{\sqrt{\alpha^2 + 1}} (\omega_{max} - \epsilon_\omega) + \left(k_1 - \frac{1}{2}\right) (\gamma_2 - 1) \epsilon_v, \end{aligned}$$

and k_1 , γ_1 , γ_2 , and m are defined in Theorem 5.2.2.

It is easy to see that M_3 , M_4 , and M_5 in Eqs. (5.29), (5.30), and (5.31) are bounded as $|\alpha|$ approaches 1. Note that $1 < (\alpha^2 + 1) < 2$ since $0 < |\alpha| < 1$. For Eq. (5.29), two cases will be considered with regard to β . In the case of $\beta = 0$, $(\alpha^2 + 1)\rho_1/\alpha^2 = (\sqrt{\alpha^2 + 1})\vartheta \sin(\frac{\alpha}{m})/\alpha$, which is bounded by $1/m$ as α approaches 0. In the case of $\beta \neq 0$, as $|\alpha|$ approaches 0, ρ_1 approaches $k_1(\gamma_1 - 1)\beta \sin(\frac{\beta}{m})$, which is negative since $0 < \gamma_1 < 1$ and $|\frac{\beta}{m}| < \frac{1}{m} < \frac{\pi}{4}$ following Eq. (5.15). Thus $M_3 = 1/m$ as $|\alpha|$ approaches 0. For Eq. (5.30), as $|\alpha|$ approaches 0, ρ_2 approaches $(k_1 - 1/2)(\gamma_2 - 1)[(v_{min} + \epsilon_v) \cos(\frac{\beta}{m}) - v_{min}]$, which is also negative following Eq. (5.16). Thus $M_4 = 0$ as $|\alpha|$ approaches 0. For Eq. (5.31), as $|\alpha|$ approaches 0, ρ_3 approaches $(k_1 - \frac{1}{2})(\gamma_2 - 1)\epsilon_v$, which is also negative. Thus $M_5 = 0$ as $|\alpha|$ approaches 0. Therefore M_3 , M_4 , and M_5 are finite and can be found by straightforward numerical techniques.

Define

$$\kappa_\omega = \max\left\{2\omega_{max} - \epsilon_\omega, \frac{d_3}{m-1}, \frac{d_4}{m-1}\right\} \quad (5.32)$$

$$\kappa_v = \frac{\omega_{max} - \epsilon_\omega}{2k_1 - 1} + \gamma_2\epsilon_v, \quad (5.33)$$

where

$$d_3 = M_3(v_{max} - \epsilon_v) + \gamma_0 + \frac{1}{2}(\omega_{max} - \epsilon_\omega)$$

$$d_4 = M_3(v_{max} - \epsilon_v) + \gamma_0 + \max\{M_4, M_5\}.$$

Lemma 5.2.3 *If*

$$u_0 = \text{sat}(-\eta_\omega \bar{x}_0, \underline{\omega}, \bar{\omega}) \quad (5.34)$$

$$u_1 = \text{sat}(-\eta_v x_2, \underline{v}, \bar{v}) \quad (5.35)$$

where $\eta_\omega > \kappa_\omega$ and $\eta_v > \kappa_v$ and κ_ω and κ_v are defined as above, then $k_{sat}(t, x) = [u_0, u_1]^T$ satisfies the conditions of Theorem 5.2.3.

Proof: Obviously $k_{sat}(t, x)$ satisfies the first and third conditions in Theorem 5.2.3. We will show that it also stays in the feasible control set $\mathcal{F}(t, x)$, that is, $\dot{V} = \frac{\partial V}{\partial x}(f_1 + g_1 k_{sat}(t, x)) \leq -W(x)$.

Note that

$$\dot{V} + W(x) = \delta_1 + \delta_2 + \delta_3 + \delta_4, \quad (5.36)$$

where

$$\begin{aligned} \delta_1 &= k_1 \left(\frac{x_1}{\pi_1} \right) \left[v_r \sin\left(\frac{\bar{x}_0}{m} - \frac{x_1}{m\pi_1}\right) + \gamma_1(v_{\min} + \epsilon_v) \sin\left(\frac{x_1}{m\pi_1}\right) \right] \\ &\quad + \frac{\bar{x}_0}{\pi_2} \frac{1+x_2^2}{\pi_1^3} v_r \sin\left(\frac{\bar{x}_0}{m} - \frac{x_1}{m\pi_1}\right) \\ \delta_2 &= \frac{\bar{x}_0}{\pi_2} \left(m - \frac{x_2}{\pi_1} \right) u_0 + \gamma_0 \left(\frac{\bar{x}_0}{\pi_2} \right)^2 \\ \delta_3 &= \frac{\bar{x}_0}{\pi_2} \frac{x_2}{\pi_1} \omega_r \\ \delta_4 &= \left(k_1 - \frac{\bar{x}_0 x_1}{\pi_2 \pi_1^2} \right) \left(\frac{x_2}{\pi_1} \right) u_1 \\ &\quad + \gamma_2 \left(k_1 - \frac{1}{2} \right) \left(\frac{x_2}{\pi_1} \right)^2 \left[(v_{\min} + \epsilon_v) \cos\left(\frac{x_1}{m\pi_1}\right) - v_{\min} \right]. \end{aligned}$$

Four cases will be considered as follows:

Case 1: $-\eta_\omega \bar{x}_0 \notin [\underline{\omega}, \bar{\omega}]$ and $-\eta_v x_2 \notin [\underline{v}, \bar{v}]$.

In this case, the saturation functions are the same as the discontinuous signum like functions in Theorem 5.2.2, which implies that $\dot{V} \leq -W(x)$ in this case.

Case 2: $-\eta_\omega \bar{x}_0 \in [\underline{\omega}, \bar{\omega}]$ and $-\eta_v x_2 \in [\underline{v}, \bar{v}]$.

In this case, we can see that $u_0 = -\eta_\omega \bar{x}_0$ and $u_1 = -\eta_v x_2$. We also know that $|\bar{x}_0| < 1$ since $\eta_\omega > \kappa_\omega \geq 2\omega_{max} - \epsilon_\omega$.

Noting that

$$\delta_1 \leq M_3(v_{max} - \epsilon_v) \left(\frac{\bar{x}_0}{\pi_2} \right)^2 \quad (5.37)$$

$$\delta_2 \leq [-(m-1)\eta_\omega + \gamma_0] \left(\frac{\bar{x}_0}{\pi_2} \right)^2 \quad (5.38)$$

$$\delta_3 \leq \frac{1}{2} \left[\left(\frac{\bar{x}_0}{\pi_2} \right)^2 + \left(\frac{x_2}{\pi_1} \right)^2 \right] (\omega_{max} - \epsilon_\omega) \quad (5.39)$$

$$\delta_4 \leq (k_1 - \frac{1}{2})(\gamma_2 \epsilon_v - \eta_v) \left(\frac{x_2}{\pi_1} \right)^2, \quad (5.40)$$

where Eq. (5.37) comes from Eq. (5.29) by letting $\alpha = \bar{x}_0$, $\beta = x_1/\pi_1$, and $\vartheta = (1+x_2^2)/\pi_1^3$, and Eq. (5.39) follows Young's Inequality. Therefore,

$$\begin{aligned} \dot{V} + W(x) &\leq [d_3 - (m-1)\eta_\omega] \left(\frac{\bar{x}_0}{\pi_2} \right)^2 \\ &+ \left[\frac{1}{2}(\omega_{max} - \epsilon_\omega) + (k_1 - \frac{1}{2})(\gamma_2 \epsilon_v - \eta_v) \right] \left(\frac{x_2}{\pi_1} \right)^2, \end{aligned}$$

which is nonpositive since $\eta_\omega > \kappa_\omega \geq d_3/(m-1)$ and $\eta_v > \kappa_v = \frac{\omega_{max} - \epsilon_\omega}{2k_1 - 1} + \gamma_2 \epsilon_v$.

Case 3: $-\eta_\omega \bar{x}_0 \in [\underline{\omega}, \bar{\omega}]$ and $-\eta_v x_2 \notin [\underline{v}, \bar{v}]$.

In this case, $|\bar{x}_0| < 1$, δ_1 and δ_2 follow the same inequalities (5.37) and (5.38), and $\delta_3 \leq \left(\frac{|x_2|}{\pi_1} \right) \left(\frac{|\bar{x}_0|}{\pi_2} \right) (\omega_{max} - \epsilon_\omega)$. Note that $\underline{v} < 0$ from the property of m and $\bar{v} \leq \epsilon_v$. If $-\eta_v x_2 < \underline{v}$, we can get that $x_2 > -\frac{\underline{v}}{\eta_v} > 0$. Thus $(\delta_3 + \delta_4) \leq \left(\frac{|x_2|}{\pi_1} \right) M_4 \left(\frac{\bar{x}_0}{\pi_2} \right)^2 \leq M_4 \left(\frac{\bar{x}_0}{\pi_2} \right)^2$. If $-\eta_v x_2 > \bar{v}$, we can get that $x_2 < -\frac{\bar{v}}{\eta_v} < 0$. Thus $(\delta_3 + \delta_4) \leq \left| \frac{x_2}{\pi_1} \right| M_5 \left(\frac{\bar{x}_0}{\pi_2} \right)^2 \leq M_5 \left(\frac{\bar{x}_0}{\pi_2} \right)^2$. Therefore, $\dot{V} + W(x) \leq 0$ since $\eta_\omega > \kappa_\omega \geq d_4/(m-1)$.

Case 4: $-\eta_\omega \bar{x}_0 \notin [\underline{\omega}, \bar{\omega}]$ and $-\eta_v x_2 \in [\underline{v}, \bar{v}]$.

In this case, $u_0 \text{sign}(\bar{x}_0) \leq -\epsilon_\omega$ and δ_4 follows the same inequality (5.40). It can be seen

that $(\sigma_1 u_1 + \sigma_2) \triangleq \delta_4 \leq 0$ since $\eta_v > \kappa_v > \gamma_2 \epsilon_v$. We can see that $\dot{V} + W(x) \leq -\epsilon_\omega \frac{|\bar{x}_0|}{\pi_2} (m - \frac{x_2}{\pi_1}) + \sigma_3 + \sigma_4$. Then following the proof for Theorem 5.2.2, we know that $\dot{V} + W(x) \leq 0$ is guaranteed based on the choice of m .

Combining these four cases gives the desired result. ■

In Lemma 5.2.3 we used a simple control law that stays in the feasible control set. Other continuous saturation functions like atan , tanh are also possible as long as they stay in the feasible control set. In the case of v_r and ω_r being uniformly continuous, it is also possible to use geometrical strategies to find feasible control laws (e.g. choose the geometrical center of the feasible control set $\mathcal{F}(t, x)$ as feasible controls).

Note that the commanded velocity and heading rate to the autopilots are defined as $v^c \triangleq u_1 + v_r \cos(x_0)$ and $\omega^c \triangleq \omega_r - u_0$.

Physically, there may exist perturbation terms in system (5.11) due to uncertainties and external disturbances. We address the issue of uncertainties and disturbances under the input-to-state (ISS) framework [114].

Consider the system

$$\dot{x} = f(t, x) + g(t, x)u + d, \quad (5.41)$$

which introduces a perturbation term $d \in \mathbb{R}^n$ to the nominal system (5.12).

Definition 5.2.4 [115] *A continuously differentiable function $V : \mathbb{R}_+ \times \mathbb{R}^n \rightarrow \mathbb{R}$ is an ISS-CLF for system (5.41) if it is positive-definite, decrescent, radially unbounded in x and there exist class \mathcal{K} functions $\chi(\cdot)$ and $\rho(\cdot)$ such that*

$$\inf_{u \in \mathbb{R}^m} \frac{\partial V}{\partial t} + \frac{\partial V}{\partial x} f + \frac{\partial V}{\partial x} g u + \frac{\partial V}{\partial x} d \leq -\chi(\|x\|), \forall \|x\| \geq \rho(\|d\|).$$

Given $W(x)$ in Eq. (5.14), there exists a class \mathcal{K} function χ_w such that $\chi_w(\|x\|) \leq W(x)$, $\forall x$ ([110], Lemma 3.5).

Lemma 5.2.4 *Let $\mu = \sup_{\|x\| \rightarrow \infty} \chi_w(\|x\|)$ and $b_1 = [1, k_1, k_1]^T$. If $\|d\| < \frac{\lambda \mu}{\|b_1\|}$, where $0 < \lambda < 1$, then $V(x)$ is also an ISS-CLF with input constraints (5.10) for system*

$$\dot{x} = f_1(t, x) + g_1(t, x)u + d, \quad (5.42)$$

where d is the perturbation term to the nominal system (5.11).

Proof: Note that $\frac{\partial V}{\partial x} = [\frac{\bar{x}_0}{\pi_2}, k_1 \frac{x_1}{\pi_1}, k_1 \frac{x_2}{\pi_1}]$, where $|\frac{\bar{x}_0}{\pi_2}| < 1$, $|\frac{x_1}{\pi_1}| < 1$, and $|\frac{x_2}{\pi_1}| < 1$.

It can be seen that

$$\begin{aligned} & \inf_{u \in \mathcal{U}_2} \frac{\partial V}{\partial x} f_1 + \frac{\partial V}{\partial x} g_1 u + \frac{\partial V}{\partial x} d \\ & \leq -W(x) + \left\| \frac{\partial V}{\partial x} d \right\| \\ & \leq -(1 - \lambda) \chi_w(\|x\|) - \lambda \alpha_w(\|x\|) + \|b_1\| \|d\| \\ & \leq -(1 - \lambda) \chi_w(\|x\|), \quad \forall \|x\| \geq \alpha_w^{-1} \left(\frac{\|b_1\| \|d\|}{\lambda} \right) \end{aligned}$$

Note that $\alpha_w^{-1}(\cdot)$ in the last inequality is also a class \mathcal{K} function of $\|d\|$ and is well defined since $\frac{\|b_1\| \|d\|}{\lambda} < \mu$. ■

Note that here $\chi_w(\cdot)$ is a class \mathcal{K} function instead of a class \mathcal{K}_∞ function, which in turn imposes constraints for $\|d\|$. This can be explained from the constrained input perspective. In the case of $d = 0$, the derivative of the CLF cannot approach $-\infty$ as the tracking errors approach ∞ even with maximum control authority due to the saturated controls. As a result, $\chi_w(\cdot)$ can only be a class \mathcal{K} function given the input constraints. Also note that with control inputs given by Eqs. (5.34) and (5.35) $V(x)$ is an ISS-Lyapunov function under the same assumptions of Lemma 5.2.4.

It is obvious that the commanded control v^c and ω^c rely on the state measurement x , y , and ψ . Due to measurement noise, there exist input uncertainties for $[v^c, \omega^c]^T$. Equivalently, we may consider input uncertainties for $[u_0, u_1]^T$ in system (5.11). We denote the actual control input to system (5.11) as $u = [u_0 + \Delta u_0, u_1 + \Delta u_1]^T$, where Δu_0 and Δu_1 represent the uncertainties. Due to saturation constraints, we know that $|\Delta u_0| \leq 2\omega_{max}$ and $|\Delta u_1| \leq v_{max} - v_{min}$.

We have the following lemma considering input uncertainties.

Lemma 5.2.5 *Let $b_2 = [m + 1, k_1 + \frac{1}{2}]^T$ and $\Delta u = [\Delta u_0, \Delta u_1]^T$. If $\|\Delta u\| < \frac{\lambda \mu}{\|b_2\|}$, where $0 < \lambda < 1$, then $V(x)$ is an ISS-Lyapunov function for system (5.11) with control inputs given by Eqs. (5.34) and (5.35) and $d = g_1 \Delta u$.*

Proof: Noting that

$$\frac{\partial V}{\partial x} g_1 = \left[\left(m - \frac{x_2}{\pi_1} \right) \frac{\bar{x}_0}{\pi_2}, -\frac{\bar{x}_0}{\pi_2} \frac{x_1 x_2}{\pi_1^3} + k_1 \frac{x_2}{\pi_1} \right],$$

where $\left| \left(m - \frac{x_2}{\pi_1} \right) \frac{\bar{x}_0}{\pi_2} \right| < m + 1$, and $\left| -\frac{\bar{x}_0}{\pi_2} \frac{x_1 x_2}{\pi_1^3} + k_1 \frac{x_2}{\pi_1} \right| < k_1 + \frac{1}{2}$, the result then directly follows Lemma 5.2.4. ■

One advantage of the CLF-based approach used in this section is that it only requires v_r and ω_r to be piecewise continuous instead of being uniformly continuous, which results in wider potential applications than other approaches which require uniform continuity. The other advantage is that it provides the possibility to use other advanced strategies to choose feasible controls from $\mathcal{F}(t, x)$. For example, at each time t , a feasible control may be generated from $\mathcal{F}(t, x)$ while optimizing some performance index function or minimizing some cost function at the same time. This may introduce more flexibility and benefits to the tracking control problem than specifying a fixed control law in advance. In addition, it is also possible to propose a suboptimal controller from $\mathcal{F}(t, x)$ based on the combination of model predictive techniques and the tracking CLF.

Although the approach in this section is designed specifically for system (5.3), the design strategy can be applied to general nonlinear systems. That is, if a constrained control Lyapunov function (CLF) can be found for a system with polytopic input constraints, the feasible control set that defines all the stabilizing controls with respect to the CLF satisfying the input constraints can be specified accordingly. Ref. [30] provides a complete parametrization of the unconstrained stabilizing controls with respect to a certain CLF. Following this idea, a direct parametrization of the feasible control set or selection from the feasible control set is applicable, e.g. finding the geometric mean of the feasible control set or a parametrization based on the vertices of the feasible control set (a polygon in this case).

5.2.4 Simulation Results

In this section, we simulate a scenario where a UAV is assigned to transition through several known targets in the presence of dynamic threats. The parameters used in this section are given in Table 5.1, which are the parameters of a three foot wingspan UAV used at BYU. The simulation results in this section are based on a full six-degree-of-freedom, twelve-state model. Note that the value for m is much lower than the theoretical

Table 5.1: Parameter values used in simulation.

Parameter	Value	Parameter	Value
v_{\min}	8.0 (m/s)	v_{\max}	13.0 (m/s)
ω_{\max}	0.671 (rad/s)	ϵ_v	1.5 (m/s)
ϵ_ω	0.2 (rad/s)	v_r	$\in [9.5, 11.5]$ (m/s)
ω_r	$\in [-0.471, 0.471]$ (rad/s)	α_ψ	0.55
α_v	0.192	m	1
k_1	2	$\gamma_0, \gamma_1, \gamma_2$	0.5
η_0	10	η_1	10

lower bound defined in Theorem 5.2.2. However, as we will see in the following, the saturation controller works well using this value, which implies the robustness of the controller to parameter variations.

Fig. 5.3 shows the reference trajectory generated by the dynamic trajectory smoother described in [112] and the actual trajectories generated by the saturation controller proposed in Lemma 5.2.3 and controller based on state-dependent Riccati equation (SDRE) approach [116], respectively. We note that the SDRE controller has been saturated to satisfy the input constraints. The diamonds denote threat locations to be avoided. Each trajectory at $t = 0$ is denoted by a circle while each trajectory at $t = 30$ is denoted by a square. Also each trajectory at $t = \{6, 12, 18, 24\}$ is denoted by a plus symbol. The trajectory tracking errors are plotted in Fig. 5.4. Note that the performance of the SDRE controller is much worse than that of the saturation controller since the SDRE design does not account for input constraints explicitly. In fact, the SDRE controller is not guaranteed to stay in the feasible control set. Without input constraints, the SDRE controller can achieve much better performance at the expense of huge velocity and heading rate commands. Fig. 5.5 shows the reference control inputs v_r and ω_r and commanded control inputs v^c and ω^c . Obviously, ω_r is only piecewise continuous instead of being uniformly continuous. The reference control inputs generated by the trajectory generator satisfy their constraints respectively. We can also see that v^c and ω^c satisfy their input constraints respectively.

Fig. 5.6 shows the reference trajectory and the actual trajectory of the 6-DOF model using the saturation controller under model uncertainties and disturbances. As in

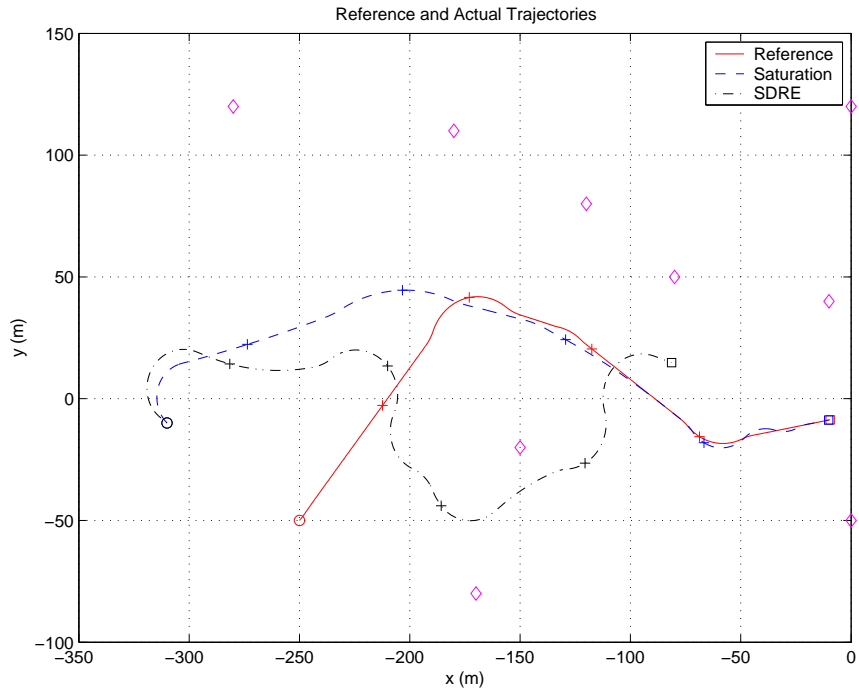


Figure 5.3: The reference and actual trajectories of the 6-DOF model.

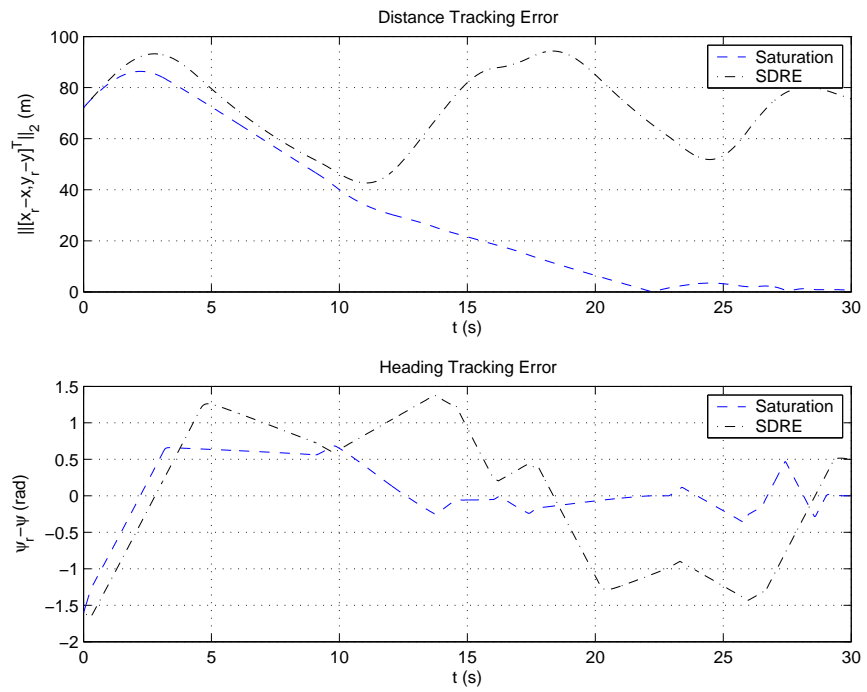


Figure 5.4: The trajectory tracking errors of the 6-DOF model.

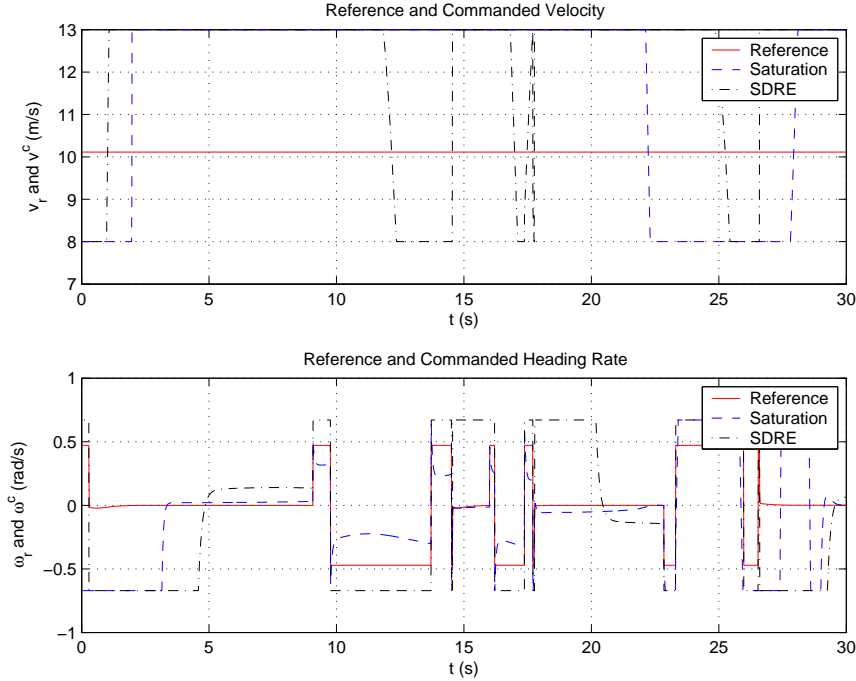


Figure 5.5: The reference and commanded control inputs of the 6-DOF model.

Fig. 5.3, a circle denotes the starting point of a trajectory and a square denotes the ending point. A diamond symbol denotes the trajectory at $t = \{10, 20, 30, 40\}$. Fig. 5.7 shows the corresponding tracking errors. Here each sensor measurement is corrupted with zero mean white noise. We can see that the saturation controller is robust to model uncertainties and disturbances.

5.3 Experimental Study of Saturated Tracking Control for Mobile Robots

With mobile robots programmed to emulate UAVs flying at a constant altitude in hardware, the main purpose of this section is to demonstrate experimental results of the tracking controllers accounting for velocity and heading rate constraints similar to those of UAVs. The experimental study here is related to the simulation studies in Section 5.2. In this section, we conduct experimental tests where a nonholonomic mobile robot is assigned to follow a desired trajectory so as to transition through several targets in the presence of static and dynamic threats. We present experimental results of two velocity controllers, where one is a saturation controller and the other is a discontinuous controller. These

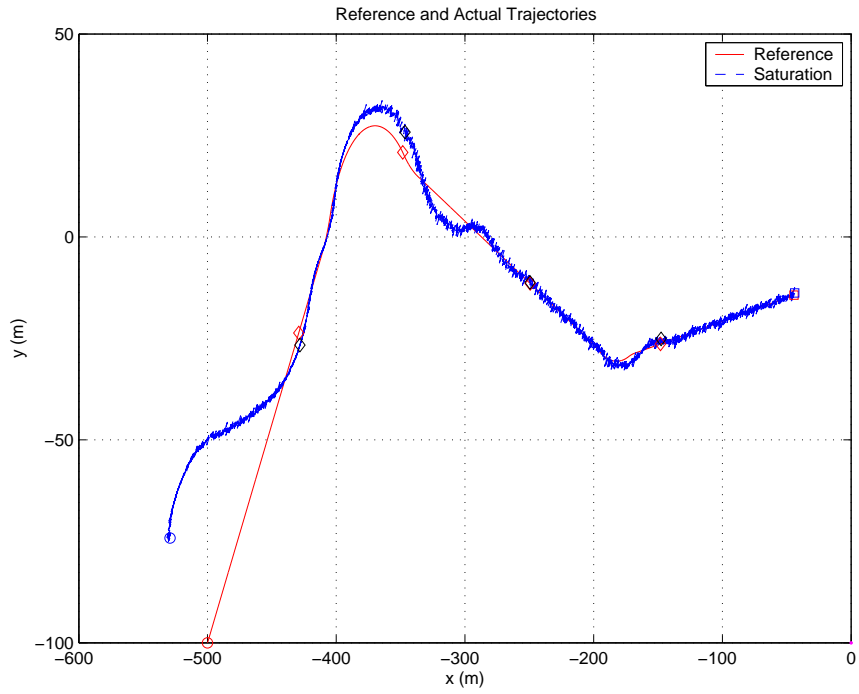


Figure 5.6: The simulation scenario of the 6-DOF model with model uncertainties and disturbances.

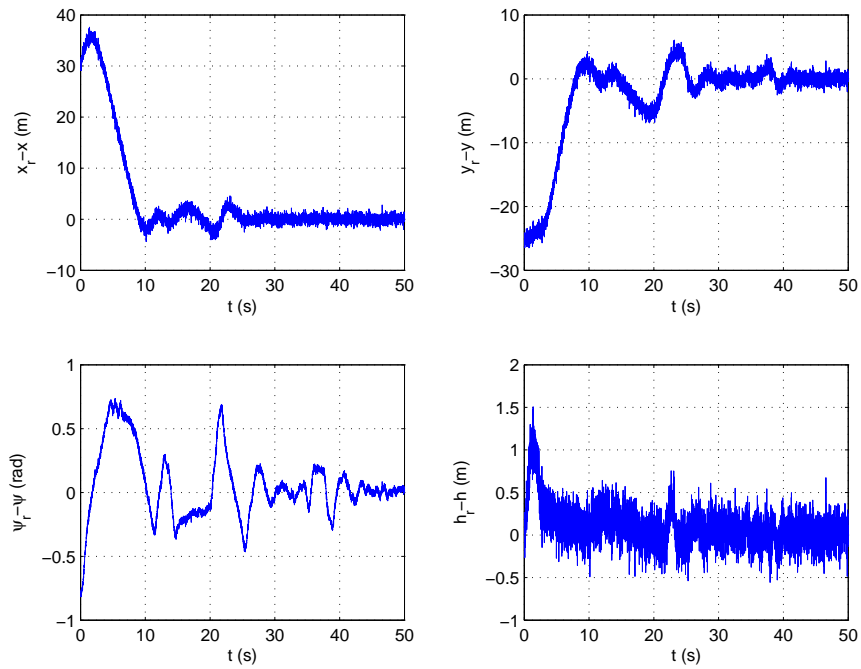


Figure 5.7: The trajectory tracking errors of the 6-DOF model with model uncertainties and disturbances.

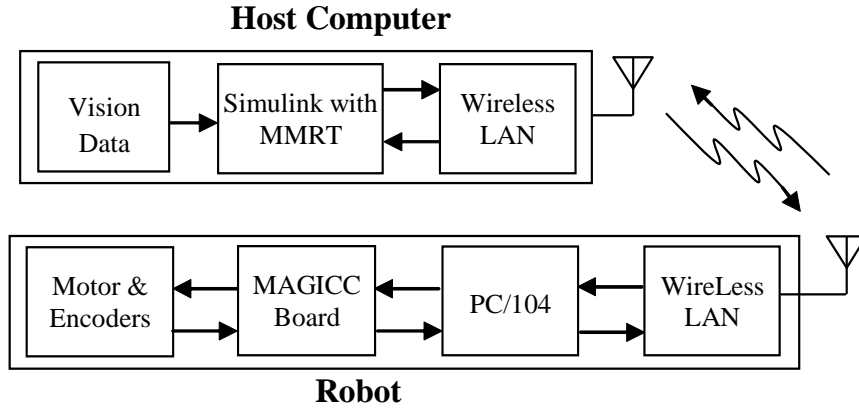


Figure 5.8: Hardware/software structure for the mobile robot testbed.

hardware results are also compared to simulation results of two dynamic controllers that are based on nonsmooth backstepping.

5.3.1 Experimental Setup

The experimental tests were conducted in the Multi-Agent Intelligent Coordination and Control (MAGICC) Laboratory at Brigham Young University.

Mobile Robot Testbed

The MAGICC Lab mobile robot testbed consists of a 5 m by 5 m field. Fig. 5.8 shows the schematic hardware/software structure for the testbed.

In our experiments, all high-level controls including the trajectory tracker are performed on a host computer. In the MAGICC Lab, host computers communicate with mobile robots over a wireless LAN. An overhead camera is mounted on the ceiling directly above the testbed to measure the position and heading of each robot. Using vision data, Simulink and the MMRT toolbox [117] are used to implement control algorithms. Control commands are then sent to a PC/104 computer onboard a mobile robot over the wireless LAN. The MAGICC board¹ is an integrated circuit board with a microprocessor, motor drivers, encoder channels, and analog input channels [103]. The MAGICC board produces

¹a circuit board designed by students from Multiple Agent Intelligent Coordination and Control (MAGICC) Laboratory at Brigham Young University



Figure 5.9: Canister robots.

PWM output to the motors and calculates the robot linear and angular velocities, which can then be sent to the host computer to estimate robot state information. Fig. 5.9 shows the canister robots used in our experiments.

Software Architecture

Fig. 5.10 shows the software architecture implemented in our experiments. The architecture consists of five components: target manager, waypoint path planner, waypoint manager, real-time trajectory generator, trajectory tracker, and low-level robot control.

The top three components in Fig. 5.10 have been addressed in [27, 118, 112]. Next, we describe low-level robot control. Trajectory tracker will be discussed in the next section.

Low-level control algorithms are implemented in the MAGICC board with the objective of maintaining commanded robot linear and angular velocities during the experiments. Fig. 5.11 shows a PID control loop for the commanded linear and angular velocities. Note that the trajectory tracker outputs the commanded linear and angular velocities v^c and ω^c . They are then converted to the commanded left and right wheel voltages denoted by V_l^c

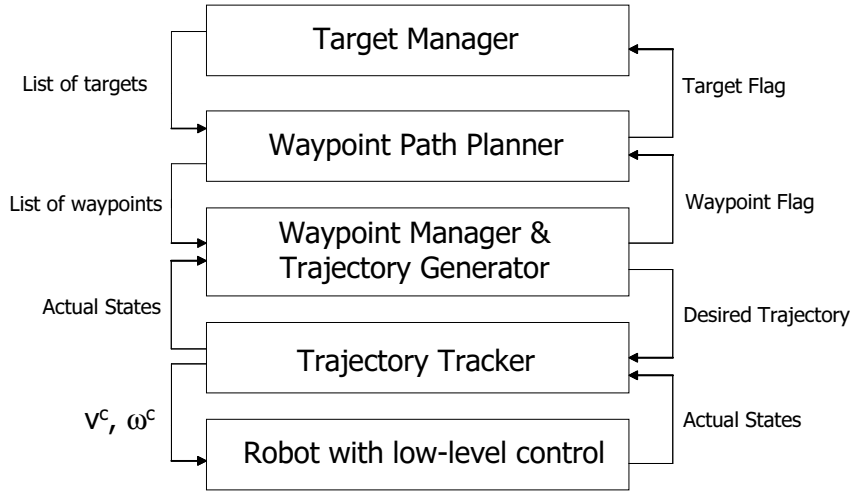


Figure 5.10: Software architecture.

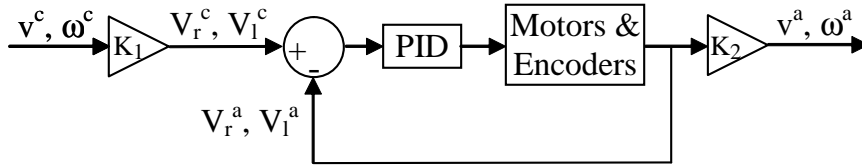


Figure 5.11: PID control loop for v^c and ω^c .

and V_r^c respectively via the conversion factor K_1 . The actual left and right wheel voltages denoted V_l^a and V_r^a respectively are then converted back to the actual linear and angular velocities v^a and ω^a respectively via the conversion factor K_2 .

5.3.2 Tracker Design

The tracker design for nonholonomic mobile robots follows a similar procedure as that in Section 5.2. For clarity of notations, we restate the tracking problem in the context of mobile robot tracking control.

The kinematic equations of a nonholonomic mobile robot are given by

$$\begin{aligned}
 \dot{x} &= v \cos(\theta) \\
 \dot{y} &= v \sin(\theta) \\
 \dot{\theta} &= \omega
 \end{aligned} \tag{5.43}$$

where (x, y) is the Cartesian position of the robot center, θ is the orientation, v is the linear velocity, and ω is the angular velocity. The simplified dynamic equations of motion are given by

$$\begin{aligned} m\dot{v} &= F \\ J\dot{\omega} &= \tau, \end{aligned} \quad (5.44)$$

where m is the mass, J is the mass moment of inertia, F is the force, and τ is the torque applied to the robot.

In order to simulate fixed-wing unmanned air vehicles flying at a constant altitude, the following input constraints are imposed on the robot:

$$\begin{aligned} 0 < v_{min} \leq v \leq v_{max} \\ -\omega_{max} \leq \omega \leq \omega_{max}, \end{aligned} \quad (5.45)$$

where $\omega_{max} > 0$.

In this section, the desired reference trajectory $(x_r, y_r, \theta_r, v_r, \omega_r)$ generated by the trajectory generator satisfies

$$\begin{aligned} \dot{x}_r &= v_r \cos(\theta_r) \\ \dot{y}_r &= v_r \sin(\theta_r) \\ \dot{\theta}_r &= \omega_r \end{aligned} \quad (5.46)$$

where v_r and ω_r are piecewise continuous and satisfy $\inf_{t \geq 0} v_r(t) > v_{min}$, $\sup_{t \geq 0} v_r(t) < v_{max}$, and $\sup_{t \geq 0} |\omega_r(t)| < \omega_{max}$.

Without loss of generality, the constraints for v_r and ω_r can be written as

$$\begin{aligned} v_{min} + \epsilon_{v1} \leq v_r \leq v_{max} - \epsilon_{v2} \\ -\omega_{max} + \epsilon_{\omega1} \leq \omega_r \leq \omega_{max} - \epsilon_{\omega2}, \end{aligned} \quad (5.47)$$

where ϵ_{v1} , ϵ_{v2} , $\epsilon_{\omega1}$, and $\epsilon_{\omega2}$ are positive control parameters.

With regard to the kinematic model (5.43), the control objective is to find feasible inputs v and ω such that $|x_r - x| + |y_r - y| + |\theta_r - \theta| \rightarrow 0$ as $t \rightarrow \infty$.

Transforming the tracking errors expressed in the inertial frame to the robot frame, the error coordinates [113] become

$$\begin{bmatrix} x_e \\ y_e \\ \theta_e \end{bmatrix} = \begin{bmatrix} \cos(\theta) & \sin(\theta) & 0 \\ -\sin(\theta) & \cos(\theta) & 0 \\ 0 & 0 & 1 \end{bmatrix} \begin{bmatrix} x_r - x \\ y_r - y \\ \theta_r - \theta \end{bmatrix}. \quad (5.48)$$

Accordingly, the tracking error model can be represented as

$$\begin{aligned} \dot{x}_e &= \omega y_e - v + v_r \cos(\theta_e) \\ \dot{y}_e &= -\omega x_e + v_r \sin(\theta_e) \\ \dot{\theta}_e &= \omega_r - \omega. \end{aligned} \quad (5.49)$$

Following [84], Eq. (5.49) can be simplified as

$$\dot{x}_0 = u_0 \quad (5.50a)$$

$$\dot{x}_1 = (\omega_r - u_0)x_2 + v_r \sin(x_0) \quad (5.50b)$$

$$\dot{x}_2 = -(\omega_r - u_0)x_1 + u_1, \quad (5.50c)$$

where

$$(x_0, x_1, x_2) \triangleq (\theta_e, y_e, -x_e) \quad (5.51)$$

and $u_0 \triangleq \omega_r - \omega$ and $u_1 \triangleq v - v_r \cos(x_0)$.

The input constraints under the transformation become

$$\begin{aligned} \underline{\omega} &\leq u_0 \leq \bar{\omega} \\ \underline{v} &\leq u_1 \leq \bar{v}, \end{aligned} \quad (5.52)$$

where $\underline{\omega} \triangleq \omega_r - \omega_{max}$, $\bar{\omega} \triangleq \omega_r + \omega_{max}$, $\underline{v} \triangleq v_{min} - v_r \cos(x_0)$, and $\bar{v} \triangleq v_{max} - v_r \cos(x_0)$ are time-varying due to state dependence and time-varying properties of v_r and ω_r .

Note from Eq. (5.50) that x_1 is not directly controllable when both x_0 and x_2 go to zero. To avoid this situation we introduce another change of variables.

Let

$$\bar{x}_0 = \lambda x_0 + \frac{x_1}{\sqrt{x_1^2 + x_2^2 + 1}}, \quad (5.53)$$

where $\lambda > 0$. Accordingly, $x_0 = \frac{1}{\lambda}(\bar{x}_0 - \frac{x_1}{\sqrt{x_1^2 + x_2^2 + 1}})$. Obviously, $(\bar{x}_0, x_1, x_2) = (0, 0, 0)$ is equivalent to $(x_0, x_1, x_2) = (0, 0, 0)$, which is in turn equivalent to $(x_e, y_e, \theta_e) = (0, 0, 0)$ and $(x_r, y_r, \theta_r) = (x, y, \theta)$ since Eqs. (5.48) and (5.51) are invertible transformations. Therefore, the original tracking control objective is converted to a stabilization objective, that is, it is sufficient to find feasible control inputs u_0 and u_1 to stabilize \bar{x}_0 , x_1 , and x_2 . With the same input constraints (5.52), Eq. (5.50a) can be rewritten as

$$\begin{aligned} \dot{x}_0 = & \frac{1 + x_2^2}{\sqrt{x_1^2 + x_2^2 + 1}^3} v_r \sin(x_0) + \frac{x_2}{\sqrt{x_1^2 + x_2^2 + 1}} \omega_r \\ & + \left(\lambda - \frac{x_2}{\sqrt{x_1^2 + x_2^2 + 1}} \right) u_0 - \frac{x_1 x_2}{\sqrt{x_1^2 + x_2^2 + 1}^3} u_1. \end{aligned} \quad (5.54)$$

In the sequel, we first design velocity controllers based on the kinematic model (5.43), where a saturation controller and a discontinuous controller will be given. Then we apply the nonsmooth backstepping approach proposed in [119] to design force and torque controllers based on the dynamic model (5.44) for comparison purposes in Section 5.3.3.

Let $\chi = [\bar{x}_0, x_1, x_2]^T$. In Section 5.2 we have shown that for $k > \frac{1}{2}$ and $\lambda > \kappa$ in Eq. (5.53), where κ is a positive constant expressed precisely in Section 5.2,

$$V_0(\chi) = \sqrt{\bar{x}_0^2 + 1} + k\sqrt{x_1^2 + x_2^2 + 1} - (1 + k) \quad (5.55)$$

is a constrained CLF for system (5.50) with input constraints (5.52) such that $\inf \dot{V}_0(\chi) \leq -W(\chi)$, where $W(\chi)$ is a continuous positive-definite function.

Define a signum like function as

$$\text{sgn}(a, b, c) = \begin{cases} b, & a < 0 \\ 0, & a = 0 \\ c, & a > 0 \end{cases}$$

By mimicking the proof in Section 5.2 that V_0 is a constrained CLF for system (5.50), it is straightforward to verify that V_0 is a constrained Lyapunov function for system (5.50) with control inputs $u_0 = \text{sgn}(\bar{x}_0, \bar{\omega}, \underline{\omega})$ and $u_1 = \text{sgn}(x_2, \bar{v}, \underline{v})$. Noting that $v = u_1 + v_r \cos(x_0)$ and $\omega = \omega_r - u_0$, a discontinuous controller for the kinematic

model (5.43) is given by

$$v^c = \begin{cases} v_{min}, & x_2 > 0 \\ v_r, & x_2 = 0, \\ v_{max}, & x_2 < 0 \end{cases} \quad (5.56)$$

$$\omega^c = \begin{cases} \omega_{max}, & \bar{x}_0 > 0 \\ \omega_r, & \bar{x}_0 = 0. \\ -\omega_{max}, & \bar{x}_0 < 0 \end{cases} \quad (5.57)$$

Define the saturation function as

$$\text{sat}(a, b, c) = \begin{cases} b, & a < b \\ a, & b \leq a \leq c, \\ c, & a > c \end{cases}$$

where it is assumed that $b < c$.

Similarly, V_0 is also a constrained Lyapunov function for system (5.50) with control inputs $u_0 = \text{sat}(-\eta_\omega \bar{x}_0, \underline{\omega}, \bar{\omega})$ and $u_1 = \text{sat}(-\eta_v x_2, \underline{v}, \bar{v})$, where η_ω and η_v are required to be greater than some positive constants which are expressed precisely in Lemma 5.2.3.

Therefore, a saturation controller for the kinematic model (5.43) is given by

$$v^c = \begin{cases} v_{min}, & -\eta_v x_2 < \underline{v} \\ v_r \cos(x_0) - \eta_v x_2, & \underline{v} \leq -\eta_v x_2 \leq \bar{v}, \\ v_{max}, & -\eta_v x_2 > \bar{v} \end{cases} \quad (5.58)$$

$$\omega^c = \begin{cases} \omega_{max}, & -\eta_\omega \bar{x}_0 < \underline{\omega} \\ \omega_r + \eta_\omega \bar{x}_0, & \underline{\omega} \leq -\eta_\omega \bar{x}_0 \leq \bar{\omega}. \\ -\omega_{max}, & -\eta_\omega \bar{x}_0 > \bar{\omega} \end{cases} \quad (5.59)$$

Given kinematic control laws, a standard way to extend the kinematic control laws to dynamic strategies is to apply backstepping techniques. It is obvious that both v^c and ω^c are not differentiable for the discontinuous controller and the saturation controller.

Note that the continuity of the saturation controller depends on the continuity of v_r and ω_r . In this section, v_r and ω_r are only assumed to be piecewise continuous. As a result, traditional backstepping techniques are not applicable to find dynamic control laws for the dynamic model (5.44). Therefore we resort to the nonsmooth backstepping approach proposed in [119] to tackle this problem.

Note that Eqs. (5.54), (5.50b), (5.50c), and (5.44) can be rewritten as

$$\begin{aligned}\dot{\chi} &= f(t, \chi) + g(\chi)\xi \\ \dot{\xi} &= \nu,\end{aligned}\tag{5.60}$$

where $\xi = [v, \omega]^T$, $\nu = [F/m, \tau/J]^T$,

$$f(t, \chi) = \begin{bmatrix} \lambda\omega_r + \frac{1+x_2^2}{\sqrt{x_1^2+x_2^2+1}}v_r \sin(x_0) + \frac{x_1x_2}{\sqrt{x_1^2+x_2^2+1}}v_r \cos(x_0) \\ v_r \sin(x_0) \\ -v_r \cos(x_0) \end{bmatrix}$$

and

$$g(\chi) = \begin{bmatrix} -\frac{x_1x_2}{\sqrt{x_1^2+x_2^2+1}} & -\left(\lambda - \frac{x_2}{\sqrt{x_1^2+x_2^2+1}}\right) \\ 0 & x_2 \\ 1 & -x_1 \end{bmatrix}.$$

Let $[v^c, \omega^c]^T = \phi(t, \chi)$ represent the saturation or discontinuous control law described above for the kinematic model (5.43). Let $\dot{\phi}(t, \chi)$ denote the generalized time derivative of ϕ and let μ represent the minimum norm element of $\dot{\phi}(t, \chi)$ (see [120, 119]).

Define

$$\nu = \mu - K(\xi - \phi(t, \chi)) - \left(\frac{\partial V_0}{\partial \chi}g(\chi)\right)^T,\tag{5.61}$$

where K is a 2×2 symmetric positive definite matrix and

$$\left(\frac{\partial V_0}{\partial \chi}g(\chi)\right)^T = \begin{bmatrix} -\frac{\bar{x}_0}{\sqrt{\bar{x}_0^2+1}}\frac{x_1x_2}{\sqrt{x_1^2+x_2^2+1}} + k\frac{x_2}{\sqrt{x_1^2+x_2^2+1}} \\ -\left(\lambda - \frac{x_2}{\sqrt{x_1^2+x_2^2+1}}\right)\frac{\bar{x}_0}{\sqrt{\bar{x}_0^2+1}} \end{bmatrix}.$$

Let the dynamic control law be given by

$$\begin{bmatrix} F \\ \tau \end{bmatrix} = \begin{bmatrix} m & 0 \\ 0 & J \end{bmatrix} \nu.\tag{5.62}$$

Table 5.2: Specifications of the robot and velocity controller parameters.

Parameter	Value
m	10.1 (kg)
J	0.13 (kg m ²)
v_{\min}	0.075 (m/s)
v_{\max}	0.24 (m/s)
ω_{\max}	2 (rad/s)
v_r	$\in [0.15, 0.19]$ (m/s)
ω_r	$\in [-1.25, 1.25]$ (rad/s)
λ	1
η_v	3
η_ω	10

Consider a Lyapunov function candidate $V = V_0(\chi) + \frac{1}{2}(\xi - \phi(t, \chi))^T(\xi - \phi(t, \chi))$. Note that $\dot{V}_0 \leq -W(\chi)$ if $\xi = \phi(t, \chi)$ from the argument that V_0 is a Lyapunov function for the kinematic model (5.43). Following Theorem 5 in [119], it can be verified that the control law (5.62) guarantees that $\|\chi\| + \|\xi - \phi(t, \chi)\| \rightarrow 0$ asymptotically as $t \rightarrow \infty$. Note that unlike the case of Theorem 5 in [119], ξ does not approach zero since here we consider a tracking problem where $\phi(t, 0) = [v_r, \omega_r]^T$ while Theorem 5 in [119] considers a stabilization problem where $\phi(0) = 0$. Therefore, it is straightforward to see that $|\bar{x}_0| + |x_1| + |x_2| + |v - v_r| + |\omega - \omega_r| \rightarrow 0$ asymptotically as $t \rightarrow \infty$.

5.3.3 Experimental Results

In this section, we present hardware results of the tracker using both the saturation velocity controller and the discontinuous velocity controller derived in Section 5.3.2. These hardware results are also compared to simulation results using the dynamic controller (5.62).

Table 5.2 shows the specifications of the robot and parameters used to obtain the experimental results.

Figs. 5.12, 5.13, and 5.14 show the hardware results of the tracker using the two velocity controllers under relatively large control authority $|\omega^c| \leq 2$ (rad/s), that is,

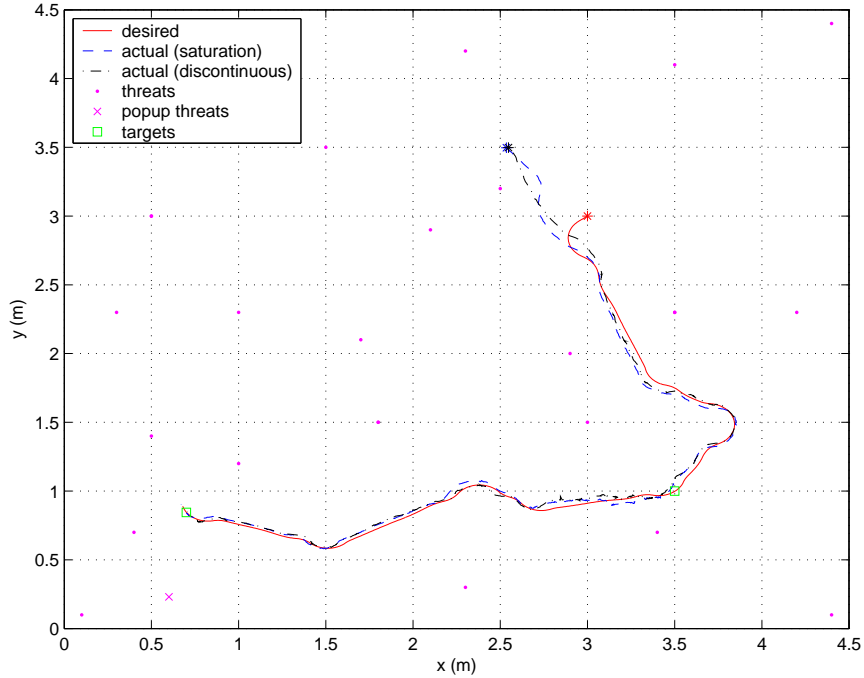


Figure 5.12: Desired and actual robot trajectories using velocity controllers when there are two targets and $\epsilon_{\omega_1} = \epsilon_{\omega_2} = 0.75$ (rad/s).

$\epsilon_{\omega_1} = \epsilon_{\omega_2} = 0.75$ (rad/s). In Fig. 5.12, we show the trajectories of the robot transitioning through two targets in the presence of static threats and popup threats, where stars indicate the starting points of the trajectories. Fig. 5.13 compares the tracking errors of the two velocity controllers. Due to vision noise, there exist a steady-state tracking error of about 0.05 meters and glitches in the heading tracking errors for both controllers. Note that the controllers are robust to glitches in the robot orientation measurement. Fig. 5.14 compares the reference and commanded velocities for both controllers. We can see that the velocities of the discontinuous controller switch frequently in time. Although similar performance is achieved using both controllers, we notice that the motion of the robot using the saturation controller is smooth while the motion of the robot using the discontinuous controller has significant jerks in the velocity results.

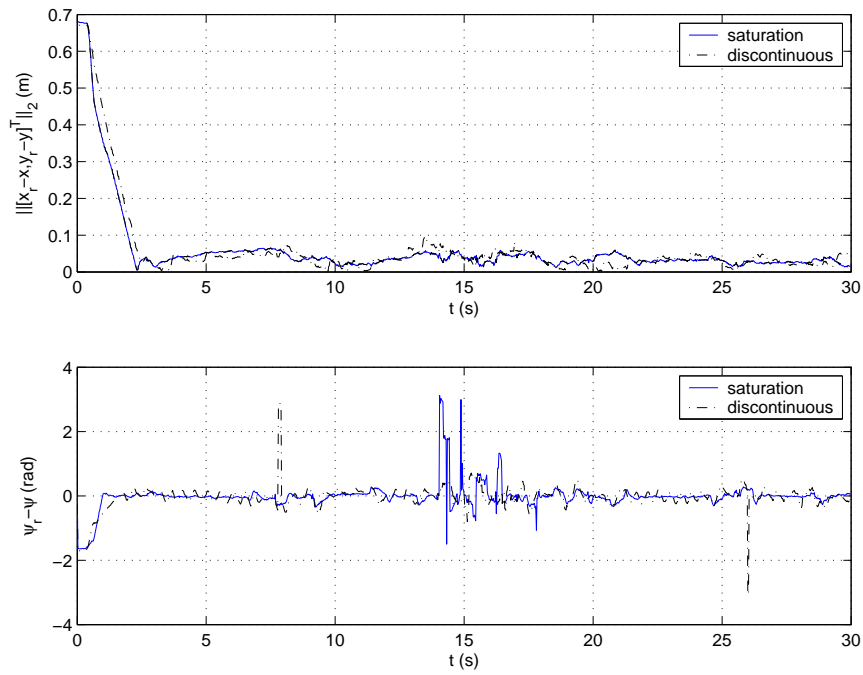


Figure 5.13: Tracking errors using velocity controllers when there are two targets and $\epsilon_{\omega 1} = \epsilon_{\omega 2} = 0.75$ (rad/s).

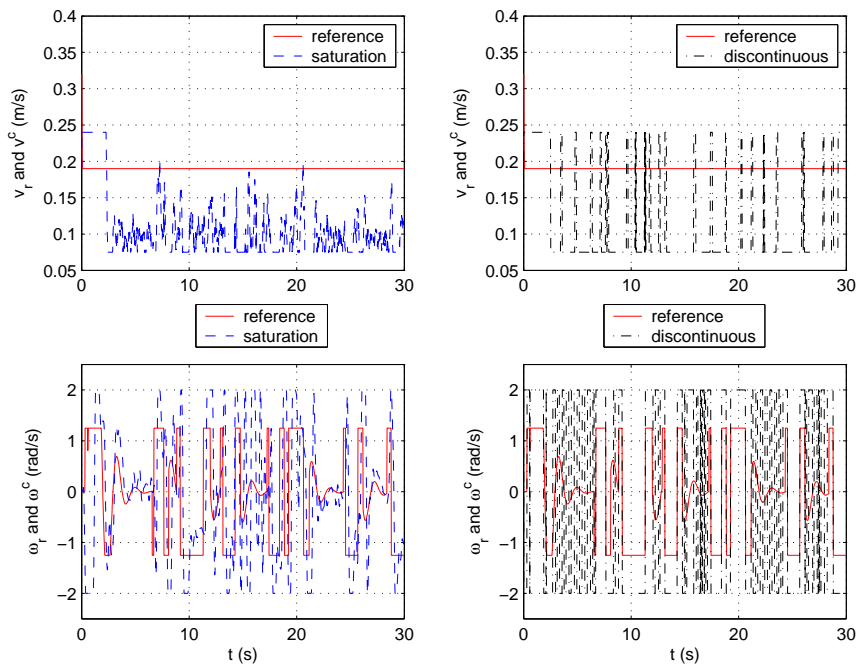


Figure 5.14: Reference and commanded velocities using velocity controllers when there are two targets and $\epsilon_{\omega 1} = \epsilon_{\omega 2} = 0.75$ (rad/s).

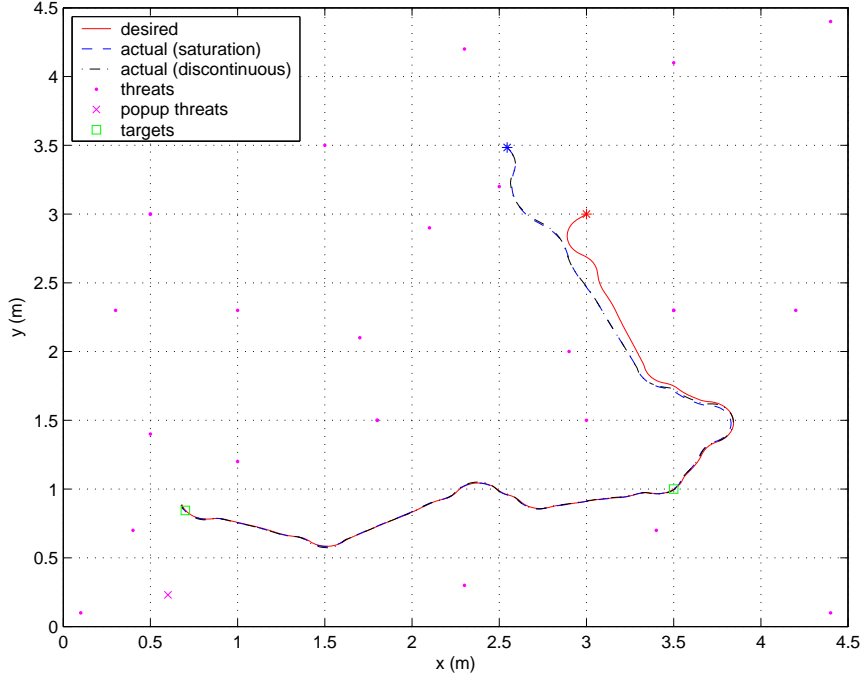


Figure 5.15: Desired and actual robot trajectories using nonsmooth backstepping when there are two targets and $\epsilon_{\omega_1} = \epsilon_{\omega_2} = 0.75$ (rad/s).

As a comparison to the above hardware results using velocity controllers, we also show simulation results using the dynamic controller based on nonsmooth backstepping in Figs. 5.15, 5.16, 5.17, and 5.18. The robot used in our testbed has physical constraints for force and torque of $|F| \leq 30$ N and $|\tau| \leq 230$ Nm. We choose $k = 2$ in Eq. (5.61). Note that nonsmooth backstepping is applied to both the saturation velocity controller and the discontinuous velocity controller. The dynamic controllers based on nonsmooth backstepping for both velocity controllers have similar tracking performances as shown in Figs. 5.15 and 5.16. However, compared to the case using nonsmooth backstepping for the saturation velocity controller, switching phenomena for actual linear and angular velocities and control forces and torques are more severe than in the case of using nonsmooth backstepping for the discontinuous controller as shown in Fig. 5.17 and 5.18.

As a final test, we reduce the control authority to $|\omega^c| \leq 1.45$ (rad/s), that is, $\epsilon_{\omega_1} = \epsilon_{\omega_2} = 0.2$ (rad/s), and introduce one more target in the test field. Figs. 5.19, 5.20, and 5.21 show the hardware results of the tracker using the saturation velocity controller

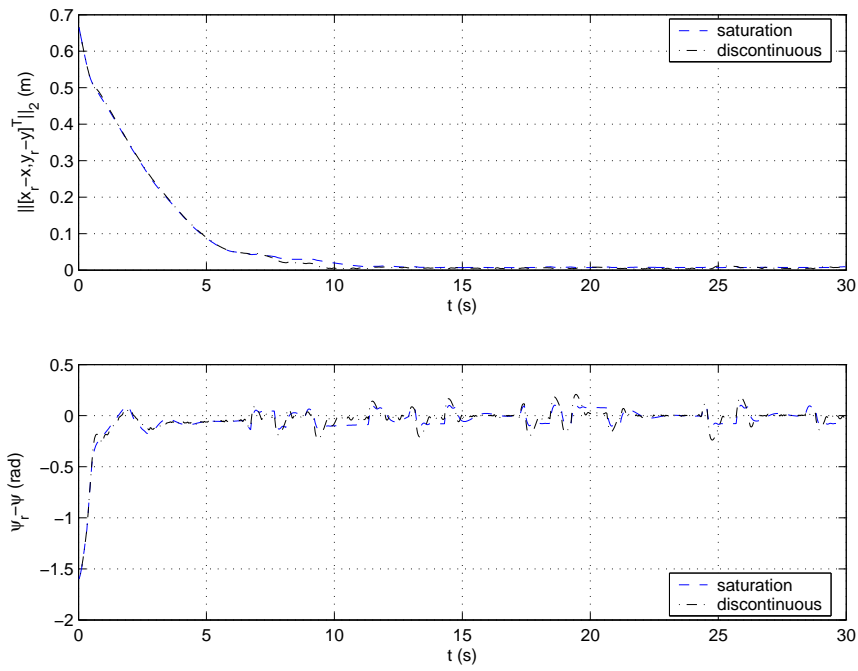


Figure 5.16: Tracking errors using nonsmooth backstepping when there are two targets and $\epsilon_{\omega 1} = \epsilon_{\omega 2} = 0.75$ (rad/s).

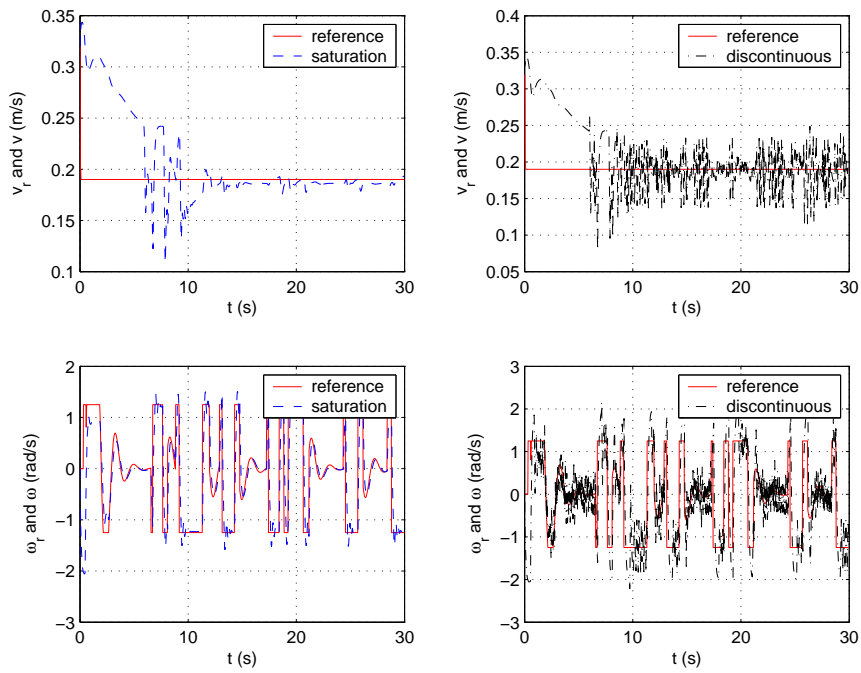


Figure 5.17: Reference and actual velocities using nonsmooth backstepping when there are two targets and $\epsilon_{\omega 1} = \epsilon_{\omega 2} = 0.75$ (rad/s).

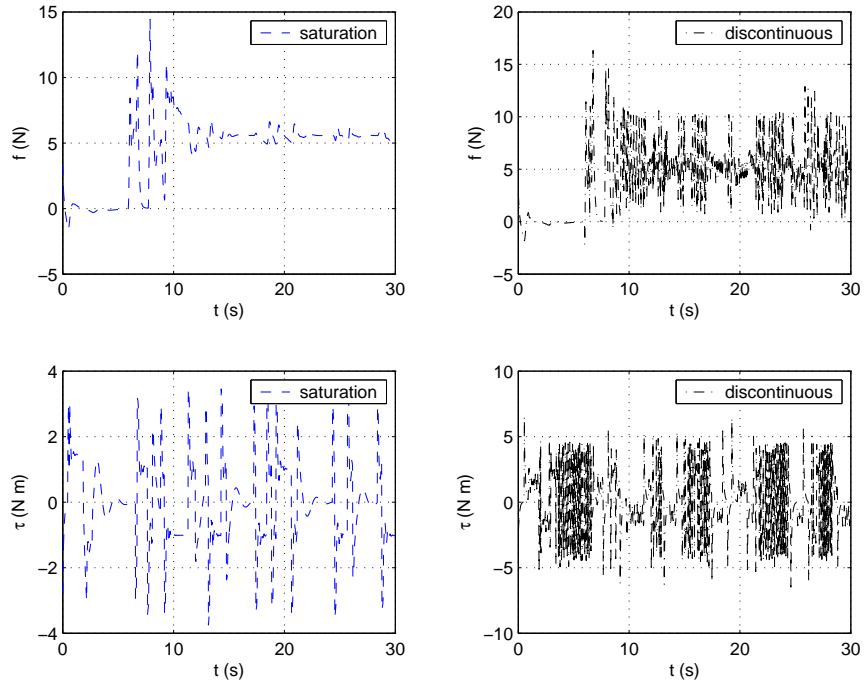


Figure 5.18: Control forces and torques using nonsmooth backstepping controller when there are two targets and $\epsilon_{\omega_1} = \epsilon_{\omega_2} = 0.75$ (rad/s).

in this situation. As shown in Fig. 5.21, ω^c is constrained within $[-1.45, 1.45]$ (rad/s) compared to Fig. 5.14 where ω^c is constrained within $[-2, 2]$ (rad/s). Note that similar performances are still achieved with much smaller control authority for ω^c and the robot transitions through three target consecutively as desired.

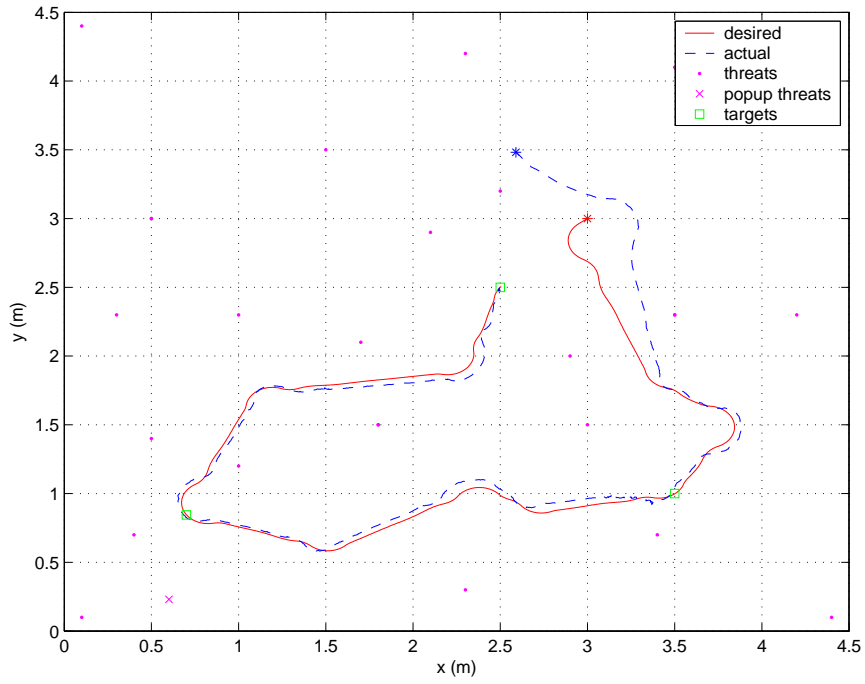


Figure 5.19: Desired and actual robot trajectories using the saturation controller when there are three targets and $\epsilon_{\omega 1} = \epsilon_{\omega 2} = 0.2$ (rad/s).

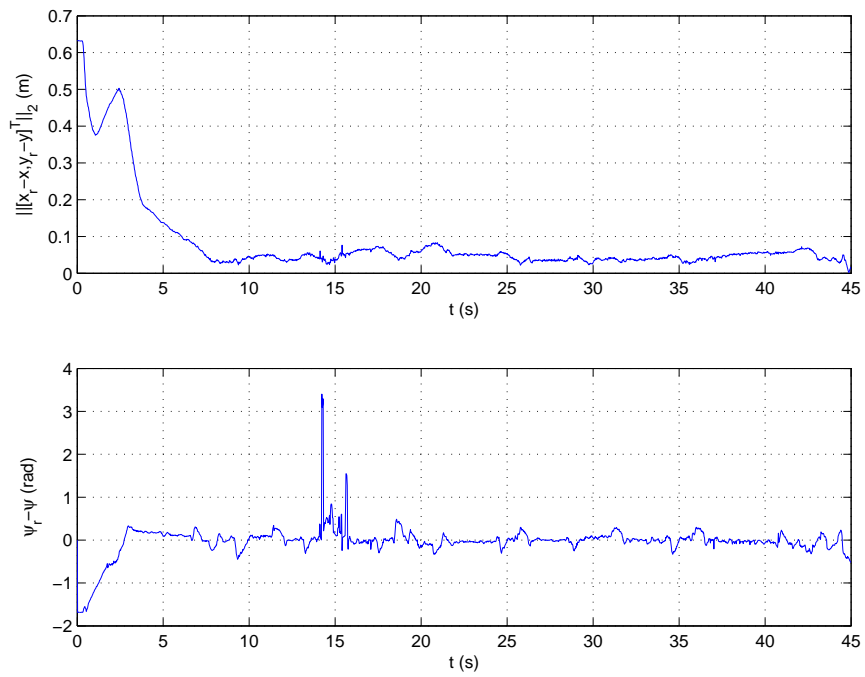


Figure 5.20: Tracking errors using the saturation controller when there are three targets and $\epsilon_{\omega 1} = \epsilon_{\omega 2} = 0.2$ (rad/s).

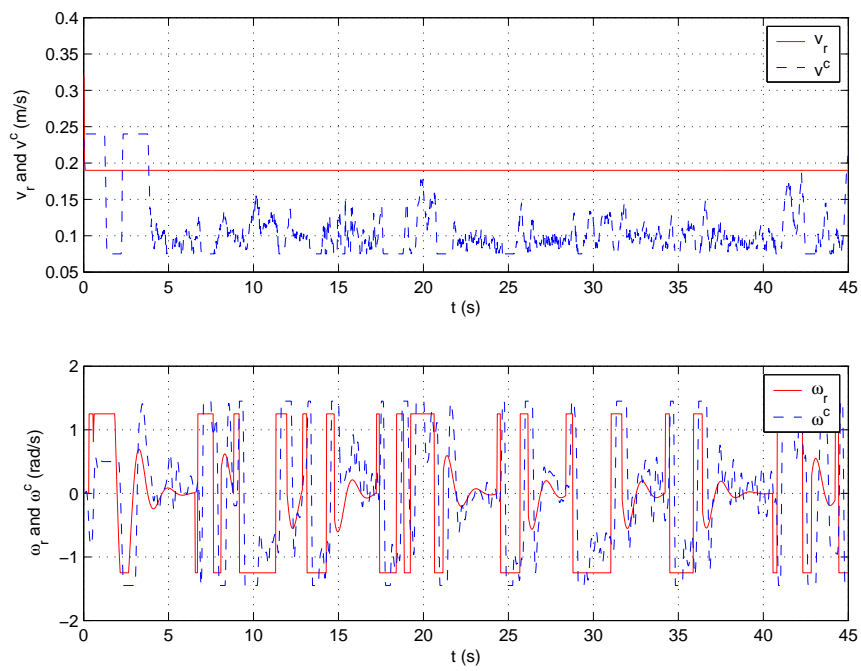


Figure 5.21: Reference and commanded velocities using the saturation controller when there are three targets and $\epsilon_{\omega_1} = \epsilon_{\omega_2} = 0.2$ (rad/s).

Chapter 6

Conclusion and Future Work

6.1 Summary of Main Results

The motivation for the research of cooperative control results from the hope that many coordinated small, inexpensive vehicles can achieve the same or better performance than one monolithic vehicle. The main purpose of this dissertation is to address three important and correlated issues in cooperative control: consensus seeking, formation keeping, and trajectory tracking.

The study of information flow and interaction among multiple agents in a group plays an important role in understanding the coordinated movements of these agents. In Chapter 3, we investigate algorithms and protocols so that a team of vehicles can reach consensus on the values of the coordination data in the presence of (i) imperfect sensors, (ii) communication dropout, (iii) sparse communication topologies, and (iv) noisy and unreliable communication links. We show necessary and/or sufficient conditions for consensus seeking with limited, unidirectional, and unreliable information exchange under fixed and switching interaction topologies (through either communication or sensing).

Multi-agent formation keeping is a field of active research in the literature. In Chapter 4, we apply a so-called “virtual structure” approach to spacecraft formation flying and multi-vehicle formation maneuvers. As a result, single vehicle path planning and trajectory generation techniques can be employed for the virtual structure while trajectory tracking strategies can be employed for each vehicle. For multiple spacecraft formation flying, we propose a decentralized architecture with formation feedback introduced. This architecture ensures the necessary precision in the presence of actuator saturation, internal

and external disturbances, and stringent inter-vehicle communication limitations. We also apply a constructive approach based on the satisficing control paradigm to multiple robot coordination.

The study of constrained nonlinear tracking control for vehicles using the satisficing paradigm facilitates the cooperative timing and formation keeping missions. In Chapter 5, we extend the satisficing control paradigm to the case of time-varying nonlinear systems with input constraints and explore applications of the approach to trajectory tracking for nonholonomic mobile robots and unmanned air vehicles subject to polytopic velocity and heading rate constraints. Our proposed tracking controllers are shown to be robust to input uncertainties and measurement noise, and are computationally simple and can be implemented with low-cost, low-power microcontrollers. In addition, our approach allows piecewise continuous reference velocity and heading rate and can be extended to derive a variety of other trajectory tracking strategies.

6.2 Future Work

For consensus seeking, we assumed single integrator dynamics in our previous study. It is possible to extend the results to double integrator dynamics. Our results also suggest that the same framework could be applied to decentralized spacecraft formation flying scenario, where the communication topologies between spacecraft could be switching with time. In addition, the coordination data might be driven by nonlinear dynamics, which is also an interesting topic to study in the future. Furthermore, the issue of time delay in multi-agent consensus seeking should also be taken into account in the future.

For multi-agent formation keeping, the current work in this dissertation focuses on fixed formations. An interesting topic of research might be reconfigurable formations. Another direction could be the study of optimization issues for multi-agent formation keeping.

For constrained tracking control, future work may be involved in exploring a parameterization of control laws with input constraints if a constrained control Lyapunov function is known. In addition, there is no feedback introduced from the trajectory tracker to the trajectory generator in our current software architecture. In the future, the trajectory

generator should be evolving based on the tracking performance of the trajectory tracker. Future work may also be involved in considering the effect of wind on trajectory tracking and testing the trajectory tracker in hardware. In addition, because the parameter α_ϕ is unknown in general, adaptive control technique could be used to extend the current trajectory tracker in order to estimate this parameter.

6.3 Conclusion

Three important issues of cooperative control including consensus seeking, formation keeping, and trajectory tracking have been addressed. For consensus seeking, we analyze protocols under both fixed and switching interaction topologies. For formation keeping, we propose a decentralized scheme for multiple spacecraft formation flying in deep space and a satisficing approach to multiple vehicle coordination. For trajectory tracking, we investigate nonlinear tracking controllers for both fixed wing unmanned air vehicles and nonholonomic mobile robots with polytopic input constraints.

Bibliography

- [1] P. K. C. Wang, "Navigation strategies for multiple autonomous mobile robots moving in formation," *Journal of Robotic Systems*, vol. 8, no. 2, pp. 177–195, 1991.
- [2] T. Balch and R. C. Arkin, "Behavior-based formation control for multirobot teams," *IEEE Transactions on Robotics and Automation*, vol. 14, pp. 926–939, December 1998.
- [3] M. A. Lewis and K.-H. Tan, "High precision formation control of mobile robots using virtual structures," *Autonomous Robots*, vol. 4, pp. 387–403, 1997.
- [4] P. Ogren, E. Fiorelli, and N. E. Leonard, "Formations with a mission: Stable coordination of vehicle group maneuvers," in *15th International Symposium on Mathematical Theory of Networks and Systems*, (Notre Dame, Indiana), 2002.
- [5] H. G. Tanner, G. J. Pappas, and V. Kumar, "Input-to-state stability on formation graphs," in *Proceedings of the IEEE Conference on Decision and Control*, (Las Vegas, NV), pp. 2439–2444, December 2002.
- [6] P. Ogren, M. Egerstedt, and X. Hu, "A control Lyapunov function approach to multiagent coordination," *IEEE Transactions on Robotics and Automation*, vol. 18, pp. 847–851, October 2002.
- [7] F. Giuliatti, L. Pollini, and M. Innocenti, "Autonomous formation flight," *IEEE Control Systems Magazine*, vol. 20, pp. 34–44, December 2000.
- [8] D. J. Stilwell and B. E. Bishop, "Platoons of underwater vehicles," *IEEE Control Systems Magazine*, vol. 20, pp. 45–52, December 2000.

- [9] W. Kang and H.-H. Yeh, "Co-ordinated attitude control of multi-satellite systems," *International Journal of Robust and Nonlinear Control*, vol. 12, pp. 185–205, 2002.
- [10] J. R. Carpenter, "Decentralized control of satellite formations," *International Journal of Robust and Nonlinear Control*, vol. 12, pp. 141–161, 2002.
- [11] M. R. Anderson and A. C. Robbins, "Formation flight as a cooperative game," in *Proceedings of the AIAA Guidance, Navigation and Control Conference*, (Boston, MA), pp. 244–251, American Institute of Aeronautics and Astronautics, August 1998. AIAA-98-4124.
- [12] P. K. C. Wang and F. Y. Hadaegh, "Coordination and control of multiple microspacecraft moving in formation," *The Journal of the Astronautical Sciences*, vol. 44, no. 3, pp. 315–355, 1996.
- [13] A. Robertson, G. Inalhan, and J. P. How, "Formation control strategies for a separated spacecraft interferometer," in *Proceedings of the American Control Conference*, (San Diego), June 1999.
- [14] M. Mesbahi and F. Y. Hadaegh, "Formation flying control of multiple spacecraft via graphs, matrix inequalities, and switching," *AIAA Journal of Guidance, Control, and Dynamics*, vol. 24, pp. 369–377, March-April 2000.
- [15] R. W. Beard, J. R. Lawton, and F. Y. Hadaegh, "A coordination architecture for formation control," *IEEE Transactions on Control Systems Technology*, vol. 9, pp. 777–790, November 2001.
- [16] S. Sheikholeslam and C. A. Desoer, "Control of interconnected nonlinear dynamical systems: The platoon problem," *IEEE Transactions on Automatic Control*, vol. 37, pp. 806–810, June 1992.
- [17] F. Brandt, W. Brauer, and G. Weiß, "Task assignment in multiagent systems based on vickrey-type auctioning and leveled commitment contracting," in *CIA-2000 (Cooperative Information Agents) workshop proceedings*, (Boston, USA), 2000.

- [18] M. Schneider-Fontan and M. J. Mataric, "Territorial multi-robot task division," *IEEE Transactions on Robotics and Automation*, vol. 14, pp. 815–822, October 1998.
- [19] Q. Chen and J. Y. S. Luh, "Coordination and control of a group of small mobile robots," in *Proceedings of the IEEE International Conference on Robotics and Automation*, pp. 2315–2320, 1994.
- [20] M. Hashimoto, F. Oba, and S. Zenitani, "Object-transportation control by multiple wheeled vehicle planar cartesian manipulator systems," in *Proceedings of the IEEE International Conference on Robotics and Automation*, pp. 2267–2272, 1995.
- [21] N. Miyata, J. Ota, Y. Aiyama, H. Asama, and T. Arai, "Cooperative transport in unknown environment: Application of real-time task assignment," in *Proceedings of the IEEE International Conference on Robotics and Automation*, (San Francisco, CA), pp. 3176–3182, April 2000.
- [22] R. Emery, K. Sikorski, and T. Balch, "Protocols for collaboration, coordination and dynamic role assignment in a robot team," in *Proceedings of the IEEE International Conference on Robotics and Automation*, (Washington D.C.), pp. 3008–3015, May 2002.
- [23] G. Inalhan, D. M. Stipanovic, and C. J. Tomlin, "Decentralized optimization, with application to multiple aircraft coordination," in *Proceedings of the IEEE Conference on Decision and Control*, (Las Vegas, NV), pp. 1147–1155, December 2002.
- [24] T. W. McLain, P. R. Chandler, S. Rasmussen, and M. Pachter, "Cooperative control of UAV rendezvous," in *Proceedings of the American Control Conference*, (Arlington, VA), pp. 2309–2314, June 2001.
- [25] J. S. Bellingham, M. Tillerson, M. Alighanbari, and J. P. How, "Cooperative path planning for multiple UAVs in dynamic and uncertain environments," in *Proceedings of the IEEE Conference on Decision and Control*, (Las Vegas, NV), pp. 2816–2822, December 2002.

- [26] I. M. Rekleitis, G. Dudek, and E. E. Milios, “Multi-robot collaboration for robust exploration,” in *Proceedings of the IEEE International Conference on Robotics and Automation*, (San Francisco), pp. 3164–3168, April 2000.
- [27] R. W. Beard, T. W. McLain, M. Goodrich, and E. P. Anderson, “Coordinated target assignment and intercept for unmanned air vehicles,” *IEEE Transactions on Robotics and Automation*, vol. 18, no. 6, pp. 911–922, 2002.
- [28] F. Y. Hadaegh, W.-M. Lu, and P. K. C. Wang, “Adaptive control of formation flying spacecraft for interferometry,” in *IFAC*, IFAC, 1998.
- [29] T. W. McLain and R. W. Beard, “Coordination variables, coordination functions, and cooperative timing missions,” *AIAA Journal of Guidance, Control, and Dynamics*, 2004. (to appear).
- [30] J. W. Curtis and R. W. Beard, “Satisficing: A new approach to constructive nonlinear control,” *IEEE Transactions on Automatic Control*, (to appear).
- [31] W. Ren, R. W. Beard, and T. W. McLain, “Coordination variables and consensus building in multiple vehicle systems,” in *Cooperative Control, Ser. Lecture Notes in Control and Information Sciences* (V. Kumar, N. E. Leonard, and A. S. Morse, eds.), (Block Island, RI), Springer-Verlag, 2003. (to appear).
- [32] W. Ren and R. W. Beard, “Consensus of information under dynamically changing interaction topologies,” in *Proceedings of the American Control Conference*, (Boston, MA), pp. 4939–4944, June 2004.
- [33] W. Ren and R. W. Beard, “Consensus seeking in multi-agent systems under dynamically changing interaction topologies,” *IEEE Transactions on Automatic Control*, 2003. (in review).
- [34] W. Ren and R. W. Beard, “Dynamic consensus seeking in distributed multi-agent coordinated control,” Tech. Rep. MAGICC Technical Report Nov.-02, MAGICC Lab, Brigham Young University, Provo, UT 84602, November 2003.

- [35] A. Jadbabaie, J. Lin, and A. S. Morse, "Coordination of groups of mobile autonomous agents using nearest neighbor rules," *IEEE Transactions on Automatic Control*, vol. 48, pp. 988–1001, June 2003.
- [36] W. Ren and R. W. Beard, "Virtual structure based spacecraft formation control with formation feedback," in *AIAA Guidance, Navigation, and Control Conference*, (Monterey, CA), August 2002. Paper No. AIAA-2002-4963.
- [37] W. Ren and R. W. Beard, "Formation feedback control for multiple spacecraft via virtual structures," *IEE Proceedings - Control Theory and Applications*, 2003. (to appear).
- [38] W. Ren and R. W. Beard, "Decentralized scheme for spacecraft formation flying via the virtual structure approach," *AIAA Journal of Guidance, Control, and Dynamics*, vol. 27, pp. 73–82, January-February 2004.
- [39] W. Ren and R. W. Beard, "A decentralized scheme for spacecraft formation flying via the virtual structure approach," in *Proceedings of the American Control Conference*, (Denver, CO), pp. 1746–1751, June 2003.
- [40] W. Ren, R. W. Beard, and J. W. Curtis, "Satisficing control for multi-agent formation maneuvers," in *Proceedings of the IEEE Conference on Decision and Control*, (Las Vegas, NV), pp. 2433–2438, December 2002.
- [41] W. Ren, J.-S. Sun, R. W. Beard, and T. W. McLain, "Experimental nonlinear tracking control for nonholonomic mobile robots with input constraints," Tech. Rep. MAG-ICC Technical Report Nov.-03, MAGICC Lab, Brigham Young University, Provo, UT 84602, November 2003.
- [42] W. Ren and R. W. Beard, "Clf-based tracking control for UAV kinematic models with saturation constraints," in *Proceedings of the IEEE Conference on Decision and Control*, (Maui, Hawaii), pp. 3924–3929, December 2003.

- [43] W. Ren and R. W. Beard, "Trajectory tracking for unmanned air vehicles with velocity and heading rate constraints," *IEEE Transactions on Control Systems Technology*, 2003. (to appear).
- [44] W. Ren and R. W. Beard, "Constrained nonlinear tracking control for small fixed-wing unmanned air vehicles," in *Proceedings of the American Control Conference*, (Boston, MA), pp. 4663–4668, June 2004.
- [45] D. Kingston, R. Beard, T. McLain, M. Larsen, and W. Ren, "Autonomous vehicle technologies for small fixed wing UAVs," in *AIAA 2nd Unmanned Unlimited Systems, Technologies, and Operations—Aerospace, Land, and Sea Conference and Workshop & Exhibit*, (San Diego, CA), September 2003. Paper no. AIAA-2003-6559.
- [46] W. Ren and R. W. Beard, "A control Lyapunov function approach to safeguarded shared control," Tech. Rep. MAGICC Technical Report Nov.-01, MAGICC Lab, Brigham Young University, Provo, UT 84602, November 2003.
- [47] D. Swaroop and J. K. Hedrick, "String stability of interconnected systems," *IEEE Transactions on Automatic Control*, vol. 41, no. 3, pp. 349–357, 1996.
- [48] S. S. Stankovic, M. J. Stanojevic, and D. D. Siljak, "Decentralized overlapping control of a platoon of vehicles," *IEEE Transactions on Control Systems Technology*, vol. 8, no. 5, pp. 816–832, 2000.
- [49] J. T. Feddema, C. Lewis, and D. A. Schoenwald, "Decentralized control of cooperative robotic vehicles: Theory and application," *IEEE Transactions on Robotics and Automation*, vol. 18, no. 5, pp. 852–864, 2002.
- [50] J. M. Fowler and R. D'Andrea, "Distributed control of close formation flight," in *Proceedings of the IEEE Conference on Decision and Control*, (Las Vegas, NV), pp. 2972–2977, December 2002.
- [51] N. A. Lynch, *Distributed Algorithms*. San Francisco, California: Morgan Kaufmann Publishers, Inc., 1996.

- [52] J. A. Fax and R. M. Murray, "Information flow and cooperative control of vehicle formations," in *IFAC World Congress*, (Barcelona, Spain), 2002.
- [53] J. A. Fax and R. M. Murray, "Graph Laplacians and stabilization of vehicle formations," in *IFAC World Congress*, (Barcelona, Spain), 2002.
- [54] R. Olfati-Saber and R. M. Murray, "Consensus protocols for networks of dynamic agents," in *Proceedings of the American Control Conference*, (Denver, CO), pp. 951–956, June 2003.
- [55] R. Olfati-Saber and R. M. Murray, "Agreement problems in networks with directed graphs and switching topology," in *Proceedings of the IEEE Conference on Decision and Control*, (Maui, Hawaii), pp. 4126–4132, December 2003.
- [56] L. Moreau, "Leaderless coordination via bidirectional and unidirectional time-dependent communication," in *Proceedings of the IEEE Conference on Decision and Control*, (Maui, Hawaii), pp. 3070–3075, December 2003.
- [57] R. W. Beard and V. Stepanyan, "Synchronization of information in distributed multiple vehicle coordinated control," in *Proceedings of the IEEE Conference on Decision and Control*, (Maui, Hawaii), pp. 2029–2034, December 2003.
- [58] L. Xiao and S. Boyd, "Fast linear iterations for distributed averaging," in *Proceedings of the IEEE Conference on Decision and Control*, (Maui, Hawaii), pp. 4997–5002, December 2003.
- [59] Z. Lin, M. Broucke, and B. Francis, "Local control strategies for groups of mobile autonomous agents," *IEEE Transactions on Automatic Control*, 2004. (to appear).
- [60] W. Lohmiller and J.-J. E. Slotine, "Contraction analysis for nonlinear systems," *Automatica*, vol. 34, no. 6, pp. 683–696, 1998.
- [61] J.-J. E. Slotine, "Modular stability tools for distributed computation and control," *International Journal on Adaptive Control and Signal Processing*, 2002. (to appear).

- [62] L. G. Dario Bauso and R. Pesenti, “Optimal distributed consensus protocols,” in *Proceedings of the IEEE Conference on Decision and Control*, (Atlantis, Paradise Island, Bahamas), December 2004. (submitted).
- [63] H. G. Tanner, A. Jadbabaie, and G. J. Pappas, “Flocking in fixed and switching networks,” *Automatica*, 2003. (submitted).
- [64] A. Muhammad and M. Egerstedt, “Decentralized coordination with local interactions: Some new directions,” in *Cooperative Control, Ser. Lecture Notes in Control and Information Sciences* (V. Kumar, N. E. Leonard, and A. S. Morse, eds.), (Block Island, RI), Springer-Verlag, 2003. (to appear).
- [65] R. Sepulchre, D. Paley, and N. Leonard, “Collective motion and oscillator synchronization,” in *Cooperative Control, Ser. Lecture Notes in Control and Information Sciences* (V. Kumar, N. E. Leonard, and A. S. Morse, eds.), (Block Island, RI), Springer-Verlag, 2003. (to appear).
- [66] T. Sugar and V. Kumar, “Decentralized control of cooperating mobile manipulators,” in *Proceedings of the IEEE International Conference on Robotics and Automation*, (Leuven, Belgium), pp. 2916–2921, May 1998.
- [67] R. Fierro, A. K. Das, V. Kumar, and J. P. Ostrowski, “Hybrid control of formations of robots,” in *Proceedings of the IEEE International Conference on Robotics and Automation*, (Seoul, Korea), pp. 157–162, May 2001.
- [68] T. Eren, P. N. Belhumeur, and A. S. Morse, “Closing ranks in vehicle formations based on rigidity,” in *Proceedings of the IEEE Conference on Decision and Control*, (Las Vegas, NV), pp. 2959–2964, December 2002.
- [69] B. Wie, H. Weiss, and A. Apapostathis, “Quaternion feedback regulator for spacecraft eigenaxis rotations,” *AIAA Journal of Guidance, Control, and Dynamics*, vol. 12, pp. 375–380, May 1989.

- [70] N. E. Leonard and E. Fiorelli, “Virtual leaders, artificial potentials and coordinated control of groups,” in *Proceedings of the IEEE Conference on Decision and Control*, (Orlando, Florida), pp. 2968–2973, December 2001.
- [71] B. Young, R. W. Beard, and J. Kelsey, “A control scheme for improving multi-vehicle formation maneuvers,” in *Proceedings of the American Control Conference*, (Arlington, VA), June 2001.
- [72] J. R. Lawton, R. W. Beard, and B. Young, “A decentralized approach to formation maneuvers,” *IEEE Transactions on Robotics and Automation*, vol. 19, pp. 933–941, December 2003.
- [73] J. R. Lawton and R. W. Beard, “Synchronized multiple spacecraft rotations,” *Automatica*, vol. 38, no. 8, pp. 1359–1364, 2002.
- [74] I. Kolmanovsky and N. H. McClamroch, “Developments in nonholonomic control problems,” *IEEE Control Systems Magazine*, vol. 15, pp. 20–36, December 1995.
- [75] R. W. Brockett, “Asymptotic stability and feedback stabilization,” in *Differential Geometric Control Theory* (R. S. Millman and H. J. Sussmann, eds.), pp. 181–191, Birkhäuser, 1983.
- [76] C. C. de Wit, B. Siciliano, and G. Bastin, *Theory of Robot Control*. London: Springer-Verlag, 1996.
- [77] Z.-P. Jiang and H. Nijmeijer, “Tracking control of mobile robots: A case study in backstepping,” *Automatica*, vol. 33, pp. 1393–1399, 1997.
- [78] J.-M. Yang and J.-H. Kim, “Sliding mode motion control of nonholonomic mobile robots,” *Control Systems Magazine*, vol. 19, pp. 15–23, April 1999.
- [79] T. Fukao, H. Nakagawa, and N. Adachi, “Adaptive tracking control of a nonholonomic mobile robot,” *IEEE Transactions on Robotics and Automation*, vol. 16, pp. 609–615, October 2000.

- [80] A. W. Proud, M. Pachter, and J. J. D’Azzo, “Close formation flight control,” in *Proceedings of the AIAA Guidance, Navigation, and Control Conference*, (Portland, OR), pp. 1231–1246, August 1999. Paper No. AIAA-99-4207.
- [81] A. M. Bloch, N. H. McClamroch, and M. Reyhanoglu, “Controllability and stabilizability properties of a nonholonomic control system,” in *Proceedings of the 29th Conference on Decision and Control*, (Honolulu, HI), pp. 1312–1314, December 1990.
- [82] A. W. Divelbiss and J. T. Wen, “Trajectory tracking control of a car-trailer system,” *IEEE Transactions on Control Systems Technology*, vol. 5, pp. 269–278, May 1997.
- [83] R. Fierro and F. L. Lewis, “Control of a nonholonomic mobile robot: backstepping kinematics into dynamics,” in *Proceedings of the 34th Conference on Decision and Control*, (New Orleans, LA), pp. 3805–3810, December 1995.
- [84] T.-C. Lee, K.-T. Song, C.-H. Lee, and C.-C. Teng, “Tracking control of unicycle-modeled mobile robots using a saturation feedback controller,” *IEEE Transactions on Control Systems Technology*, vol. 9, pp. 305–318, March 2001.
- [85] Z.-P. Jiang, E. Lefeber, and H. Nijmeijer, “Saturated stabilization and track control of a nonholonomic mobile robot,” *Systems and Control Letters*, vol. 42, pp. 327–332, 2001.
- [86] Z. Artstein, “Stabilization with relaxed controls,” *Nonlinear Analysis, Theory, Methods, and Applications*, vol. 7, no. 11, pp. 1163–1173, 1983.
- [87] E. D. Sontag, “A Lyapunov-like characterization of asymptotic controllability,” *SIAM Journal on Control and Optimization*, vol. 21, pp. 462–471, May 1983.
- [88] R. A. Freeman and P. V. Kokotovic, *Robust Nonlinear Control Design: State-Space and Lyapunov Techniques*. Systems & Control: Foundations & Applications, Birkhauser, 1996.

- [89] W. C. Stirling and D. R. Morrell, "Convex bayes decision theory," *IEEE Transactions on Systems, Man, and Cybernetics*, vol. 21, pp. 173–183, January/February 1991.
- [90] M. A. Goodrich, W. C. Stirling, and R. L. Frost, "A theory of satisficing decisions and control," *IEEE Transactions on Systems, Man, and Cybernetics—Part A. Systems and Humans*, vol. 28, pp. 763–779, November 1998.
- [91] W. Stirling, *Satisficing Games and Decision Making: With Applications to Engineering and Computer Science*. Cambridge University Press, 2003.
- [92] D. Q. Mayne and H. Michalska, "Receding horizon control of nonlinear systems," *IEEE Transactions on Automatic Control*, vol. 35, no. 7, pp. 814–824, 1990.
- [93] E. F. Camacho and C. Bordons, *Model Predictive Control*. Springer Verlag, 1999.
- [94] Y. Lin and E. D. Sontag, "Control-Lyapunov universal formulas for restricted inputs," *Control-Theory and Advanced Technology*, vol. 10, pp. 1981–2004, December 1995.
- [95] Y. Lin and E. D. Sontag, "Universal formula for stabilization with bounded controls," *Systems and Control Letters*, vol. 16, pp. 393–397, June 1991.
- [96] T. W. McLain and R. W. Beard, "Coordination variables, coordination functions, and cooperative timing missions," in *Proceedings of the American Control Conference*, (Denver, CO), pp. 296–301, June 2003.
- [97] T. Balch and L. E. Parker, eds., *Robot Teams: From Diversity to Polymorphism*. Natick, Massachusetts: A. K. Peters, Ltd., 2002.
- [98] G. Royle and C. Godsil, *Algebraic Graph Theory*. New York: Springer Graduate Texts in Mathematics #207, 2001.
- [99] R. A. Horn and C. R. Johnson, *Matrix Analysis*. Cambridge University Press, 1985.
- [100] W. J. Rugh, *Linear System Theory*. Englewood Cliffs, New Jersey: Prentice Hall, 2nd ed., 1996.

- [101] J. Wolfowitz, “Products of indecomposable, aperiodic, stochastic matrices,” *Proceedings of the American Mathematical Society*, vol. 15, pp. 733–736, 1963.
- [102] A. S. Morse, “Supervisory control of families of linear set-point controllers-part 1: Exact matching,” *IEEE Transactions on Automatic Control*, vol. 41, no. 10, pp. 1413–1431, 1996.
- [103] <http://www.ee.byu.edu/magicc/>.
- [104] J. R. Wertz, ed., *Spacecraft Attitude Determination and Control*. Kluwer Academic Publishers, 1978.
- [105] P. C. Hughes, *Spacecraft Attitude Dynamics*. John Wiley & Sons, 1986.
- [106] J. T.-Y. Wen and K. Kreutz-Delgado, “The attitude control problem,” *IEEE Transactions on Automatic Control*, vol. 36, pp. 1148–1162, October 1991.
- [107] A. Graham, *Kronecker Products and Matrix Calculus: with Applications*. Halsted Press, 1981. Properties of Kronecker Products.
- [108] P. Ogren, M. Egerstedt, and X. Hu, “A control Lyapunov function approach to multi-agent coordination,” in *Proceedings of the IEEE Conference on Decision and Control*, (Orlando, Florida), pp. 1150–1155, December 2001.
- [109] M. Egerstedt, X. Hu, and A. Stotsky, “Control of mobile platforms using a virtual vehicle approach,” *IEEE Transactions on Automatic Control*, vol. 46, pp. 1777–1782, November 2001.
- [110] H. K. Khalil, *Nonlinear Systems*. Upper Saddle River, NJ: Prentice Hall, 2nd ed., 1996.
- [111] J. Pomet, B. Thuilot, G. Bastin, and G. Campion, “A hybrid strategy for the feedback stabilization of nonholonomic mobile robots,” in *Proceedings of the IEEE International Conference on Robotics and Automation*, (Nice, France), pp. 129–134, May 1992.

- [112] E. P. Anderson and R. W. Beard, “An algorithmic implementation of constrained extremal control for UAVs,” in *Proceedings of the AIAA Guidance, Navigation, and Control Conference*, (Monterey, CA), August 2002. Paper no. AIAA-2002-4470.
- [113] Y. J. Kanayama, Y. Kimura, F. Miyazaki, and T. Noguchi, “A stable tracking control method for an autonomous mobile robot,” in *Proceedings of the IEEE International Conference on Robotics and Automation*, pp. 384–389, 1990.
- [114] E. Sontag and Y. Wang, “New characterizations of input-to-state stability,” *IEEE Transactions on Automatic Control*, vol. 41, pp. 1283–1294, September 1996.
- [115] M. Krstić and H. Deng, *Stabilization of Nonlinear Uncertain Systems*. Communication and Control Engineering, London: Springer, 1998.
- [116] J. R. Cloutier, C. N. D’Souza, and C. P. Mracek, “Nonlinear regulation and nonlinear H_∞ control via the state-dependent Riccati equation technique,” in *IFAC World Congress*, (San Francisco, California), 1996.
- [117] J. Kelsey, “MAGICC multiple robot toolbox (MMRT): A Simulink-based control and coordination toolbox for multiple robotic agents,” Master’s thesis, Brigham Young University, Provo, Utah 84602, April 2002.
- [118] T. W. McLain and R. W. Beard, “Cooperative rendezvous of multiple unmanned air vehicles,” in *Proceedings of the AIAA Guidance, Navigation and Control Conference*, (Denver, CO), August 2000. Paper no. AIAA-2000-4369.
- [119] H. G. Tanner and K. J. Kyriakopoulos, “Backstepping for nonsmooth systems,” *Automatica*, vol. 39, pp. 1259–1265, 2003.
- [120] D. Shevitz and B. Paden, “Lyapunov stability theory of nonsmooth systems,” *IEEE Transactions on Automatic Control*, vol. 39, no. 9, pp. 1910–1914, 1994.